Part III

Rotor-Body Coupling Elastic Blades

pp. 152-193

Outline of Multiblade Coordinates

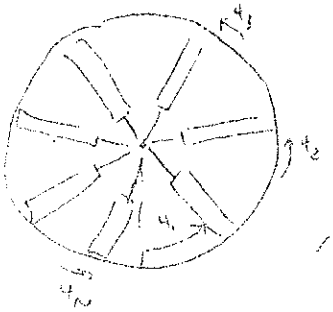

N-blades $\qquad \psi = \Omega t$

$\psi_k = \frac{k-1}{M}(2\pi) + \psi$

$$\beta_k = a_o + \sum_{n=1}^{N} a_n \cos(n\psi_k) + b_n \sin(n\psi_k)$$

even $N \Rightarrow M = \frac{N}{2} - 1 = \frac{N-2}{2} + a_d\,(-1)^{k+1}$

odd $N \Rightarrow M = \frac{N-1}{2}$, a_d removed

other names for $a_n, b_n, \beta_I, \beta_{II}$, etc.

Inverse: $\qquad a_o = \frac{1}{N}\sum_{k=1}^{N} \beta_k \qquad a_d = \frac{1}{N}\sum_{k=1}^{N} (-1)^{k+1}\,\beta_k$

$$a_n = \frac{2}{N}\sum_{k=1}^{n} \beta_k \cos(n\psi_k) \qquad b_n = \frac{2}{N}\sum_{k=1}^{N} \beta_k \sin(n\psi_k)$$

Matrix Form

$$\begin{Bmatrix} \beta_1 \\ \beta_2 \\ \vdots \\ \beta_N \end{Bmatrix} = \begin{bmatrix} 1 & \cos\psi_1 & \sin\psi_1 & \cos 2\psi_1 & \cdots & 1 \\ 1 & \cos\psi_2 & \sin\psi_2 & \cos 2\psi_2 & \cdots & -1 \\ \vdots & \vdots & \vdots & \vdots & \ddots & \vdots \\ 1 & \cos\psi_N & \sin\psi_N & \cos 2\psi_N & \cdots & (-1)^{N+1} \end{bmatrix} \begin{Bmatrix} a_o \\ a_1 \\ b_1 \\ \vdots \\ a_d \end{Bmatrix} = [T] \begin{Bmatrix} a \\ b \end{Bmatrix}$$

$$\begin{Bmatrix} a_o \\ a_1 \\ b_1 \\ a_2 \\ b_2 \\ \vdots \\ a_d \end{Bmatrix} = [Q] \begin{bmatrix} 1 & 1 & 1 & 1 & 1 \\ \cos\psi_1 & \cos\psi_2 & \cos\psi_3 & \ldots & \cos\psi_N \\ \sin\psi_1 & \sin\psi_2 & \sin\psi_3 & \ldots & \sin\psi_N \\ \cos 2\psi_1 & \cos 2\psi_2 & \cos 2\psi_3 & \ldots & \cos 2\psi_N \\ \vdots & \vdots & \vdots & \vdots & \vdots \\ 1 & -1 & 1 & -1 & \ldots \end{bmatrix} \begin{Bmatrix} \beta_1 \\ \beta_2 \\ \vdots \\ \beta_k \end{Bmatrix} = QT^T \{\beta\}$$

$QT^T\dot{T}$ = constant, anti-symmetric

of form: $\begin{bmatrix} \ddots & & & \\ & \begin{bmatrix} 0 & n\Omega \\ -n\Omega & 0 \end{bmatrix} & & \\ & & & \ddots \end{bmatrix}$.

$QT^T\ddot{T}$ of form: $\begin{bmatrix} \ddots & & \\ & -n^2\Omega^2 & \\ & & \ddots \end{bmatrix}$

$$[Q] = \begin{bmatrix} 1/N & & & & & \\ & 2/N & & & & \\ & & 2/N & & & \\ & & & \ddots & & \\ & & & & 2/N & \\ & & & & & 1/N \end{bmatrix}$$

$$[Q]^{-1/2} = \begin{bmatrix} \sqrt{N} & & & & \\ & \sqrt{N}/2 & & & \\ & & \ddots & & \\ & & & \sqrt{N}/2 & \\ & & & & \sqrt{N} \end{bmatrix}, \qquad QT^T = T^{-1}$$

Normalized Coordinates

$$\begin{Bmatrix} \bar{a} \\ b \end{Bmatrix} = [Q]^{-1/2} \begin{Bmatrix} a \\ b \end{Bmatrix}, \qquad \begin{Bmatrix} a \\ b \end{Bmatrix} = [Q]^{1/2} \begin{Bmatrix} \bar{a} \\ b \end{Bmatrix}$$

$$\overline{T} = TQ^{1/2} \qquad \{\beta\} = \{\overline{T}\} \begin{Bmatrix} \bar{a} \\ b \end{Bmatrix}$$

$$\begin{Bmatrix} \bar{a} \\ b \end{Bmatrix} = \{\overline{T}\}^T \{\beta\}$$

$$\overline{T}^T = \overline{T}^{-1}$$

Identities

$$\frac{1}{N}\sum_{k=1}^{N}\cos\left(n\psi_k\right)=\begin{cases}0 & n\neq\text{integer mult. of N}\\ \cos\left(n\psi\right) & n=\text{integer multiple}\end{cases}$$

$$\frac{1}{N}\sum_{k=1}^{N}\sin\left(n\psi_k\right)=\begin{cases}0 & n\neq\text{integer mult. of N}\\ \sin\left(n\psi\right) & n=\text{integer multiple}\end{cases}$$

$$\frac{1}{N}\sum_{k=1}^{N}\left(-1\right)^{k+1}\cos\left(l\psi_k\right)=\begin{cases}0 & l\neq\text{odd mult. of N/2}\\ \cos\left(l\psi\right) & l=\text{odd multiple}\end{cases}$$

$$\frac{1}{N}\sum_{k=1}^{N}\left(-1\right)^{k+1}\sin\left(l\psi_k\right)=\begin{cases}0 & l\neq\text{odd mult. of N/2}\\ \sin\left(l\psi\right) & l=\text{odd multiple}\end{cases}$$

$$\cos\left(l\psi_k\right)\cos\left(m\psi_k\right)=\tfrac{1}{2}\left[\cos(l-m)\psi_k+\cos\left(l+m\right)\psi_k\right]$$
$$\sin\left(l\psi_k\right)\sin\left(m\psi_k\right)=\tfrac{1}{2}\left[\cos(l-m)\psi_k-\cos\left(l+m\right)\psi_k\right]$$
$$\sin\left(l\psi_k\right)\cos\left(m\psi_k\right)=\tfrac{1}{2}\left[\sin(l-m)\psi_k+\sin\left(l+m\right)\psi_k\right]$$

e.g.

$$\frac{1}{N}\sum_{k=1}^{N}\cos\left(l\psi_k\right)\cos\left(m\psi_k\right)=\left\{\begin{array}{cc}1 & l=m=0\\ \frac{1}{2} & l=m\neq\text{integ. mult. } N/2\\ \frac{1}{2}+\frac{1}{2}\cos\left(N\psi\right) & l=m=\text{int. mult.}N/2\end{array}\right\}$$

Helpful Multi-Blade Relationships ($N = 4$)

$$x_j = a_o + a_1 \cos\psi_j + b_1 \sin\psi_j + a_d\,(-1)^{j-1}$$

$$\dot{x}_j = \dot{a}_o + \dot{a}_1 \cos\psi_j + \dot{b}_1 \sin\psi_j + \dot{a}_d\,(-1)^{j-1} - a_1\Omega \sin\psi_j + b_1\Omega \cos\psi_j$$

$$\ddot{x}_j = \ddot{a}_o + \ddot{a}_1 \cos\psi_j + \ddot{b}_1 \sin\psi_j + \ddot{a}_d\,(-1)^{j-1} - 2\dot{a}_1\Omega \sin\psi_j + 2\dot{b}_1\Omega \cos\psi_j - a_1\Omega^2 \cos\psi_j - b_1\Omega^2 \sin\psi_j$$

$$a_o = \frac{1}{4}\sum_{j=1}^{4} x_j \qquad a_d = \frac{1}{4}\sum_{j=1}^{4} x_j\,(-1)^{j-1}$$

$$a_1 = \frac{1}{2}\sum_{j=1}^{4} x_j \cos\psi_j \qquad b_1 = \frac{1}{2}\sum_{j=1}^{4} x_j \sin\psi_j$$

$$\dot{a}_1 + \Omega b_1 = \frac{1}{2}\sum_{j=1}^{4} \dot{x}_j \cos\psi_j \qquad \dot{b}_1 - \Omega a_1 = \frac{1}{2}\sum_{j=1}^{4} \dot{x}_j \sin\psi_j$$

$$\ddot{a}_1 - 2\Omega\dot{b}_1 - \Omega^2 a_1 = \frac{1}{2}\sum_{j=1}^{4} \ddot{x}_j \cos\psi_j$$

$$\ddot{b}_1 - 2\Omega\dot{a}_1 - \Omega^2 b_1 = \frac{1}{2}\sum_{j=1}^{4} \ddot{x}_j \sin\psi_j$$

Multi-Blade Example
David Peters
4-5-16

$$\overset{*}{X}_k + (K + \mu\cos\psi_k) X_k = 1 + \mu\sin\psi_k$$

$$k = 1,2,3,4$$

$$X_k = a_0 + a_1\cos\psi_k + b_1\sin\psi_k + (-1)^{k+1} a_d$$

$$\overset{*}{X}_k = \overset{*}{a}_0 + \overset{*}{a}_1\cos\psi_k + \overset{*}{b}_1\sin\psi_k + \overset{*}{a}_d(-1)^{k+1} - a_1\sin\psi_k + b_1\cos\psi_k$$

Substitute Multi-Blade Transform into Differential Equation

$$\dot{a}_0 + \dot{a}_1\cos\psi_k + \dot{b}_1\sin\psi_k + \dot{a}_d(-1)^{k+1} - a_1\sin\psi_k + b_1\cos\psi_k + K a_0 + K a_1\cos\psi_k + K b_1\sin\psi_k + K a_d(-1)^{k+1} + \mu\cos\psi_k a_0 + \frac{\mu}{2}(1+\cos 2\psi_k) a_1 + \frac{\mu}{2}\sin(2\psi_k) b_1 + (-1)^{k+1}\cos\psi_k a_d\mu = 1 + \mu\sin\psi_k$$

a_0 equation $\frac{1}{4}\sum_{k=1}^{4}\left[Eq^{\Delta}_{k}\right]$

$$\dot{a}_0 + K a_0 + \frac{\mu}{2} a_1 = 1$$

---

a_1 equation $\frac{2}{4}\sum_{k=1}^{4}\left[Eq^{\Delta}\right]_k \cos(\psi_k)$

$$\dot{a}_1 + b_1 + K a_1 + \mu a_0 + \mu \cos(2\psi) a_d = 0$$

---

b_1 equation $\frac{2}{4}\sum_{k=1}^{4}\left[Eq^{\Delta}\right]_k \sin(\psi_k)$

$$\dot{b}_1 - a_1 + K b_1 = \mu$$

---

a_d equation $\frac{1}{4}\sum_{k=1}^{4}(-1)^{k+1}\left[Eq^{\Delta}\right]_k$

$$\dot{a}_d + K a_d + \frac{\mu}{2}\cos(2\psi) a_1 + \frac{\mu}{2}\sin(2\psi) b_1 = 0$$

Matrix Form

$$\begin{bmatrix} 1 & 0 & 0 & 0 \\ 0 & 1 & 0 & 0 \\ 0 & 0 & 1 & 0 \\ 0 & 0 & 0 & 1 \end{bmatrix} \begin{Bmatrix} a_0 \\ a_1 \\ b_1 \\ a_d \end{Bmatrix}^{*}$$

$$+ \left[\begin{array}{c|c|c|c} K & \frac{\mu}{2} & 0 & 0 \\ \hline \mu & K & 1 & \mu\cos(24) \\ \hline 0 & -1 & K & 0 \\ \hline 0 & \frac{\mu}{2}\cos(24) & \frac{\mu}{2}\sin(24) & K \end{array}\right] \begin{Bmatrix} q_0 \\ q_1 \\ b_1 \\ q_d \end{Bmatrix}$$

$$= \begin{Bmatrix} 1 \\ 0 \\ \mu \\ 0 \end{Bmatrix}$$

E 3

ROTOR-BODY COUPLING & MULT-BLADE COORDINATES

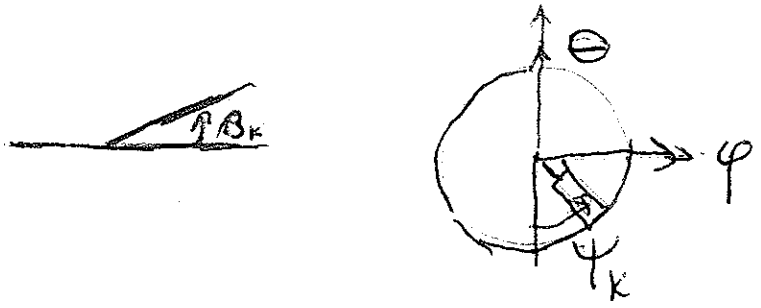

$\psi_k = \psi + (k-1)\frac{2\pi}{N}$

Must define order:

a) $\theta, \phi, \psi, \beta$ ang. rotation $= \Omega + \dot{\phi}\theta$

or *b*) $\phi, \theta, \psi, \beta$ ang. rotation $= \Omega - \phi\dot{\theta}$

c) quasi-coordinates rotation $= \Omega - \frac{1}{2}\phi\dot{\theta} + \frac{1}{2}\dot{\phi}\theta$

‡ $T = \frac{1}{2} I_\theta \dot{\theta}^2 + \frac{1}{2} I_\psi \dot{\varphi}^2 + \sum_{k=1}^{N} \int_0^R m \frac{1}{2} \left[\{ (\Omega + \dot{\varphi}\theta)\cos\beta_k + \dot{\theta}\sin\beta_k \cos\psi_k - \dot{\varphi}\sin\beta_k \sin\psi_k \}^2 + (\dot{\beta}_k - \dot{\theta}\sin\psi_k - \dot{\varphi}\cos\psi_k)^2 \right] x^2 dx$ or $\Omega - \dot{\theta}\varphi$ or $\Omega - \frac{1}{2}\dot{\theta}\varphi + \frac{1}{2}\theta\dot{\varphi}$

$T = \frac{1}{2} I_\theta \dot{\theta}^2 + \frac{1}{2} I_\varphi \dot{\varphi}^2 + \sum_{k=1}^{N} \frac{1}{2} I_\beta \left[\Omega^2 (1 - \beta_k^2 + 2\dot{\varphi}\theta/\Omega) + \dot{\theta}^2 \sin^2\beta_k \cos^2\psi_k + \dot{\varphi}^2 \sin^2\beta_k \sin^2\psi_k + 2\Omega\dot{\theta}\sin\beta_k \cos\beta_k \cos\psi_k - 2\Omega\dot{\varphi}\sin\beta_k \cos\beta_k \sin\psi_k - 2\dot{\theta}\dot{\varphi}\sin^2\beta_k \sin\psi_k \cos\psi_k + \dot{\beta}_k^2 + \dot{\theta}^2 \sin^2\psi_k + \dot{\varphi}^2 \cos^2\psi_k - 2\dot{\beta}_k\dot{\theta}\sin\psi_k - 2\dot{\beta}_k\dot{\varphi}\cos\psi_k + 2\dot{\theta}\dot{\varphi}\sin\psi_k\cos\psi_k \right]$ or $-2\Omega\theta$ or $\underline{\underline{\text{or}}}$ etc.

Linearize $\sin\beta_k = \beta_k, \beta_k, \theta, \phi$ small,

Keep quadratic terms,

$\frac{\mathrm{d}}{\mathrm{d}\psi} \equiv ()^* = \frac{1}{\Omega}\frac{\mathrm{d}}{\mathrm{d}t}, \qquad \frac{2I_\theta}{NI_\beta} = \rho_\theta, \qquad \frac{2I_\phi}{NI_\beta} = \rho_\phi$

‡ Note $\int_0^R \left(\sqcup_T^2 + \sqcup_p^2\right) \mathrm{d}x$

$$\frac{T}{\Omega^2 I_\beta} = \frac{1}{2}\dot{\theta}^2\left[\frac{N}{2}\rho_\theta + \sum_k \sin^2\psi_k\right] - \frac{N}{2}\dot{\theta}\phi + \frac{N}{2}\dot{\phi}\theta$$
$$+ \frac{1}{2}\dot{\phi}^2\left[\frac{N}{2}\rho_\phi + \sum_k \cos^2\psi_k\right]$$
$$+ \sum_k \left[\frac{1}{2}\dot{\beta}_k^2 - \beta_k^2 + \dot{\theta}\beta_k\cos\psi_k - \dot{\phi}\beta_k\sin\psi_k\right.$$
$$\left. - \dot{\beta}_k\dot{\theta}\sin\psi_k - \dot{\beta}_k\dot{\phi}\cos\psi_k + \dot{\theta}\dot{\phi}\sin\psi_k\cos\psi_k\right]$$

$$\frac{T}{\Omega^2 I_\beta} = \frac{1}{2}\dot{\theta}^2\left(\frac{N}{2}\right)(\rho_\theta + 1) + \frac{1}{2}\dot{\phi}^2\left(\frac{N}{2}\right)(\rho_\phi + 1) - \frac{N}{2}\dot{\theta}\phi + \frac{N}{2}\dot{\phi}\theta$$
$$+ \sum_k \left[\frac{1}{2}\dot{\beta}_k^2 - \frac{1}{2}\beta_k^2 + \dot{\theta}\left(\beta_k\cos\psi_k - \dot{\beta}_k\sin\psi_k\right)\right.$$
$$\left. - \dot{\phi}\left(\beta_k\sin\psi_k + \dot{\beta}_k\cos\psi_k\right)\right]$$

$$\beta_k = \beta_c\cos\psi_k + \beta_s\sin\psi_k$$
$$\beta_k^2 = \beta_c^2\cos^2\psi_k + \beta_s^2\sin^2\psi_k + 2\beta_s\beta_c\cos\psi_k\sin\psi_k$$
$$\dot{\beta}_k = \dot{\beta}_c\cos\psi_k + \dot{\beta}_s\sin\psi_k - \beta_c\sin\psi_k + \beta_s\cos\psi_k$$
$$\dot{\beta}_k^2 = \dot{\beta}_c^2\cos^2\psi_k + \dot{\beta}_s^2\sin^2\psi_k - \beta_c^2\sin^2\psi_k + \beta_s^2\cos^2\psi_k$$
$$+ 2\left(\dot{\beta}_c\dot{\beta}_s - \dot{\beta}_c\beta_c + \dot{\beta}_s\beta_s - \beta_c\beta_s\right)\sin\psi_k\cos\psi_k$$
$$+ 2\dot{\beta}_c\beta_c\cos^2\psi_k - 2\dot{\beta}_s\beta_c\sin^2\psi_k$$

$$\beta_c \equiv \frac{2}{N}\sum_k \beta_k \cos\psi_k \qquad \beta_s \equiv \frac{2}{N}\sum_k \beta_k \sin\psi_k$$

$$\overset{*}{\beta}_c = \frac{2}{N}\sum_k \left(\overset{*}{\beta}_k \cos\psi_k - \beta_k \sin\psi_k\right) = \frac{2}{N}\sum_k \overset{*}{\beta}_k \cos\psi_k - \beta_s$$

$$\overset{*}{\beta}_s = \frac{2}{N}\sum_k \left(\overset{*}{\beta}_k \sin\psi_k + \beta_k \cos\psi_k\right) = \frac{2}{N}\sum_k \overset{*}{\beta}_k \sin\psi_k + \beta_c$$

$$\frac{2T}{N\Omega^2 I_\beta} = \frac{1}{2}\overset{*2}{\theta}\ (1+\rho_\theta) + \frac{1}{2}\overset{*2}{\phi}\ (1+\rho_\phi) - \overset{*}{\theta}\phi + \overset{*}{\phi}\theta$$
$$+ \frac{1}{2}\left(\overset{*2}{\beta}_c + \overset{*2}{\beta}_s + 2\overset{*}{\beta}_c\beta_s - 2\overset{*}{\beta}_s\beta_c\right)$$
$$+ \overset{*}{\theta}\left(2\beta_c - \overset{*}{\beta}_s\right) - \overset{*}{\phi}\left(2\beta_s + \overset{*}{\beta}_c\right) = \overline{T}$$

$$V = \tfrac{1}{2}K_\theta\theta^2 + \tfrac{1}{2}K_\phi\phi^2 + \sum_k \tfrac{1}{2}K_\beta\beta_k^2$$

$$\frac{2K_\theta}{N\Omega^2 I_\beta} = \overline{K}_\theta, \qquad \frac{2K_\phi}{N\Omega^2 I_\beta} = \overline{K}_\phi, \qquad \frac{K_\beta}{\Omega^2 I_\beta} = p^2 - 1$$

$$\frac{2V}{N\Omega^2 I_\beta} = \frac{1}{2}\overline{K}_\theta\theta^2 + \frac{1}{2}\overline{K}_\phi\phi^2 + \frac{1}{2}\left(p^2-1\right)\left(\beta_c^2 + \beta_s^2\right) = \overline{V}$$

$$\delta W = \sum_{k=1}^{N} \int_0^R \tfrac{1}{2}\rho a c \Omega x \left[-\dot{\beta}_k x + \dot{\theta} x \sin\psi_k + \dot{\phi} x \cos\psi\right] \cdot$$

(from $\sqcup_p$) $\qquad [x\delta\beta_k - x\delta\theta \sin\psi_k - x\delta\phi\cos\psi_k]\,\mathrm{d}x$

$$\frac{\delta W}{\Omega^2 I_\beta} = \sum_k \tfrac{\gamma}{8} \left[-\overset{*}{\beta}_k + \overset{*}{\theta}\sin\psi_k + \overset{*}{\phi}\cos\psi\right] \cdot$$

$$[\delta\beta_k - \sin\psi_k\delta\theta - \cos\psi_k\delta\phi]$$

$$\frac{\delta W}{\Omega^2 I_\beta} = \sum_k \tfrac{\gamma}{8} \left[\left(-\overset{*}{\beta}_c - \beta_s + \overset{*}{\phi}\right)\cos\psi_k + \left(-\overset{*}{\beta}_s + \beta_c + \overset{*}{\theta}\right)\sin\psi_k\right] \cdot$$

$$[(\delta\beta_s - \delta\theta)\sin\psi_k + (\delta\beta_c - \delta\phi)\cos\psi_k]$$

$$\frac{2\delta W}{N\Omega^2 I_\beta} = \delta\overline{W} = \tfrac{\gamma}{8}\left[\left(-\overset{*}{\beta}_c + \beta_s + \overset{*}{\phi}\right)(\delta\beta_c - \delta\phi)\right.$$

$$\left. + \left(-\overset{*}{\beta}_s + \beta_c + \overset{*}{\theta}\right)(\delta\beta_s - \delta\theta)\right]$$

$$\frac{\mathrm{d}}{\mathrm{d}\psi}\frac{\partial\overline{T}}{\partial\overset{*}{\theta}}-\frac{\partial\overline{T}}{\partial\theta}=\overset{**}{\theta}\left(1+\rho_\theta\right)+2\overset{*}{\beta}_c-\overset{**}{\beta}_s-2\overset{*}{\phi}$$

$$\frac{\mathrm{d}}{\mathrm{d}\psi}\frac{\partial\overline{T}}{\partial\overset{*}{\phi}}-\frac{\partial\overline{T}}{\partial\phi}=\overset{**}{\phi}\left(1+\rho_\phi\right)-2\overset{*}{\beta}_s-\overset{**}{\beta}_c+2\overset{*}{\theta}$$

$$\frac{\mathrm{d}}{\mathrm{d}\psi}\frac{\partial\overline{T}}{\partial\overset{*}{\beta}_s}-\frac{\partial\overline{T}}{\partial\beta_s}=\overset{**}{\beta}_s-\overset{*}{\beta}_c-\overset{**}{\theta}-\overset{*}{\beta}_c+2\overset{**}{\phi}$$

$$\frac{\mathrm{d}}{\mathrm{d}\psi}\frac{\partial\overline{T}}{\partial\overset{*}{\beta}_c}-\frac{\partial\overline{T}}{\partial\beta_c}=\overset{**}{\beta}_c-\overset{*}{\beta}_s-\overset{**}{\phi}-\overset{*}{\beta}_s+2\overset{**}{\theta}$$

$$\begin{bmatrix}1+\rho_\theta & 0 & -1 & 0\\ 0 & 1+\rho_\phi & 0 & -1\\ -1 & 0 & 1 & 0\\ 0 & -1 & 0 & 1\end{bmatrix}\begin{Bmatrix}\overset{**}{\theta}\\ \overset{**}{\phi}\\ \overset{**}{\beta}_s\\ \overset{**}{\beta}_c\end{Bmatrix}+\begin{bmatrix}n & -2 & -n & 2\\ 2 & n & -2 & -n\\ -n & 2 & n & -2\\ -2 & -n & 2 & n\end{bmatrix}\begin{Bmatrix}\overset{*}{\theta}\\ \overset{*}{\phi}\\ \overset{*}{\beta}_s\\ \overset{*}{\beta}_c\end{Bmatrix}$$

$$+\begin{bmatrix}\overline{K}_\theta & 0 & 0 & n\\ 0 & \overline{K}_\phi & -n & 0\\ 0 & 0 & p^2-1 & -n\\ 0 & 0 & n & p^2-1\end{bmatrix}\begin{Bmatrix}\theta\\ \phi\\ \beta_s\\ \beta_s\end{Bmatrix}=\begin{Bmatrix}0\\ 0\\ 0\\ 0\end{Bmatrix}$$

$$n=\gamma/8$$

Adding eqns (1) & (3), (2) & (4)

$$\rho_\theta \overset{**}{\theta} + \overline{K}_\theta \theta + \left(p^2 - 1\right) \beta_s = 0$$

$$\rho_\phi \overset{**}{\phi} + \overline{K}_\phi \theta + \left(p^2 - 1\right) \beta_c = 0$$

($p = 1 \Rightarrow$ no β coupling possible wiht no ϕ or θ)

1) βmode, no θ or ϕ

$$\begin{Bmatrix} \overset{**}{\beta_s} \\ \overset{**}{\beta_c} \end{Bmatrix} + \begin{bmatrix} n & -2 \\ 2 & n \end{bmatrix} \begin{Bmatrix} \overset{*}{\beta_s} \\ \overset{*}{\beta_c} \end{Bmatrix} + \begin{bmatrix} p^2 - 1 & -n \\ n & p^2 - 1 \end{bmatrix} \begin{Bmatrix} \beta_s \\ \beta_c \end{Bmatrix} = \begin{Bmatrix} 0 \\ 0 \end{Bmatrix}$$

$$\begin{bmatrix} s^2 + ns + p^2 - 1 & -2s - n \\ 2s + n & s^2 + ns + p^2 - 1 \end{bmatrix} \begin{Bmatrix} \beta_s \\ \beta_c \end{Bmatrix} = \begin{Bmatrix} 0 \\ 0 \end{Bmatrix}$$

$$\left(s^2 + ns + p^2 - 1\right)^2 + (2s + n)^2 = 0$$

$$s^2 + ns + p^2 - 1 = \pm i\,(2s + n)$$

$$s^2 + s\,(n \pm 2i) \pm in + p^2 - 1 \qquad s = \frac{-n \pm 2i \pm \sqrt{n^2 - 4 - 4p^2 + 4}}{2}$$

$$s = \tfrac{-n}{2} \pm i\sqrt{p^2 - \tfrac{n^2}{4}} \pm i \qquad \text{(1/rev) shift}$$

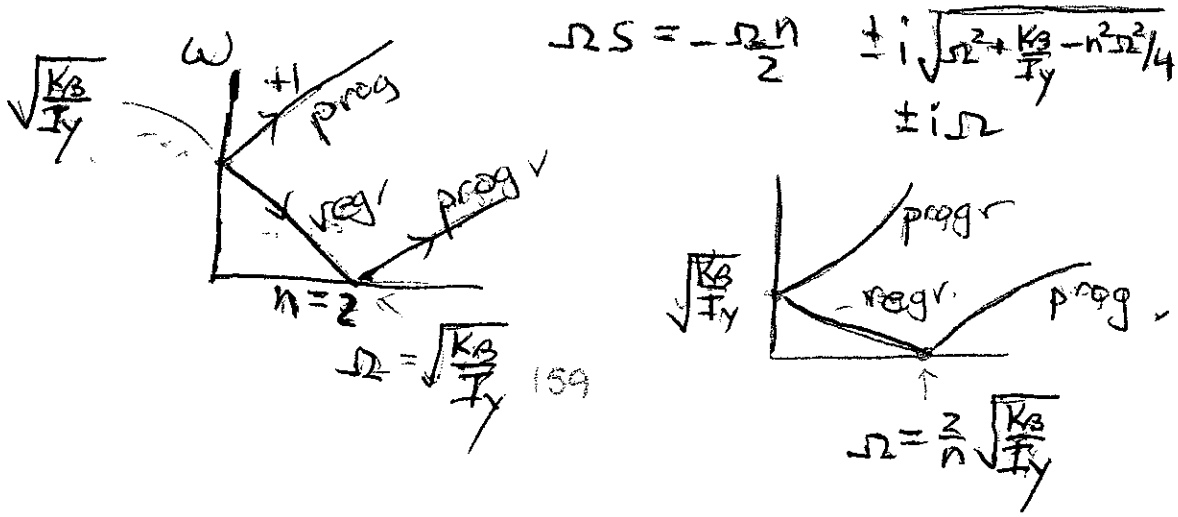

2) $p = \infty,\ \beta = 0,$ pure gyroscopic

$$\begin{Bmatrix} 0 \\ 0 \end{Bmatrix} = \begin{bmatrix} 1+\rho_\theta & 0 \\ 0 & 1+\rho_\phi \end{bmatrix} \begin{Bmatrix} \overset{**}{\theta} \\ \overset{**}{\phi} \end{Bmatrix} + \begin{bmatrix} n & -2 \\ 2 & n \end{bmatrix} \begin{Bmatrix} \overset{*}{\theta} \\ \overset{*}{\phi} \end{Bmatrix} + \begin{bmatrix} \overline{K}_\theta & 0 \\ 0 & \overline{K}_\phi \end{bmatrix} \begin{Bmatrix} \theta \\ \phi \end{Bmatrix} = \begin{Bmatrix} 0 \\ 0 \end{Bmatrix}$$

$$\begin{bmatrix} (1+\rho_\theta)\, s^2 + ns + \overline{K}_\theta & -2s \\ 2s & (1+\rho_\phi)\, s^2 + ns + \overline{K}_\phi \end{bmatrix} \begin{Bmatrix} \theta \\ \phi \end{Bmatrix} = \begin{Bmatrix} 0 \\ 0 \end{Bmatrix}$$

Let n = 0 (vacuum)

$$\left[(1+\rho_\theta)\, s^2 + \overline{K}_\theta\right] \left[(1+\rho_\phi)\, s^2 + \overline{K}_\phi\right] + 4s^2 = 0$$

$$(1+\rho_\theta)\,(1+\rho_\phi)\, s^4 + \left[\overline{K}_\theta\,(1+\rho_\theta)\,\overline{K}_\phi\,(1+\rho_\phi) + 4\right] s^2 + \overline{K}_\theta \overline{K}_\phi = 0$$

For $\rho_\theta = \rho_\phi, 1+\rho_\theta = 1+\rho_\phi = A \qquad A \geq 1$

$$\frac{K_\theta}{1+\rho_\theta} \equiv w_\theta^2 \qquad \frac{K_\phi}{1+\rho_\phi} \equiv w_\phi^2$$

$$s^4 + \left(w_\theta^2 + w_\phi^2 + \frac{4}{A^2}\right) s^2 + w_\theta^2 w_\phi^2 = 0$$

$$s^2 = \frac{-\left(w_\theta^2 + w_\phi^2 + \frac{4}{A^2}\right) \pm \sqrt{\left(w_\theta^2 - w_\phi^2\right)^2 + \frac{8}{A^2}\left(w_\theta^2 + w_\phi^2\right) + \frac{16}{A^4}}}{2}$$

For $w_\theta = w_\phi \equiv w, \quad A = 1$

$$s^2 = -w^2 - 2 \pm \sqrt{4w^2 + 4}$$

$$s = \pm i\sqrt{w^2 + 2 \pm 2\sqrt{w^2 + 1}}$$

$$\Omega s = \pm i\sqrt{\frac{K}{I} + 2\Omega^2 \pm 2\Omega\sqrt{\frac{K}{I} + \Omega^2}}$$

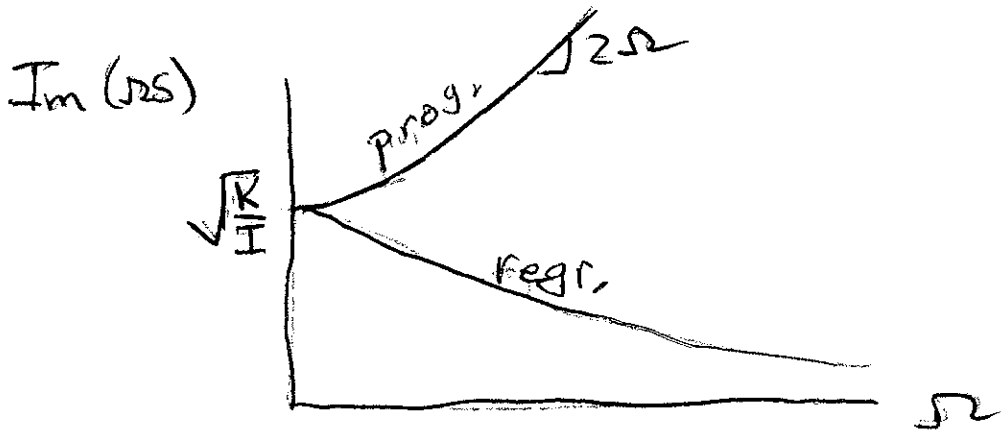

Ground Resonance

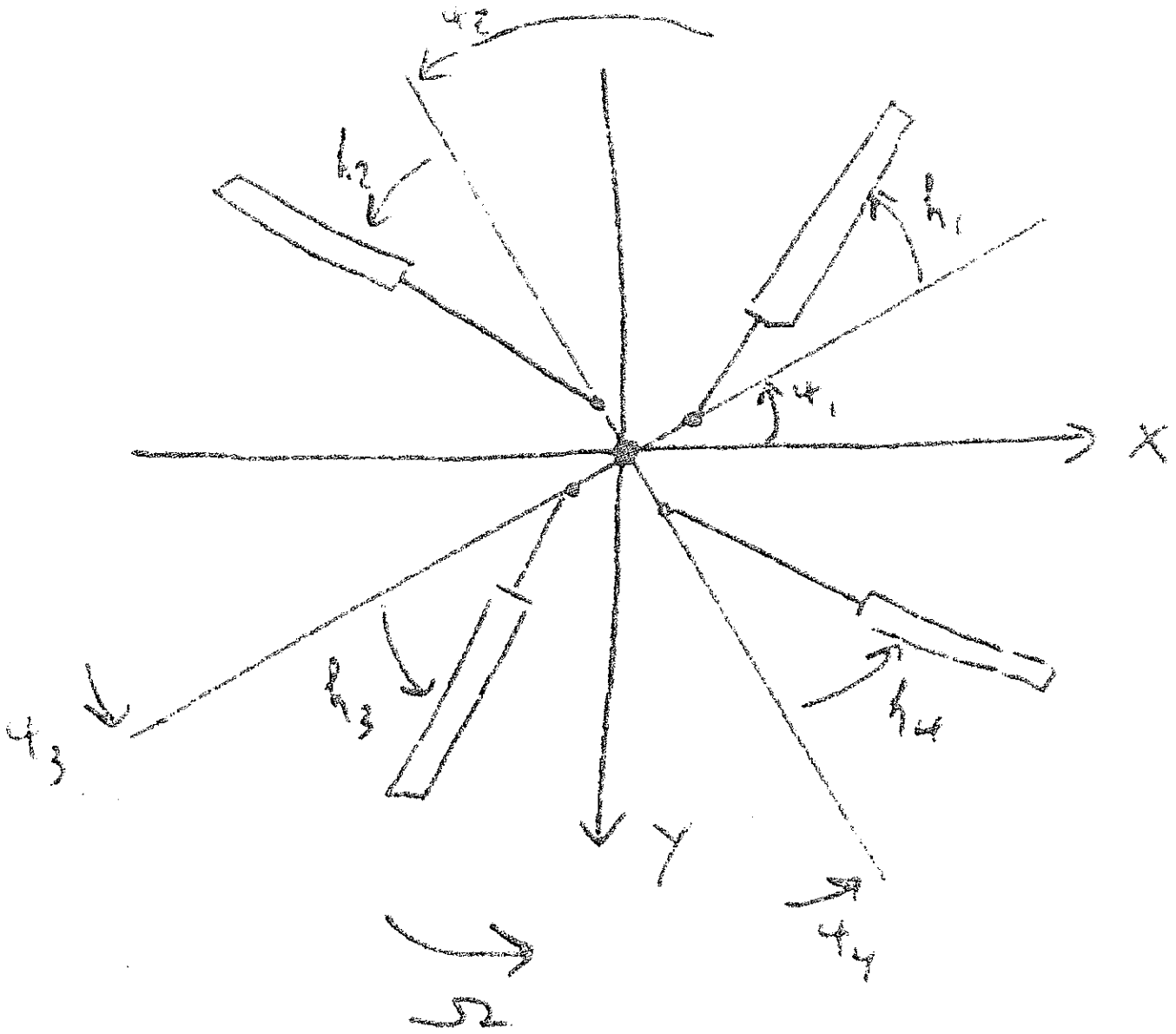

$$\psi_k = \Omega t + \left(\frac{k-1}{b}\right) 2\pi$$

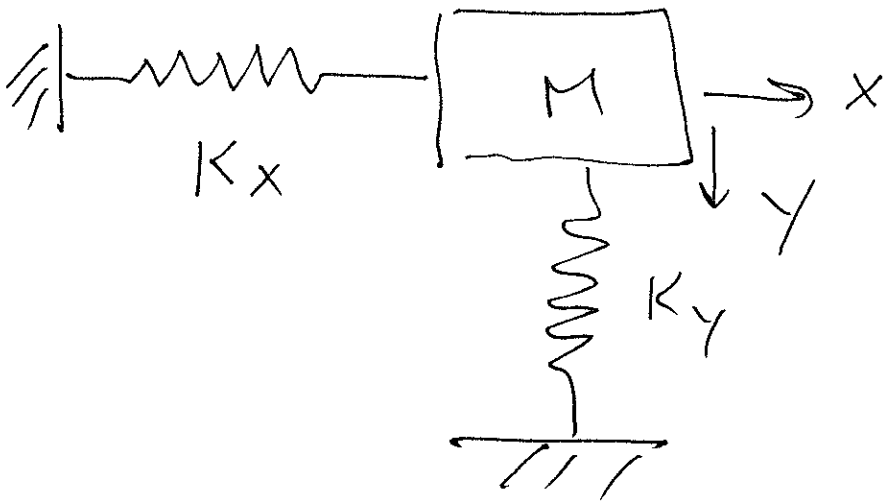

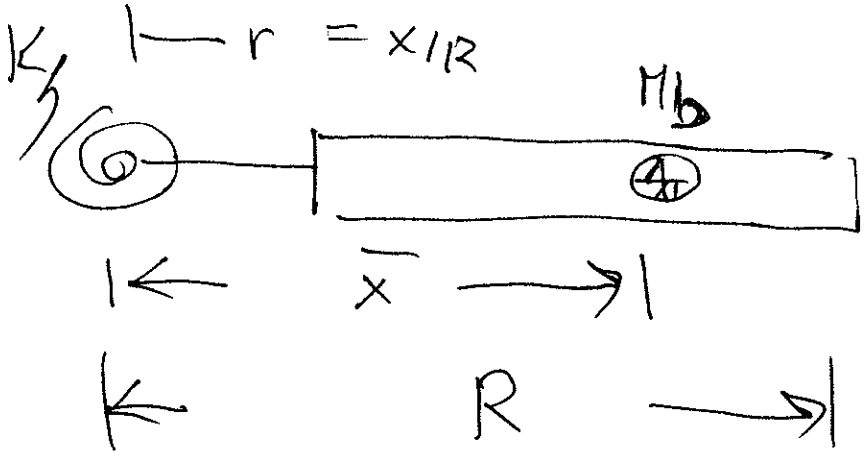

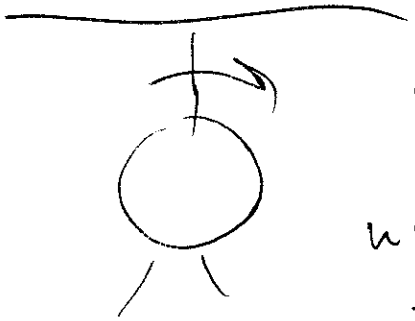

roll + pitch replaced with equivalent lateral vibrations in x + y

$$T = \tfrac{1}{2}M\dot{x}^2 + \tfrac{1}{2}M\dot{y}^2$$

$$+ \sum_{i=1}^{Q} \tfrac{1}{2} \int_0^R m \left\{ \left[r\left(\Omega + \dot{\zeta}_i\right) + \dot{x}\cos\left(\psi_i + \zeta_i\right) \ldots \dot{y}\sin\left(\psi_i + \zeta_i\right) \right]^2 \right.$$

$$\left. + \left[\dot{y}\cos\left(\psi_i + \zeta_i\right) + \dot{x}\sin\left(\psi_i + \zeta_i\right)\right]^2 \right\} \mathrm{d}r$$

$$\int_0^R mr^2 \mathrm{d}r = I_\zeta, \qquad \int_0^R m\mathrm{d}r = M_b, \qquad \overline{x} = \int_0^R mr\mathrm{d}r/M_b$$

$$T = \tfrac{1}{2}M\left(\dot{x}^2 + \dot{y}^2\right) + \sum_{i=1}^{b} \left[\tfrac{1}{2} I_\zeta \left(\Omega + \dot{\zeta}_i\right)^2 \right.$$

$$+ M_b\overline{x}\left(\Omega + \dot{\zeta}_i\right)\left[\dot{x}\cos\psi_i\cos\zeta_i - \dot{x}\sin\psi_i\sin\zeta_i \right.$$

$$\left. -\dot{y}\sin\psi_i\cos\zeta_i - \dot{y}\cos\psi_i\sin\zeta_i\right]$$

$$+ \tfrac{1}{2}M_b\left(\dot{x}\cos\psi_i\cos\zeta_i - \dot{y}\sin\psi_i\cos\zeta_i - \dot{x}\sin\psi_i\sin\zeta_i - \dot{y}\cos\psi_i\sin\zeta_i\right)^2$$

$$\left. + \tfrac{1}{2}M_b\left(\dot{y}\cos\psi_i\cos\zeta_i + \dot{x}\sin\psi_i\cos\zeta_i - \dot{y}\sin\psi_i\sin\zeta_i + \dot{x}\cos\psi_i\sin\zeta_i\right)^2 \right]$$

$b \equiv N\#$ of blades

Assume $\zeta_i \ll 1$ $\cos\zeta_i = 1$ $\sin\zeta_i = \zeta_i$

Assume x and y small compared to R.

Keep only quadratic terms in energy.

$$T = \tfrac{1}{2}M\left(\dot{x}^2 + \dot{y}^2\right) + \sum_{i=1}^{b}\Big[\tfrac{1}{2}T_\zeta\Omega^2 + I_\zeta\Omega\dot{\zeta}_i + \tfrac{1}{2}I_\zeta\dot{\zeta}_i^2$$

$$+ M_b\overline{x}\Omega\left(\dot{x}\cos\psi_i - \dot{y}\sin\psi_i\right)$$

$$- M_b\overline{x}\Omega\left(\dot{x}\sin\psi_i - \dot{y}\cos\psi_i\right)\zeta_i$$

$$+ M_b\overline{x}\dot{\zeta}_i\left(\dot{x}\cos\psi_i - \dot{y}\sin\psi_i\right)$$

$$+ \tfrac{1}{2}M_b\left(\dot{x}\cos\psi_i - \dot{y}\sin\psi_i\right)^2$$

$$+ \tfrac{1}{2}M_b\left(\dot{y}\cos\psi_i + \dot{x}\sin\psi_i\right)^2\Big]$$

$$\frac{\partial T}{\partial \dot{\zeta}_i} = I_\zeta \Omega + I_\zeta \dot{\zeta} + M_b \overline{x} \left(\dot{x} \cos \psi_i - \dot{y} \sin \psi_i \right)$$

$$\frac{\partial T}{\partial \zeta_i} = -M_b \overline{x} \Omega \left(\dot{x} \sin \psi_i + \dot{y} \cos \psi_i \right) \qquad \frac{\partial V}{\partial \zeta_i} = K_\zeta \zeta_i$$

$$\boxed{I_\zeta \ddot{\zeta}_i + M_b \overline{x} \left(\ddot{x} \cos \psi_i - \ddot{y} \sin \psi_i \right) + K_\zeta \zeta_i = 0}$$

$$\frac{\partial T}{\partial \dot{x}} = \left(M_b b + M \right) \dot{x} + \sum_{i=1}^{b} \left[M_b \overline{x} \Omega \cos \psi_i - M_b \overline{x} \Omega \sin \psi_i \zeta_i + M_b \overline{x} \dot{\zeta}_i \cos \psi_i \right]$$

$$\frac{\partial T}{\partial x} = 0 \qquad \frac{\partial V}{\partial x} = K_x x \qquad \frac{\partial T}{\partial y} = 0 \qquad \frac{\partial V}{\partial y} = K_y y$$

$$\frac{\partial T}{\partial \dot{y}} = M \dot{y} + \sum_{i=1}^{b} \left[M_b \right] \left[\left(-\Omega \sin \psi_i - \Omega \cos \psi_i \zeta_i - \dot{\zeta} \sin \psi_i \right) \overline{x} \right] + b M_b \dot{y}$$

Nondimesional version

$$\frac{K_\zeta}{\Omega^2 I_\zeta} = w_\zeta^2 \qquad \frac{K_x}{\Omega^2 M} = w_x^2 \qquad \frac{K_y}{\Omega^2 M} = w_y^2$$

$$\frac{M_b \bar{x} R}{I_\zeta} = \bar{\sigma} = \left(\tfrac{3}{2} \text{ for uniform blade}\right) \qquad \frac{b M_b R^2}{I_\zeta} = r_g^2 = 3\text{b} \text{ if uniform}$$

$$u \equiv x/R, \qquad \upsilon \equiv y/R, \qquad \frac{MR^2}{I_\zeta} \equiv \rho^2, \qquad \psi = \Omega t$$

$$\overset{**}{\zeta}_i + \sigma\left(\overset{**}{u}\cos\psi_i - \overset{**}{\upsilon}\sin\psi_i\right) + w_\zeta^2 \zeta_i = 0$$

$$\frac{R}{I_\zeta \Omega}\frac{\partial T}{\partial \dot{x}} = \left(\rho^2 + r_g^2\right)\overset{*}{u} + \sum_{i=1}^{b}\left[\sigma\cos\psi_i - \bar{\sigma}\zeta_i \sin\psi_i + \sigma\overset{*}{\zeta}_i\cos\psi_i\right]$$

$$\frac{R}{I_\zeta \Omega}\frac{\partial T}{\partial \dot{y}} = \left(\rho^2 + r_g^2\right)\overset{*}{\upsilon} + \sum_{i=1}^{b}\left[\bar{\sigma}\left(-\sin\psi_i - \zeta_i\cos\psi_i + \overset{*}{\zeta}_i\sin\psi_i\right)\right]$$

$$\frac{R}{I_\zeta \Omega^2}\frac{\partial V}{\partial x} = \rho^2 w_x^2 \qquad \frac{R}{I_\zeta \Omega^2}\frac{\partial V}{\partial y} = \rho^2 w_y^2$$

Multiblade Transform

$$\zeta_s = \frac{2}{b}\sum_{i=1}^{b} \zeta_i \sin\psi_i$$

$$\zeta_i = \zeta_{1s}\sin\psi_i + \zeta_{1c}\cos\psi_i + \underbrace{\zeta_{2s}\sin 2\psi_i + \zeta_{2c}\cos 2\psi_i}_{= (-1)^i \zeta_o \text{ for } b=4}$$

$$\zeta_o = \frac{1}{b}\sum_{i=1}^{b} \zeta_i \qquad \zeta_o = \frac{1}{b}\sum_{i=1}^{b} (-1)^i \zeta_i \qquad \zeta_c = \frac{2}{b}\sum_{i=1}^{b} \zeta_i \cos\psi_i$$

$$\overset{*}{\zeta}_i = \overset{*}{\zeta}_o + (-1)^i \overset{*}{\zeta}_o + \left(\overset{*}{\zeta}_{1s} - \zeta_{1c}\right)\sin\psi_i + \left(\overset{*}{\zeta}_{1c} + \zeta_{1s}\right)\cos\psi_i$$

$$\overset{**}{\zeta}_i = \overset{**}{\zeta}_o + (-1)^i \overset{**}{\zeta}_o + \left(\overset{**}{\zeta}_{1s} - 2\overset{*}{\zeta}_{1c} - \zeta_{1s}\right)\sin\psi_i + \left(\overset{**}{\zeta}_{1c} + 2\overset{*}{\zeta}_{1s} - \zeta_{1c}\right)\cos\psi_i$$

$\frac{1}{b}\sum_{i=1}^{b} \zeta_i$ equations $\Rightarrow$ $\overset{**}{\zeta}_o + w_\zeta^2 \zeta_o = 0$ wind-up (collective)

$\frac{1}{b}\sum_{i=1}^{b} (-1)^i \zeta_i$ equations $\Rightarrow$ $\overset{**}{\zeta}_o + w_\zeta^2 \zeta_o = 0$ (differential) scissors

$\frac{2}{b}\sum_{i=1}^{b} (\sin\psi_i)\,\zeta_i$ equations & $\frac{2}{b}\sum_{i=1}^{b} (\cos\psi_i)\,\zeta_i$ equations $\Rightarrow$

$$\boxed{\begin{aligned} \overset{**}{\zeta}_{1s} - 2\overset{*}{\zeta}_{1c} + \left(w_\zeta^2 - 1\right)\zeta_{1s} - \bar{\sigma}\left(\overset{**}{v}\right) &= 0 \\ \overset{**}{\zeta}_{1c} + 2\overset{*}{\zeta}_{1s} + \left(w_\zeta^2 - 1\right)\zeta_{1c} + \bar{\sigma}\left(\overset{**}{u}\right) &= 0 \end{aligned}}$$

D'Alembert Forces

Body Equations with Multi-blade Coordinates

$$\frac{\mathrm{d}}{\mathrm{d}\psi}\left[\rho^2 \overset{*}{u} + \bar{\sigma} b \left(-\frac{\zeta_{1s}}{2} + \frac{\overset{*}{\zeta}_{1c}}{2} + \frac{\zeta_{1s}}{2} \right) + r_g^2 \overset{*}{u} \right] + \rho^2 w_x^2 u = 0$$

$$\frac{\mathrm{d}}{\mathrm{d}\psi}\left[\rho^2 \overset{*}{v} + \bar{\sigma} b \left(-\frac{\zeta_{1c}}{2} - \frac{\overset{*}{\zeta}_{1s}}{2} + \frac{\zeta_{1c}}{2} \right) + r_g^2 \overset{*}{v} \right] + \rho^2 w_y^2 v = 0$$

$$\boxed{\begin{aligned} \frac{2\left(\rho^2 + r_g^2\right)}{b} \overset{**}{u} + \bar{\sigma} \overset{**}{\zeta}_{1c} + \frac{2\rho^2 w_x^2}{b} u = 0 \\ \frac{2\left(\rho^2 + r_g^2\right)}{b} \overset{**}{v} - \bar{\sigma} \overset{**}{\zeta}_{1s} + \frac{2\rho^2 w_y^2}{b} v = 0 \end{aligned}}$$

$$\begin{bmatrix} 1 & 0 & 0 & -\bar{\sigma} \\ 0 & 1 & \bar{\sigma} & 0 \\ 0 & \bar{\sigma} & \frac{2\left(\rho^2+r_g^2\right)}{b} & 0 \\ -\bar{\sigma} & 0 & 0 & \frac{2\left(\rho^2+r_g^2\right)}{b} \end{bmatrix} \begin{Bmatrix} \overset{**}{\zeta}_{1s} \\ \zeta_{1c} \\ u \\ v \end{Bmatrix} + \begin{bmatrix} 0 & -2 & 0 & 0 \\ 2 & 0 & 0 & 0 \\ 0 & 0 & 0 & 0 \\ 0 & 0 & 0 & 0 \end{bmatrix} \begin{Bmatrix} \overset{*}{\zeta}_{1s} \\ \zeta_{1c} \\ u \\ v \end{Bmatrix}$$

$$+ \begin{bmatrix} w_\zeta^2 - 1 & 0 & 0 & 0 \\ 0 & w_\zeta^2 - 1 & 0 & 0 \\ 0 & 0 & \frac{2\rho^2 w_x^2}{b} & 0 \\ 0 & 0 & 0 & \frac{2\rho^2 w_y^2}{b} \end{bmatrix} \begin{Bmatrix} \zeta_{1s} \\ \zeta_{1c} \\ u \\ v \end{Bmatrix} = \begin{Bmatrix} 0 \\ 0 \\ 0 \\ 0 \end{Bmatrix}$$

$$\frac{2\left(\rho^2 + r_g^2\right)}{b} = \frac{MR^2}{bI_\zeta/2} + \frac{M_b R^2}{I_\zeta/2} \qquad \rho^2 = MR^2/I_\zeta$$

$$\frac{2\rho^2 w_x^2}{b} = \frac{K_x}{b(I_\zeta/2)} \frac{1}{\Omega^2}$$

Another normalization (with damping)

$$\frac{w_x^2}{1+r_g^2/\rho^2} = w_u^2 \qquad \frac{w_y^2}{1+r_g^2/\rho^2} = w_v^2$$

$$\frac{b\bar{\sigma}}{2\left(\rho^2+r_g^2\right)} = \overline{Q} = \frac{\frac{b}{2}M_b\overline{x}/R}{M+bM_b}$$

$\delta =$ damping ratio

$$\begin{bmatrix} 1 & 0 & 0 & -\overline{\sigma} \\ 0 & 1 & \overline{\sigma} & 1 \\ 0 & \overline{Q} & 1 & 0 \\ -\overline{Q} & 0 & 0 & 1 \end{bmatrix} \overset{**}{\begin{Bmatrix} \zeta_{1s} \\ \zeta_{1c} \\ u \\ v \end{Bmatrix}} + \begin{bmatrix} 2\delta & -2 & 0 & 0 \\ 2 & 2\delta & 0 & 0 \\ 0 & 0 & \delta_u & 0 \\ 0 & 0 & 0 & \delta_v \end{bmatrix} \overset{*}{\begin{Bmatrix} \zeta_{1s} \\ \zeta_{1c} \\ u \\ v \end{Bmatrix}}$$

$$+ \begin{bmatrix} w_\zeta^2 - 1 & -2\delta & 0 & 0 \\ 2\delta & w_\zeta^2 - 1 & 0 & 0 \\ 0 & 0 & w_u^2 & 0 \\ 0 & 0 & 0 & w_v^2 \end{bmatrix} \begin{Bmatrix} \zeta_{1s} \\ \zeta_{1c} \\ u \\ v \end{Bmatrix} = \begin{Bmatrix} 0 \\ 0 \\ 0 \\ 0 \end{Bmatrix}$$

$\delta =$ f damping ratio $* \omega_f$

$\delta_v =$ 2 * v-damping ratio $* \omega_v$

$\delta_u =$ 2 * u-damping ratio $* \omega_u$

Special Cases

$$K_x = \infty, x = 0, u = 0, w_u^2 = \infty$$

$$\begin{bmatrix} 1 & 0 & -\bar{\sigma} \\ 0 & 1 & 0 \\ -\bar{Q} & 0 & 1 \end{bmatrix} \overset{**}{\begin{Bmatrix} \zeta_{1s} \\ \zeta_{1c} \\ v \end{Bmatrix}} + \begin{bmatrix} 2\delta & -2 & 0 \\ 2 & 2\delta & 0 \\ 0 & 0 & \delta_v \end{bmatrix} \overset{*}{\begin{Bmatrix} \zeta_{1s} \\ \zeta_{1c} \\ v \end{Bmatrix}}$$

$$+ \begin{bmatrix} w_\zeta^2 - 1 & -2\delta & 0 \\ 2\delta & w_\zeta^2 - 1 & 0 \\ 0 & 0 & w_v^2 \end{bmatrix} \begin{Bmatrix} \zeta_{1s} \\ \zeta_{1c} \\ v \end{Bmatrix} = \begin{Bmatrix} 0 \\ 0 \\ 0 \end{Bmatrix}$$

$$(\delta\delta_v) > \frac{\bar{Q}\bar{\sigma}w_v^2}{8w_\zeta(1 - w_v)} \text{ for stability}$$

special case

$$w_\zeta = 1 - w_v$$

$$\Rightarrow (\delta\delta_v) > \bar{Q}\bar{\sigma}\left(\frac{w_v^2}{w_\zeta^2}\right)/8$$

$\bar{Q}$ not blade number

Note $w_v > 1$ stable

$w_\zeta < 1$ for unstable

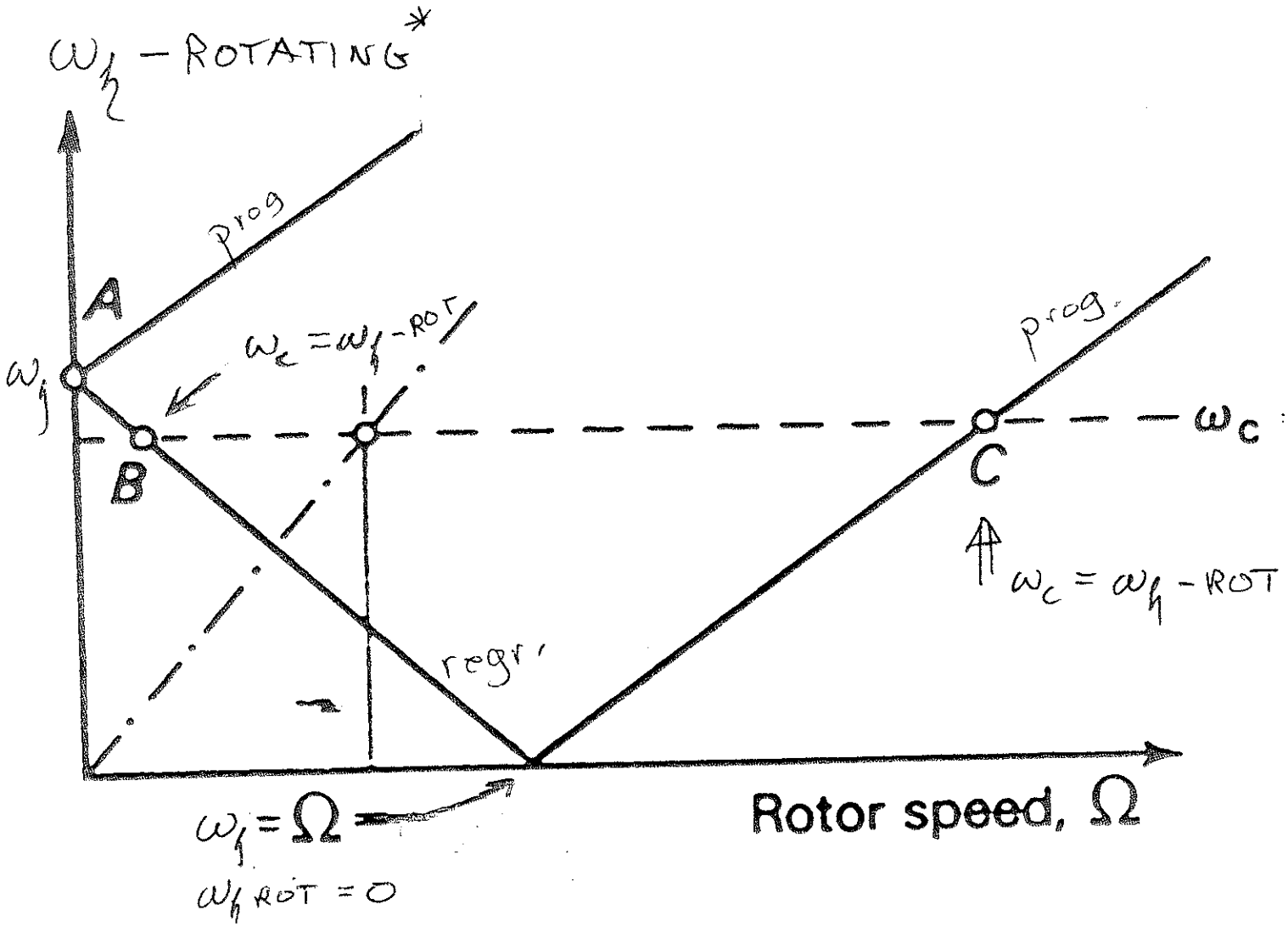

Uncoupled fuselage and whirling frequencies

* Frequency of rotating blades as seen in non-rotating system

Comparison of Methods

I. Fourier Series / Harmonic Balance

A. Expand x in Fourier Series, truncate

B. a_n and b_n are constants

C. Collect like harmonics up to truncation number

D. Algebraic Equations in $a_n b_n$

II. Hill's Determinant Method

A. Expand x in Fourier Series, truncate

B. a_n and b_n are functions of time
there will be $\dot{a}_n$ $\dot{b}_n$ $\ddot{a}_n$ $\ddot{b}_n$

C. Collect like harmonics up to truncation number

D. ordinary, constant-coefficient differential
equations in a_n and b_n

III. Multi-Blade Coordinates (Exact)

A. Expand in multi-blade equal to balde number.

B. a_n b_n a_d functions of time

$$\frac{1}{N}\sum_{k=1}^{N}(Eq)_k \qquad \frac{2}{N}\sum_{k=1}^{N}(Eq)_k \begin{matrix}\cos(m\psi_k)\\ \sin(m\psi_k)\end{matrix} \qquad \frac{1}{N}\sum_{k=1}^{N}(Eq)_k(-1)^{k+1}$$

C. Periodic-Coefficient Equations

Elastic Blade Equations

Flapping

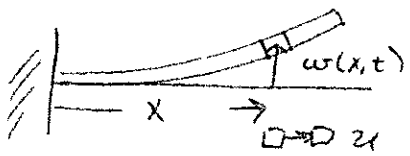

Inextensibility $\Rightarrow x+u=\int_0^x \sqrt{\mathrm{d}x^2-\mathrm{d}w^2}=\int_0^x \sqrt{1-w'^2}\mathrm{d}\xi$

$$x+u\approx\int_0^x \mathrm{d}\xi-\int_0^x \tfrac{1}{2}w'^2\mathrm{d}\xi=x-\int_0^x \tfrac{1}{2}\left(\tfrac{\mathrm{d}w}{\mathrm{d}\xi}^2\right)\mathrm{d}\xi$$

$$u=-\tfrac{1}{2}\int_0^x \left(\tfrac{\mathrm{d}w}{\mathrm{d}\xi}\right)^2\mathrm{d}\xi$$

Kinetic Energy:

$$T=\tfrac{1}{2}\int_0^R m\left(\tfrac{\partial w}{\partial t}\right)^2\mathrm{d}x+\int_0^R \tfrac{1}{2}m\Omega^2\left(x+u\right)^2\mathrm{d}x$$

$$T=\tfrac{1}{2}\int_0^R m\left(\tfrac{\partial w}{\partial t}\right)^2\mathrm{d}x+\tfrac{1}{2}\Omega^2\int_0^R mx^2\mathrm{d}x-\Omega^2\int_0^R mx\int_0^x \tfrac{1}{2}\left(\tfrac{\mathrm{d}w}{\mathrm{d}\xi}\right)^2\mathrm{d}\xi$$

Integrate last term by parts $\left(\frac{1}{2}\Omega^2\right)$

$$u=\int_0^x \left(\tfrac{\partial w}{\partial \xi}\right)^2\mathrm{d}\xi \qquad \mathrm{d}v=-\int_0^R mx\mathrm{d}x$$

$$\mathrm{d}u=\left(\tfrac{\partial w}{\partial x}\right)^2\mathrm{d}x \qquad v=-\int_0^R m\xi\mathrm{d}\xi+C=0$$

note (Integration constant is C = 0 to make $v(R)=0$)

$$T=\tfrac{1}{2}\int_0^R m\left(\tfrac{\partial w}{\partial t}\right)^2\mathrm{d}x+\tfrac{\Omega^2}{2}\int_0^R mx^2\mathrm{d}x+\tfrac{1}{2}\left[\int_0^x \left(\tfrac{\partial w}{\partial \xi}\right)^2\mathrm{d}\xi\int_x^R m\xi\mathrm{d}\xi\right]_0^R\Omega^2$$

(= 0 at x = 0 and x = R)

$$-\tfrac{1}{2}\int_0^R \left(\tfrac{\partial w}{\partial x}\right)^2\int_x^R \Omega^2 m\xi\mathrm{d}\xi\mathrm{d}x$$

$$T = \tfrac{1}{2}\int_0^R m\left(\tfrac{\partial w}{\partial t}\right)^2 \mathrm{d}x - \tfrac{1}{2}\int_0^R B\left(\tfrac{\partial w}{\partial x}\right)^2 \mathrm{d}x$$

where $B = \int_x^R m\Omega^2 \xi \mathrm{d}\xi = \text{tension}$

$$\text{Potential Energy} = V = \int_0^R \tfrac{1}{2} EI\left(\tfrac{\partial^2 w}{\partial x^2}\right)^2 \mathrm{d}x$$

$$\text{Action} = \int_{t_1}^{t_2} (\text{Lagrange})\,\mathrm{d}t = \int_{t_1}^{t_2} (T - V)\,\mathrm{d}t$$

$$A = \int_{t_1}^{t_2}\int_0^R \tfrac{1}{2}\left[m\left(\tfrac{\partial w}{\partial t}\right)^2 - B\left(\tfrac{\partial w}{\partial x}\right)^2 - EI\left(\tfrac{\partial^2 w}{\partial x^2}\right)^2\right]\mathrm{d}x\mathrm{d}t$$

$$A = \int_{t_1}^{t_2}\int_0^R \pounds\,\mathrm{d}x\mathrm{d}t, \quad \pounds = \text{Lagrange density}$$

$$\text{Virtual Work} = \int_0^R f\left(x, t, w, \dot{w}, w', \dot{w}'\right)\delta w \mathrm{d}x$$
$$+ M_L \delta w'(L) - M_o \delta w'(0) - V_L \delta w(L) + V_o \delta w(0) = \delta W$$

$$\delta a = \text{Virtual Action} = \int_{t_1}^{t_2} \delta W \mathrm{d}t + \overline{p}_1 \delta w\left(t_1\right) - \overline{p}_2 \delta w\left(t_2\right)$$

$\overline{p}_i$ are momenta at $t = t_i$, $\frac{\partial}{\partial x}() = ()'$, $\frac{\partial}{\partial t}() = \dot{()}$

p_i are momenta densities $\overline{p}_i = \int_0^R m\dot{w}(x, t_i)\mathrm{d}x \equiv \int_0^R p_i(x, t_i)\mathrm{d}x$

$$\delta a = \int_{t_1}^{t_2}\int_0^R f(x, t, etc.)\delta w(x, t)\mathrm{d}x\mathrm{d}t + \int_{t_1}^{t_2} M_x \delta w'(x, t)\mathrm{d}t\Big|_{x=0}^{x=L}$$
$$- \int_{t_1}^{t_2} V_x \delta w(x, t)\mathrm{d}t\Big|_{x=0}^{x=L} - \int_0^L P_t \delta w(x, t)\mathrm{d}x\Big|_{t=t_1}^{t=t_2}$$

Modified Hamilton's Law

$$\boxed{\delta A + \delta a = 0}$$

Variation (Action) + Virtual Action = 0

Integration by Parts Gives:

$$\int_{t_1}^{t_2}\int_0^R \left[\frac{\partial \pounds}{\partial w} - \frac{\partial}{\partial t}\frac{\partial \pounds}{\partial \dot{w}} - \frac{\partial}{\partial x}\frac{\partial \pounds}{\partial w'} + f + \frac{\partial^2}{\partial x^2}\frac{\partial \pounds}{\partial w''}\right]\delta w \mathrm{d}x\mathrm{d}t$$
$$+ \int_{t_1}^{t_2}\left[M_x + \frac{\partial \pounds}{\partial w''}\right]\delta w' \mathrm{d}t\Bigg|_{x=0}^{x=L} - \int_{t_1}^{t_2}\left[V_x + \frac{\mathrm{d}}{\mathrm{d}x}\left(\frac{\partial \pounds}{\partial w''}\right) - \frac{\partial \pounds}{\partial w'} -\right]\delta w \mathrm{d}t\Bigg|_{x=0}^{L=0}$$
$$+ \int_0^L \left[\frac{\partial \pounds}{\partial \dot{w}} - P_t\right]\delta w \mathrm{d}x\Bigg|_{t=t_1}^{t=t_2} = 0$$

Double Integral $\Rightarrow$ differential equation
time integrals $\Rightarrow$ boundary conditions
spacial integral $\Rightarrow$ momentum conditions

$$m\ddot{w} - (Bw')' + (EIw'')'' = f \qquad \text{d.e.}$$
$$M_x = EIw''(x,t) \qquad (x = 0, x = L)$$
$$V_x = (EIw'')' - Bw' \qquad (x = 0, L)$$
$$P_t = m\dot{w}(x,t) \qquad t = t_1,\ t = t_2$$

Uniform Beam

$$B = \int_x^R m\Omega^2 \rho \mathrm{d}\rho = \tfrac{1}{2} m\Omega^2 \left(R^2 - x^2\right)$$

$$B' = -m\Omega^2 x$$

$$m\ddot{w} + \left(m\Omega^2 x\right) w' - \tfrac{1}{2} m\Omega^2 \left(R^2 - x^2\right) w'' + EIw'''' = f_w$$

$$\overline{w} = w/R, \quad r = x/R, \quad \overset{*}{()} = \frac{\mathrm{d}}{\mathrm{d}\psi}, \quad ()^+ = \frac{\mathrm{d}}{\mathrm{d}r}$$

$$\boxed{\overset{**}{\overline{w}} + r\overline{w}^{\dagger} - \tfrac{1}{2}\left(1 - r^2\right)\overline{w}^{\dagger\dagger} + \eta\overline{w}^{\dagger\dagger\dagger\dagger} = \overline{f}_w}$$

$$\eta = \frac{EI}{m\Omega^2 R^4}, \qquad \overline{f} = \frac{f}{m\Omega^2 R}$$

$$\text{or } \overset{**}{\overline{w}} - \left[\tfrac{1}{2}\left(1 - r^2\right)\overline{w}^{\dagger}\right]^{\dagger} + \eta\overline{w}^{\dagger\dagger\dagger\dagger} = \overline{f}$$

Inplane Equation, v

$$m\ddot{v} + \left(m\Omega^2 x\right) v' - \tfrac{1}{2} m\Omega^2 \left(\Omega^2 - x^2\right) v'' + EIv'''' - m\Omega^2 v = f_v$$

$$\overset{**}{\overline{v}} - \left[\tfrac{1}{2}\left(1 - r^2\right)\overline{v}^{\dagger}\right]^{\dagger} + \eta\overline{v}^{\dagger\dagger\dagger\dagger} - \overline{v} = \overline{f}_v$$

Special Cases (Flap)

a) $\eta = 0$, Legendre's Eqs

$\omega^2 = \frac{n(1+n)}{2} \quad n = 1, 3, 5, 7$

$\overline{w}(r) = P_n \quad r, \frac{1}{2}\left(5r^3 - 3r\right), etc$

b) $\eta \to \infty$ cantilever $w^2 = \beta^4 \eta$

$\beta_1 = 1.875, \quad \beta^4 = 12.36$

c) Approximations:

$w^2 = 1.19 + 12.36\eta$

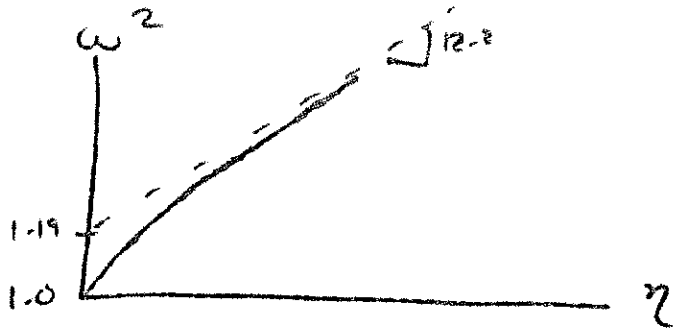

Inplane: $\omega_{\text{IP}}^2 = \omega_{\text{FLAP}}^2 - 1$

Torsion

$$mk_m^2\ddot{\phi} - (GJ\phi')' - k_A^2 (B\phi')' - D(B\theta')' + m\Omega^2 \left(k_{m_1}^2 - k_{m_2}^2\right)(\theta + \phi) = 0$$

θ = pretwist, ϕ = elastic twist

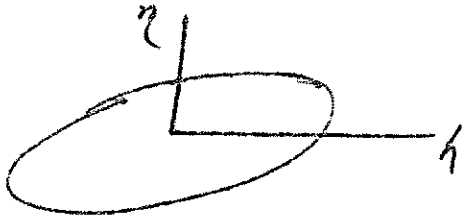

$$m = \int_A \int \rho \mathrm{d}\eta \mathrm{d}\zeta$$

$$k_{m_1}^2 = \frac{1}{m} \int_A \int \rho \zeta^2 \mathrm{d}\eta \mathrm{d}\zeta$$

$$k_{m_2}^2 = \frac{1}{m} \int_A \int \rho \eta^2 \mathrm{d}\eta \mathrm{d}\zeta$$

$$k_m^2 = k_{m_1}^2 + k_{m_2}^2 \qquad A = \int_A \int \mathrm{d}\eta \mathrm{d}\zeta, \qquad k_{A_1}^2 = \frac{1}{A} \int_A \int \zeta^2 \mathrm{d}\eta \mathrm{d}\zeta, \qquad k_{A_2}^2 = \frac{1}{A} \int_A \int \eta^2 \mathrm{d}\eta \mathrm{d}\zeta$$

$$k_A^2 = k_{A_1}^2 + k_{A_2}^2, \qquad I = \left(k_{A_1}^2 + k_{A_2}^2\right) A$$

J, D from warp function

Uniform beam, no pretwist, $\lambda = \eta\zeta$ (warp function)

$k_1^2 >> k_2^2$

$$\ddot{\phi} - \gamma\phi'' - \left[\tfrac{1}{2}\left(1 - r^2\right)\phi'\right]' + \phi = 0$$

$$\gamma = \frac{GJ}{m\Omega^2 R^2 k_M^2} \qquad \omega^2 = \frac{\pi^2}{12} + \frac{5}{4} + \frac{\pi^2}{9}\gamma \approx 2.07 + 2.47\gamma$$

Longitudinal Vibrations

$$\sigma_{xx} = E\epsilon, \quad \epsilon = u^{\dagger} + \alpha \left(u^{\dagger}\right)^2 /2$$

$$\overset{**}{u} - \alpha \left[\tfrac{1}{2}\left(1 - r^2\right) u'\right]^{\dagger} - \lambda u^{\dagger\dagger} - u = 0$$

$$-3 < \alpha < 1 \qquad \text{(typical values)}$$

Coupled Flap-Lag Equations

$$\overset{**}{w} - \left[\tfrac{1}{2}\left(1 - r^2\right) w^{\dagger}\right]^{\dagger} - 2\left[w^{\dagger} \int_r^1 \overset{*}{v} \mathrm{d}\xi\right]^{\dagger} + \eta w^{\dagger\dagger\dagger\dagger} = \overline{f}_w$$

$$\overset{**}{v} - \left[\tfrac{1}{2}\left(1 - r^2\right) v^{\dagger}\right]^{\dagger} - 2\int_0^r w^{\dagger} \overset{*}{w}^{\dagger} \mathrm{d}\xi + \eta v^{\dagger\dagger\dagger\dagger} - v = \overline{f}_v$$

$$\lambda = \frac{EA}{m\Omega^2 R^2}$$

u, w, v all normalized on R

Galerkin - Ritz

$\omega = \varphi(r)\beta \qquad v = \varphi(r)\eta$

multiply by $\varphi(r) \qquad \int_0^1 (\,)\,dr$

$$\int_0^1 \varphi^2 dr \overset{**}{\beta} - \int_0^1 \varphi\left[\tfrac{1}{2}(1-r^2)\varphi'\right]' dr\,\beta$$

$$-2\int_0^1 \varphi\left[\varphi^+\int_r^1 \varphi\,d\xi\right]^+ dr\,\beta\overset{*}{\eta}$$

$$+\ \eta\int_0^1 \varphi\varphi^{\text{IIII}}\,dr = \int_0^1 \varphi(r)\bar{f}_w\,dr$$

$$\int_0^1 \varphi^2 dr \overset{**}{\eta} - \int_0^1 \varphi\left[\tfrac{1}{2}(1-r^2)\varphi^+\right]^+ dr\,\eta$$

$$-2\int_0^1 \varphi\left[\int_0^r \varphi^+\varphi^+ d\xi\right] dr\,\beta\overset{*}{\beta} + \eta\int_0^1 \varphi\varphi^{\text{IIII}}\,dr\,\eta$$

$$-\int_0^1 \varphi^2 dr\,\eta = \int_0^1 \varphi(r)\bar{f}_v\,dr$$

Integrate by Parts

$$\int_0^1 \varphi^2 dr\, \ddot{\beta} + \int_0^1 \varphi^+ \varphi^+ \left[\tfrac{1}{2}(1-r^2)\right] dr\, \beta$$

$$+ 2\int_0^1 \varphi \int_0^r \varphi^+ \varphi^+ d\xi\, dr\, \beta \dot{\beta}$$

$$+ \eta \int_0^1 \varphi^{++} \varphi^{++} dr\, \beta = \int_0^1 \varphi(r)\, \bar{f}_\omega\, dr$$

$$\int_0^1 \varphi^2 dr\, \ddot{\eta} + \int_0^1 \varphi^+ \varphi^+ \left[\tfrac{1}{2}(1-r^2)\right] dr\, \eta$$

$$-2\int_0^1 \varphi \int_0^r \varphi^+ \varphi^+ d\xi\, dr\, \beta \dot{\beta}$$

$$+ \eta \int_0^1 \varphi^{++} \varphi^{++} dr\, \eta - \int_0^1 \varphi^2 dr\, \eta = \int_0^1 \varphi \bar{f}_\nu\, dr$$

Example = Rigid-Blade Flap-Lag

$F_a = F_y = 0$

$\phi = r \qquad \phi^+ = 1 \qquad \phi^{++} = 0$

$$\int_0^1 \phi^2 dr = \int_0^1 r^2 dr = \frac{1}{3}$$

$$\int_0^1 \frac{1}{2}\left[1 - r^2\right] dr = \frac{1}{2}\left(1 - \frac{1}{3}\right) = \frac{1}{3}$$

$$\int_0^1 r \int_0^r d\xi \, dr = \int_0^1 r^2 dr = \frac{1}{3}$$

$$\int_0^1 (\phi^{++})^2 dr = 0 \qquad \text{multiply} \times 3$$

$$\ddot{\beta}^* + \beta + 2\beta\dot{\zeta}^* = 0$$

$$\ddot{\zeta}^* + (1-1)\zeta - 2\beta\dot{\beta}^* = 0$$

Check

Matrix Form

$$\begin{bmatrix} 1 & 0 \\ 0 & 0 \end{bmatrix} \begin{Bmatrix} \ddot{\beta} \\ \ddot{\psi} \end{Bmatrix} + \begin{bmatrix} 0 & 2B \\ -2B & 0 \end{bmatrix} \begin{Bmatrix} \dot{\beta} \\ \dot{\psi} \end{Bmatrix}$$

$$+ \begin{bmatrix} 1 & 0 \\ 0 & 0 \end{bmatrix} \begin{Bmatrix} \beta \\ \psi \end{Bmatrix} = \begin{Bmatrix} 0 \\ 0 \end{Bmatrix}$$

Vertica, Vol. 5, pp. 21 to 34, 1981
Printed in Great Britain

0360-5450/81/030021-14$02.00/0
Pergamon Press Ltd

THEORETICAL PREDICTION OF DYNAMIC-INFLOW DERIVATIVES*

DALE M. PITT
U.S. Army Aviation Research and Development Command, St. Louis, MO 63166
and
DAVID A. PETERS
Washington University, Box 1185 St. Louis, MO 63130 U.S.A.

Abstract—A linear, unsteady theory is developed that relates transient rotor loads (thrust, roll moment, and pitch moment) to the overall transient response of the rotor induced-flow field. The relationships are derived from an unsteady, actuator-disc theory; and some are obtained in closed form. The results reveal both the strengths and weaknesses of previous formulations and the results also indicate areas in which further study is needed.

1. INTRODUCTION

It has been known for some thirty years that the induced-flow field associated with a lifting rotor responds in a dynamic fashion to changes in either blade pitch (i.e. pilot inputs) or rotor flapping angles (i.e. rotor or body dynamics) [1–3]. In recent years, it has been found that dynamic inflow for steady response in hover can be treated by an equivalent (i.e. reduced) Lock number [4]. For more general conditions, such as transient motions or a rotor in forward flight, it has been determined that the induced flow can be treated by additional "degrees of freedom" of the system. Each degree of freedom represents a particular inflow distribution, and each has its own particular gain and time constant [5–7].

Although the above results have provided some impressive correlation with experimental data, there is still no general theory to predict the gains and time-constants of dynamic inflow. Values from momentum theory give excellent results in hover, but are clearly inadequate in forward flight [5, 6]. A simple vortex model [5], gives some improvement in forward flight but is still not satisfactory. An empirical model based on the best fit of response data [5, 6], gives excellent results; but several peculiar singularities remain unexplained. Thus, there is a need to determine the dynamic-flow behavior from fundamental, aerodynamic considerations. One type of analysis that appears capable of producing such results is actuator-disc theory [8–10]. Although this type of analysis has been used extensively for induced-flow calculation, it has not been used to obtain the necessary gains and time constants required for dynamic inflow. There are primarily two reasons for this neglected application. First, most investigators have been interested in the details of the wake for a steady flight condition (rather than in the dynamic properties of the wake due to perturbations in flight condition). Second, investigators often include the coupled response of blade motions in their analysis. This hopelessly complicates the analysis and precludes the type of results desired here.

Figure 1 gives a schematic representation of the coupled inflow/rotor problem. The inflow dynamics and rotor dynamics of the closed-loop system are strongly coupled. It is the purpose of this paper, however, to investigate the behavior (i.e. the transfer function) of the open-loop induced flow model. The resultant theory may then be used with any model of the rotor dynamics. To do this, we extend the actuator-disc theory of [9] to the unsteady case and use it to find the dynamic relationships between the aerodynamic loading and the induced flow. Special emphasis is placed in developing these relationships in terms of a first-order dynamic model for each inflow distribution.

* Presented at the *Sixth European Rotorcraft and Powered Lift Aircraft Forum*, Bristol, England, 16–19 September 1980.

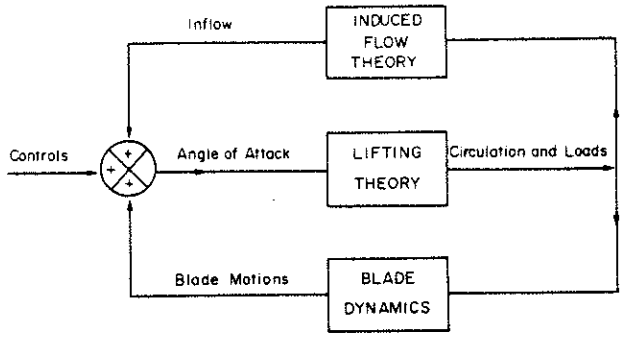

Fig. 1. Block diagram of coupled rotor and induced-flow dynamics.

2. BACKGROUND

The theory of dynamic inflow relates the airloads of a rotor (C_T, C_L, and C_M) to the induced-flow distributions (λ_0, λ_s, λ_c) where C_T, C_L and C_M are the aerodynamic perturbation in thrust, roll moment, and pitch moment; and λ_0, λ_s and λ_c are the magnitudes of uniform, side-to-side and fore-to-aft variations in induced flow.

$$\lambda = \lambda_0 + \lambda_s r \sin\psi + \lambda_c r \cos\psi \tag{1}$$

(Note that even rotors with no net hub moment can have considerable aerodynamic moments which, although balanced by inertial moments in the rotor system, can nevertheless influence the induced flow.) The dynamic inflow models of Refs [6, 7] assume that the inflow is related to the aerodynamic loads in a linear, first-order fashion.

$$[M]\begin{Bmatrix}\dot\lambda_0\\ \dot\lambda_s\\ \dot\lambda_c\end{Bmatrix} + [L]^{-1}\begin{Bmatrix}\lambda_0\\ \lambda_s\\ \lambda_c\end{Bmatrix} = \begin{Bmatrix}C_T\\ C_L\\ C_M\end{Bmatrix} \tag{2a}$$

or

$$[\tau]\begin{Bmatrix}\dot\lambda_0\\ \dot\lambda_s\\ \dot\lambda_c\end{Bmatrix} + \begin{Bmatrix}\lambda_0\\ \lambda_s\\ \lambda_c\end{Bmatrix} = [L]\begin{Bmatrix}C_T\\ C_L\\ C_M\end{Bmatrix} \tag{2b}$$

The purpose of this research is to find the elements of $[L]$ and $[M]$ from basic aerodynamic principles and to also investigate the validity of this linear, first-order form.

The actuator-disc theory that we use in this investigation is based on pressure distributions developed by Kinner (see Ref. [9]). Kinner discovered a family of pressure distributions that solve Laplace's equation, ϕ_{ii}, $e = 0$, and that also give a pressure discontinuity (i.e. lift) across a circular disc. These distributions can be combined in a general form to give the total, nondimensional pressure ϕ

$$\phi = -\sum_{\substack{m,n=0\\ m\le n}}^{\infty} P_n^m(v)Q_n^m(i\eta)[C_n^m \cos m\psi + D_n^m \sin m\psi] \tag{3}$$

where P_n^m and Q_n^m are, respectively, associated Legendre functions of the first and second kinds; C_n^m and D_n^m are arbitrary constants; and v, η, and ψ are ellipsoidal coordinates defined by the relationships

$$x = -\sqrt{1-v^2}\sqrt{1+\eta^2}\cos\psi \tag{4a}$$

$$y = \sqrt{1-v^2}\sqrt{1+\eta^2}\sin\psi \tag{4b}$$

$$z = -v\eta \tag{4c}$$

where z is normal to the rotor plane and positive down; x is in the rotor plane and positive in the forward direction, $\psi = 180°$; and Y is in the rotor plane and positive in the starboard direction, $\psi = 90°$. On the rotor disc, $\eta = 0$, $\nu = \sqrt{1 - r^2}$, and ψ is the conventional, counterclockwise azimuth angle. A schematic of the coordinate system is given in Fig. 2.

The nondimensional aerodynamic loading can be calculated from the nondimensional pressure, ϕ = pressure/$\rho\Omega^2 R^2$, by use of the following integrals, taken over the rotor disc.

$$C_T = \int\int \phi \, dA = \frac{4}{3} C_1^0 \tag{5a}$$

$$C_L = \int\int \phi(-r \sin\psi) \, dA = \frac{8}{5} i D_2^1 \tag{5b}$$

$$C_M = \int\int \phi(-r \cos\psi) \, dA = \frac{8}{5} i C_2^1 \tag{5c}$$

The variables r and dA are nondimensional ($0 \leqslant r \leqslant 1$, $\int\int dA = \pi$). For the sake of later comparisons, we also introduce two second-harmonic pressure integrals.

$$C_{L2} \equiv \int\int \phi(-r^2 \sin 2\psi) \, dA = \frac{128}{7} D_3^2 \tag{5d}$$

$$C_{M2} = \int\int \phi(-r^2 \cos 2\psi) \, dA = \frac{128}{7} C_3^2 \tag{5e}$$

It is interesting to note that each loading integral in equation (5) is uniquely determined by a single coefficient of the Kinner distribution and is independent of all others. Therefore, differing pressure distributions can result in identical average loadings. One of the purposes of this research is to find out if such pressure distributions will also result in identical averaged values of the induced flow. To do this, we will consider two types of pressure distribution. The first, called "uncorrected," will contain only the single coefficient of ϕ necessary to create the appropriate loading, as given in equation (5). The second distribution, called "corrected," will include just enough of the next-higher Kinner term to enforce the conditions $\phi = 0$, $d\phi/dr = 0$, at $r = 0$, which is a reasonable distribution for a rotor. The resulting additional terms are C_3^0, D_4^1 and C_4^1. A summary of the

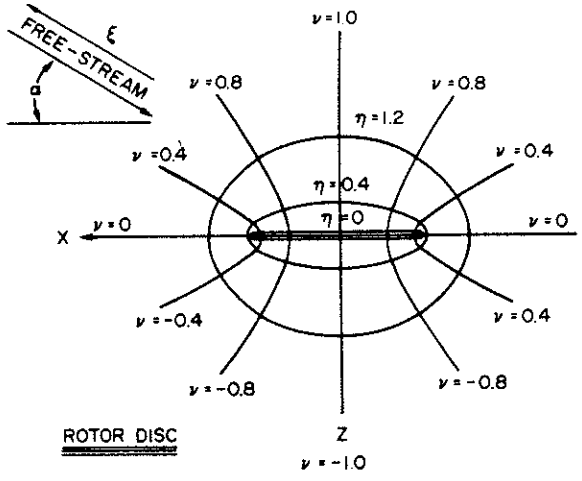

Fig. 2. Ellipsoidal coordinate system.

Table 1. Pressure terms

m, n	$P_n^m(v)$	$Q_n^m(i\eta)$	C_n^m	D_n^m	Purpose
0, 1	v	$\eta \tan^{-1}\frac{1}{\eta} - 1$	$\frac{3}{4}C_T$	—	Gives desired thrust
0, 3	$\frac{v}{2}(5v^2 - 3)$	$-\frac{\eta}{2}(5\eta^2 + 3)\tan^{-1}\frac{1}{\eta} + \frac{5}{2}\eta^2 + \frac{2}{3}$	$\frac{9}{8}C_T$	—	Hub correction for thrust
1, 2	$-3v\sqrt{1 - v^2}$	$3i\eta\sqrt{1 + \eta^2}\tan^{-1}\frac{1}{\eta} - 3i\sqrt{1 + \eta^2} + \frac{1}{\sqrt{1 + \eta^2}}$	$-\frac{5}{8}iC_M$	$-\frac{5}{8}iC_L$	Gives desired moments
1, 4	$-\frac{5}{2}v(7v^2 - 3)\sqrt{1 - v^2}$	$-\frac{5}{2}i\eta(7\eta^2 + 3)\sqrt{1 + \eta^2}\tan^{-1}\frac{1}{\eta} + \frac{5}{6}i(21\eta^2 + 2)\sqrt{1 + \eta^2} + \frac{i}{\sqrt{1 + \eta^2}}$	$-\frac{9}{64}iC_M$	$-\frac{9}{64}iC_L$	Hub correction moments
2, 3	$15v(1 - v^2)$	$-15\eta(1 + \eta^2)\tan^{-1}\frac{1}{\eta} + 15\eta^2 + 10 - \frac{2}{\sqrt{1 + \eta^2}}$	$\frac{7}{128}C_{M2}$	$\frac{7}{128}C_{L2}$	Gives higher-harmonic loading

pressure terms used in each distribution is given in Table 1 and the corrected and uncorrected distributions are plotted in Figs 3–5 as functions of radial station, r.

The pertinent integrals that define the magnitude of the basic induced-flow distributions at the disc are given by

$$\lambda_0 = \frac{1}{\pi}\int\int \lambda \, dA \tag{6a}$$

$$\lambda_s = \frac{4}{\pi}\int\int \lambda r \sin\psi \, dA \tag{6b}$$

$$\lambda_c = \frac{4}{\pi}\int\int \lambda r \cos\psi \, dA \tag{6c}$$

$$\lambda_{2s} = \frac{6}{\pi}\int\int \lambda r^2 \sin 2\psi \, dA \tag{6d}$$

$$\lambda_{2c} = \frac{6}{\pi}\int\int \lambda r^2 \cos 2\psi \, dA \tag{6e}$$

where λ is the nondimensional induced flow (velocity divided by ΩR).

3. MATHEMATICAL FORMULATION

For a free-stream velocity in the negative ξ direction (as shown in Fig. 2), the induced velocity components, q_i, must satisfy the continuity and momentum equations,

$$q_{i,i} = 0 \tag{7a}$$

$$q_{i,0} - vq_{i,\xi} = -\phi_{,i} \tag{7b}$$

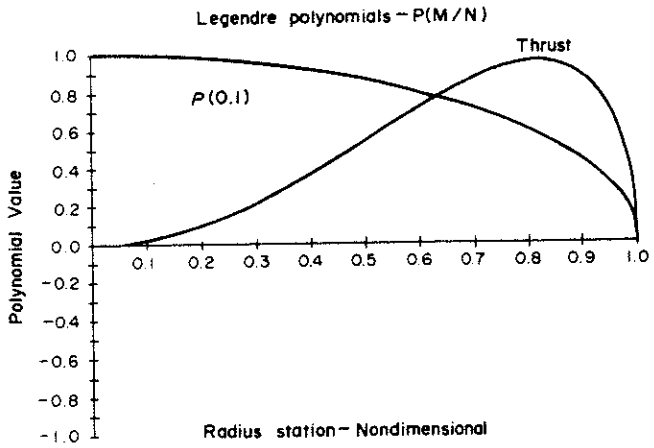

Fig. 3. Corrected (Thrust) and Uncorrected (P_1^0) Lift Distributions for C_T.

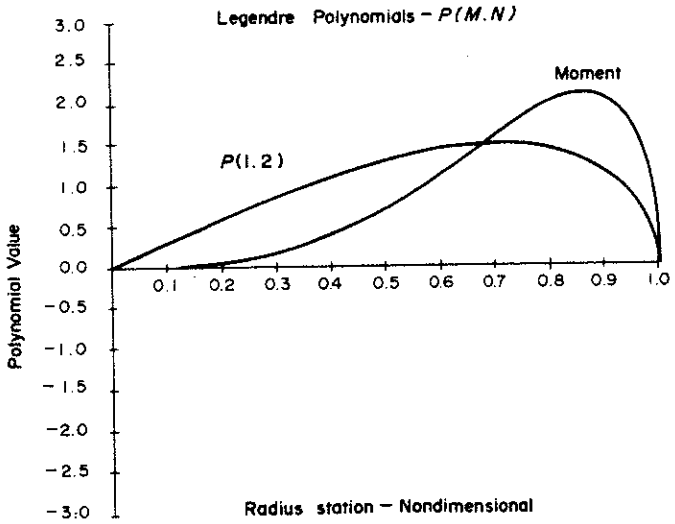

Fig. 4. Corrected (Moment) and Uncorrected (P_2^1) Lift Distributions for C_L or C_M.

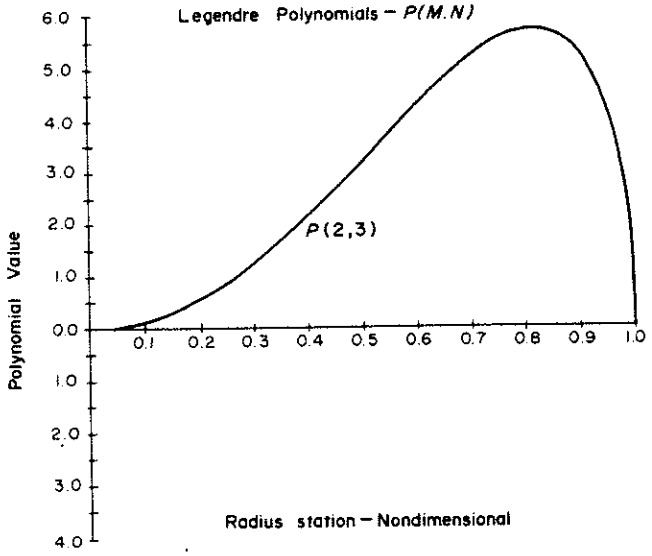

Fig. 5. Lift distribution (P_3^2) for C_{L2} or C_{M2}.

where, 0 implies $d/d\Omega t$), and v is the free-stream velocity divided by ΩR. We will now examine several special cases of equation (7) to determine relationships between loading, ϕ, and induced flow normal to the disc, q_z, at $\eta = 0$.

The first case we consider is the steady condition, $q_{i,0} = 0$. Equations (7) become

$$\phi_{,ii} = 0 \tag{8a}$$

$$q_{i,\xi} = \frac{1}{v}\phi_{,i} \tag{8b}$$

Equation (8a), the Laplace equation, implies that the Kinner distribution, equation (3), is an appropriate solution. The normal induced velocity at a point (x_0, y_0) on the rotor disc is found from equation (8b) with $i = z$

$$q_z = \lambda(x_0, y_0) = \frac{1}{v}\int_{\infty}^{0} \phi_{,z}\, d\xi \tag{9}$$

where ξ follows the streamline from (x_0, y_0) to infinity,

$$x = x_0 + \xi\cos\alpha \tag{10a}$$

$$y = y_0 \tag{10b}$$

$$z = -\xi\sin\alpha \tag{10c}$$

and α is the angle of incidence, Fig. 2. The z derivative in equation (9) may be expressed in ellipsoidal coordinates.

$$\phi_{,z} = \frac{-\eta(1 - \nu^2)}{\nu^2 + \eta^2}\frac{\partial\phi}{\partial\nu} - \frac{\nu(1 + \eta^2)}{\nu^2 + \eta^2}\frac{\partial\phi}{\partial\eta} \tag{11}$$

Thus, the induced flow for a given pressure distribution is found by intergration of the Kinner functions from the disc to the far field.

A specialization of equation (9) can be made for the condition $\alpha = 90°$ (axial flow). For such a condition z and ξ are parallel; and equation (9) reduces to

$$\lambda = -\frac{1}{v}\phi\Big|_{\eta=0}. \tag{12}$$

Thus, the induced flow may be found directly from ϕ with no integration. Another specialization of equation (9) can be made for $\alpha = 0°$ (edgewise flow). Here, ξ is parallel to x; and a portion of the integration is on the disc.

$$\lambda = -\frac{1}{v}\int_{\infty}^{\sqrt{1-y_0^2}} \frac{1}{\eta}\frac{\partial\phi}{\partial\nu}\Big|_{\nu=0} dx - \frac{1}{v}\int_{\sqrt{1-y_0^2}}^{x_0} \frac{1}{\nu}\frac{\partial\phi}{\partial\eta}\Big|_{\eta=0} dx \tag{13}$$

Thus, equation (9) and its two specializations, equations (12) and (13), summarize the steady case, $\omega = 0$.

The second general case we consider is the disc in still air, $v = 0$, with a simple-harmonic pressure distribution, $\phi = \bar{\phi}e^{i\omega\psi}$ where $\psi = \Omega t$ and ω is the oscillatory frequency, nondimensionalized on Ω (i.e. per rev). Equations (7) become, with $q = \bar{q}e^{i\omega\psi}$,

$$\bar{\phi}_{,ii} = 0 \tag{14a}$$

$$i\omega\bar{q}_i = -\bar{\phi}_{,i} \tag{14b}$$

Equation (14a) indicates that the Kinner distribution is applicable, and equation (14b)

gives the induced flow.

$$\bar{q}_z = \frac{i}{\omega}\bar{\phi}_{,z} \tag{15a}$$

$$\lambda = \frac{-i}{\omega}\frac{1}{v}\frac{\partial\bar{\phi}}{\partial\eta}\bigg|_{\eta=0} \tag{15b}$$

No integration is required.

The next case we consider is an oscillatory velocity field, $q = \bar{q}e^{i\omega\psi}$, where $\bar{q}$ is taken as real, which implies that all induced velocities are mutually in phase. If we express the pressure as $\phi = (A + Bi)e^{i\omega\psi}$, equation (7) yields

$$A_{,ii} = B_{,ii} = 0 \tag{16a}$$

$$v\bar{q}_{i,\xi} = A_{,i}\,(\text{real}) \tag{16b}$$

$$\omega\bar{q}_i = -B_{,i}\,(\text{imaginary}). \tag{16c}$$

Equation (16a) shows that both the real and imaginary portions of ϕ can be represented by Kinner solutions. Equation (16b) shows that real (i.e. inphase) portion of the pressure relates to induced velocity exactly as does the steady case, equation (8b). Equation (16c) shows that imaginary (i.e. out-of-phase) component of pressure relates to induced velocity exactly as does the case $v = 0$, equation (15a). Therefore, when all induced velocities are mutually in phase, the total pressure is simply a superposition of the steady pressure $\omega = 0$) and the apparent-mass pressure ($v = 0$). Thus, the basic assumption of the theory of dynamic inflow, equation (2a), is partially validated.

The final case we consider is an oscillatory pressure field, $\phi = \bar{\phi}e^{i\omega\psi}$, in which all pressures are mutually in phase ($\bar{\phi}$ real). If we express the resultant induced flow as $q = (u + iw)e^{i\omega\psi}$, equations (7) become

$$\bar{\phi}_{,ii} = 0 \tag{17a}$$

$$\omega w_i + v u_{i,\xi} = \bar{\phi}_{,i}\,(\text{real}) \tag{17b}$$

$$\omega u_i - v w_{i,\xi} = 0\,(\text{imaginary}). \tag{17c}$$

Equation (17a) indicates, again, that the Kinner distribution is appropriate. Equations (17b) and (17c) may be combined to give equations for the induced flow in terms of $\bar{\phi}$.

$$\omega^2 u_i + v^2 u_{i,\xi\xi} = v\bar{\phi}_{,i\xi} \tag{18a}$$

$$\omega^2 w_i + v^2 w_{i,\xi\xi} = \omega\bar{\phi}_{,i} \tag{18b}$$

Equations (18) are solved by a Laplace transform in ξ followed by application of the convolution theorem. The final solution for induced flow at the rotor disk is

$$u_z = \frac{1}{v}\int_{\infty}^{0}\bar{\phi}_{,z}\cos(k\xi)\,d\xi \tag{19a}$$

$$w_z = -\frac{1}{v}\int_{\infty}^{0}\bar{\phi}_{,z}\sin(k\xi)\,d\xi \tag{19b}$$

where k is a reduced frequency, ω/v, based on air speed (not tip speed).

Equations (19) are very interesting. They show that the in-phase and out-of-phase induced velocities may be calculated in the same manner as the steady case, equation (9), except that weighting functions ($\cos k\xi$ or $-\sin k\xi$) must be added. It should be noted that, since a true rotor should behave somewhere between "in-phase velocities," equations (16), and "in-phase pressures," equations (19), numerical comparisons of these two cases should prove very valuable for the validation of a first-order dynamic-inflow theory.

4. CLOSED-FORM RESULTS

Before proceeding to the numerical results it is good to consider some closed-form solutions. These provide added insights into the characteristics of dynamic inflow, and they also serve as checks on the accuracy of the numerical algorithms. Although we are primarily interested in the 3×3 L and M matrices of equations (2), we will also look at the elements of more general 5×5 matrices obtained by an extension of the induced-flow and loading vectors to include $\langle \lambda_0, \lambda_s, \lambda_c, \lambda_{2s}, \lambda_{2c} \rangle$ and $\langle C_T, C_L, C_M, C_{L2}, C_{M2} \rangle$, respectively. The λ's and C's are defined by equations (5) and (6). The 5×5 matrices include the effect of second-harmonic loads on the induced flow; they give the magnitude of the higher-harmaonics of induced flow; and they provide for a five-degree-of-freedom induced-flow model, should the three-degree-of-freedom model prove inadequate for a given system.

We now present closed-form results for several special cases. First, we consider $\omega = 0$, $\alpha = 90°$ (steady, axial flow). The pertinent theory is given by equation (12). Substitution of equations (3) and (12) into equation (6), with terms defined as in Table 1, yields

$$L_{11} = 1/2v,\ L_{22} = L_{33} = -2/v,\ L_{44} = L_{55} - 3/v$$
$$L_{ij} = 0,\ i \neq j \qquad \text{(20a–d)}$$

An important property of the results in equation (20) is that elements of L are entirely independent of induced-flow distribution. Thus, they are identical for the corrected and uncorrected pressure distributions. Another interesting aspect of equation (20) is that the L_{11}, L_{22}, and L_{33} elements are identical to those obtained from simple momentum theory [6]. It would appear that this correspondence is more than coincidental. In particular the lift-deficiency function obtained from the results in equation (20), (see Ref. [6]) is given by

$$\gamma^*/\gamma = \frac{1}{1 + \sigma a/8v} \qquad (21)$$

and is identical to the lift-deficiency functions obtained by Lowey (from a shed-vorticity analysis) and by Miller (from a vorticity-tube theory) [10, 11]. Thus, there is an apparent universality in the results for axial flow.

A second special case for which closed-form results can be obtained is $\omega = 0$, $\alpha = 0°$ (steady, edgewise flow), equation (13). Table 2 lists the closed-form results for both the uncorrected and the corrected pressure distributions, and these are compared with the results of the vortex and momentum theories of Ref. [5]. Several conclusions are important here. First, the L_{11} element remains $1/2v$ (as it was for $\alpha = 90°$) independent of lift distribution. The L_{22} element is about twice the value predicted by momentum theory, and it is only slightly dependent upon the lift distribution. The L_{33} element is identically zero, independent of lift distribution. The coupling terms, L_{31} (λ_c due to C_T) and L_{13} (λ_0 due to C_M), are zero in momentum theory but are present in the vortex and actuator-disc theories. They are definitely affected by the lift distribution, but not qualitatively. Of special interest is the fact that L_{31} is greater than L_{11}, which implies that C_T would create an upwash ($\lambda < 0$) at the leading edge, $\psi = 180°$. This is consistent with measurements [9]. All elements of the 3×3 L-matrix agree qualitatively with the Ormiston vortex model [5].

The higher-harmonic elements of L are also interesting. L_{51} (λ_{2c} due to C_T) is highly sensitive to lift distribution and is not at all small. L_{42} (λ_{2s} due to C_L) is much less sensitive to lift distribution but is also substantial. The L_{55} term (λ_{2c} due to C_{M2}) is twice the value of L_{55} for $\alpha = 90°$. The only nonzero coupling term is L_{24} (λ_s due to C_{L2}). It is roughly half the value of the diagonal element, L_{22}, (λ_s due to C_L). All elements not listed in Table 2 are identically zero due to conditions of symmetry.

Table 2. L-Matrix for Edgewise Flow†

Element	Uncorrected	Corrected	Vortex	Momentum
L_{11}	$\frac{1}{2} = 0.500$	$\frac{1}{2} = 0.500$	$\frac{1}{2} = 0.5$	$\frac{1}{2} = 0.5$
L_{22}	-4^*	$-\frac{79}{16} = -4.938$	$-\frac{8}{3} = -2.7$	-2
L_{33}	0	0	0	-2
L_{31}	$\frac{3\pi}{8} = 1.178$	$\frac{15\pi}{64} = 0.736$	$\frac{1}{2} = 0.5$	0
L_{13}	$\frac{15\pi}{64} = 0.736$	$\frac{1395\pi}{3072} = 1.427$	1.0	0
L_{51}	$\frac{3}{5} = 0.600$	$-\frac{3}{7} = -0.429$		
L_{42}	$-\frac{45\pi}{32} = -4.418$	$-\frac{2205\pi}{2048} = -3.382$		
L_{55}	-6^*			
L_{24}	$\frac{105\pi}{128} = 2.577$			
$^* L_{15}, L_{35}, L_{44}, L_{53}$	0			

†Multiply entries by $1/v$.
*Limited numerical integration required.

The qualitative differences between the L-matrices for $\alpha = 0°$ and $\alpha = 90°$ lead to the obvious question as to how the elements vary as functions of α (i.e. how they vary from hover to forward flight). Although we examine this behavior in detail in the next section, there are some closed-form solutions for this variation which are rather useful. In particular, the Fourier components obtained in Ref. [12] can be used to obtain the first column of L. For the corrected lift distribution, these are

$$L_{11} = \frac{1}{2v} \tag{22a}$$

$$L_{31} = \frac{15\pi}{64v}\sqrt{\frac{1 - \sin\alpha}{1 + \sin\alpha}} \tag{22b}$$

$$L_{51} = -\frac{3}{7v}\left(\frac{1 - \sin\alpha}{1 + \sin\alpha}\right) \tag{22c}$$

For the uncorrected distributions, the α-variations are the same as in equation (22); but the coefficients are altered, as appropriate, to match $\alpha = 0°$. (The L_{11} element is completely independent of lift distribution and angle of incidence.) The variation of L_{31} is approximately linear with α and is identical to the variation obtained from the vortex–element theory of Ref. [13]. The variation of L_{51} is smooth and somewhat parabolic, as α varies from 90° to 0°.

The final closed-form results to be considered are the apparent mass terms for $v = 0$, equation (15b). The evaluation of this equation, according to the entries in Table 1, results in the M-matrix given in Table 3. Several points are noteworthy. First, the uncorrected values of M_{11}, M_{22} and M_{33} are identical to the values obtained for the apparent mass of an impermeable disk [6]. Second, there are significant differences between results for corrected and uncorrected lift distributions. Therefore the apparent mass terms are more sensitive to pressure distribution than are the steady terms. Third, the apparent mass terms decrease with increasing harmonics of λ.

Table 3. Elements of M-matrix

Element	Uncorrected	Corrected
M_{11}	$\frac{8}{3\pi} = 0.8488$	$\frac{128}{75\pi} = 0.5432$
$M_{22} = M_{33}$	$-\frac{16}{45\pi} = -0.1132$	$-\frac{256}{945\pi} = -0.0862$
$M_{44} = M_{55}$	$-\frac{256}{1575\pi} = -0.0517$	—
$M_{ij}, i \neq j$	0	0

5. NUMERICAL RESULTS

We now turn to numerical results for the elements of L vs disc angle, α. The ξ integral in equation (9) is calculated by Simpson's 1/3 Rule at intervals varying from 0.01 to 0.05 and going out to $\xi = 20$. These integrals are used to find $\lambda(r, \psi)$ at 10, unequally-spaced radial stations and at 5° azimuthal increments. The averages in equation (6) are computed by Gauss quadrature in r and by Fourier analysis in ψ. The accuracy of the results may be gauged in the subsequent figures by comparison with the closed-form, starred values of $\alpha = 0°$ and $\alpha = 90°$.

Figure 6 gives corrected and uncorrected values of the elements of the first column of L (induced flow due to perturbations in C_T). These results can be compared with the closed-form expressions in equation (20); and they show an accuracy of 0.1%, for $5° < \alpha < 90°$, and an accuracy of 4% as α approaches 0°. The results illustrate the smooth transition of all elements even as α approches 0°, at which point the disc is in its own wake. Figure 7 gives the second column of L (induced flow due to C_L). The L_{22} element is nearly independent of lift distribution for $\alpha > 10°$; but for $\alpha < 10°$ a noticeable difference develops between the corrected and uncorrected values. The L_{42} element displays a dependence on lift distribution that is independent of α. Figure 8 gives the third column of L(induced flow due to C_M). The λ_0 component, L_{13}, varies smoothly with α; and there is a difference between corrected and uncorrected results only for $\alpha < 10°$. The λ_c component, L_{33}, varies smoothly and is nearly independent of pressure distribution. The higher-harmonic component, L_{53}, is zero for both $\alpha = 0°$ and $\alpha = 90°$; but it is nonzero for intermediate angles and reaches a maximum at $\alpha = 30°$.

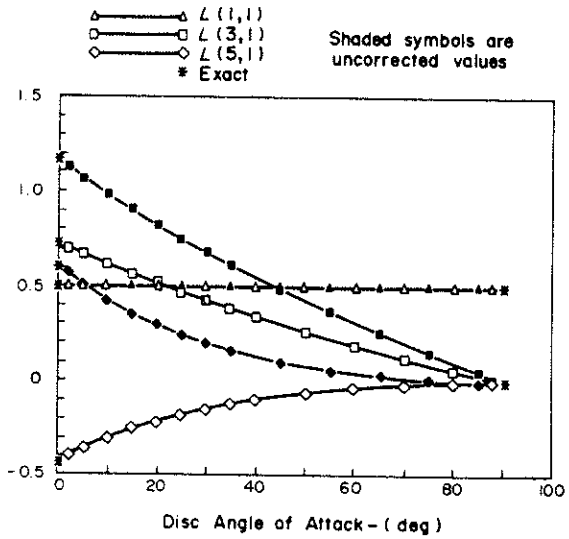

Fig. 6. First Column of L-Matrix (C_T).

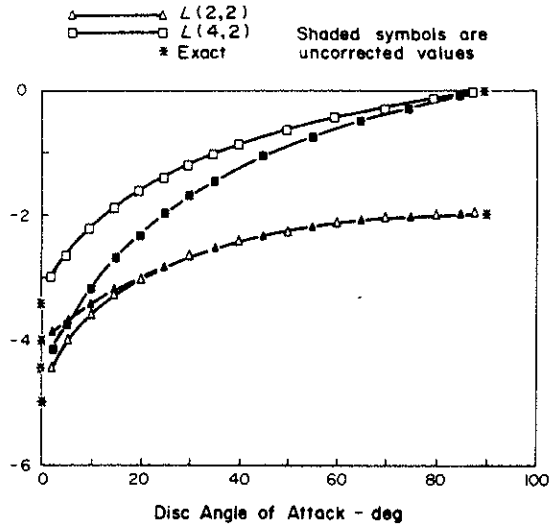

Fig. 7. Second column of L-matrix (C_L).

Figures 9 & 10 give the effect of second-harmonic loading on the L-matrix. These results can be used to determine if dynamic perturbations in the higher-harmonic loads might cause significant changes in λ_0, λ_s or λ_c and thereby invalidate the assumptions of dynamic-inflow theory. Figure 9 shows that there is some λ_s due to C_{L2} (i.e. L_{24}) and its maximum value is 2.58 at $\alpha = 0°$. Given, however, that L_{22} is twice this value and that C_{L2} is probably less than half of C_L, it is reasonable to assume that this coupling could be neglected. Figure 9 further shows that both L_{24} vary smoothly with α. Figure 10 shows that L_{15} (λ_0 due to C_{M2}) and L_{35} (λ_c due to C_{M2}) may reasonably be neglected, the former being identically zero for all α and the latter remaining less than 0.5. L_{55} varies smoothly with α.

The preceding numerical results provide a foundation for the choice of an analytic 3×3 L-matrix. For the first column of this matrix, we use the corrected, closed-form results in equations (22a) and (22b). The corrected lift distribution is used because, from Fig. 3, we see that the uncorrected distribution is unrealistic for a lifting rotor. For the second two columns of L, however, we choose the uncorrected results of Figs 7 & 8.

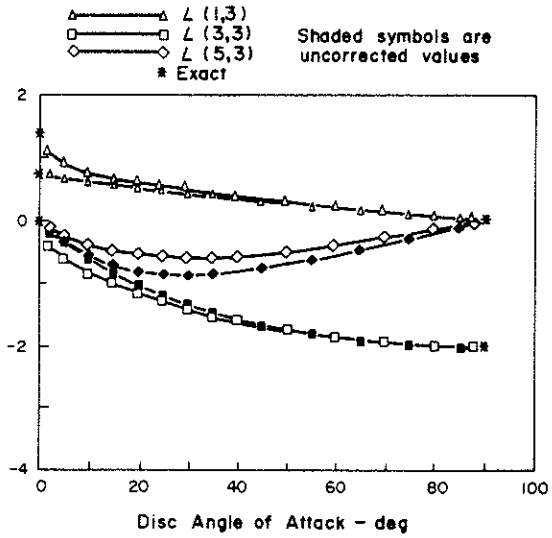

Fig. 8. Third-column of L-matrix (C_M).

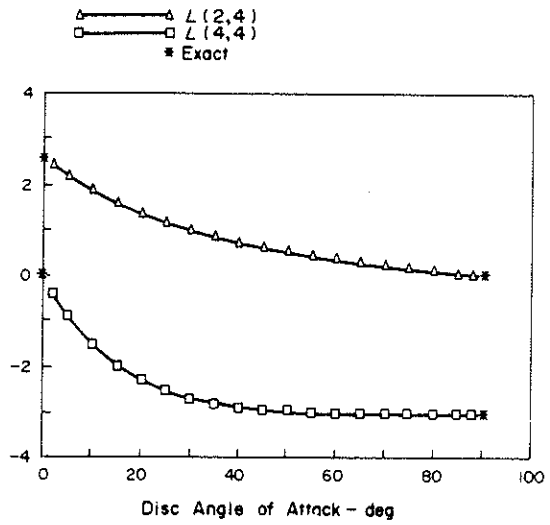

Fig. 9. Fourth Column of L-Matrix (C_{L2}).

There are several reasons for this choice. First, we see in Figs 4 & 5 that either the corrected or the uncorrected distribution for moment is reasonable for the first harmonic variation in lift. Second, Figs 7 & 8 show that the two distributions give nearly identical results (for L_{13}, L_{33} and L_{22}) when $\alpha > 10°$. Since helicopters operate with α's from 5° to 10°, there should be little practical difference between the two distributions. Third, the uncorrected distributions follow smooth curves that appear to be identical to the α-functions in equation (22). Therefore, simple analytic expressions are available for these uncorrected curves. The resultant analytic form of the L-matrix is given in Table 4. The M-matrix, also given in Table 4, is for the identical assumptions. The first column is corrected, and the second two columns are uncorrected. The choice of uncorrected apparent mass for M_{22} and M_{33} is also consistent with experimental results in Ref. [6] that show that these give realistic time constants. There is a certain symmetry to the L-matrix in Table 4 ($L_{13} = L_{31}$ and $L_{11} + L_{22} + L_{33} =$ constant). Furthermore, an eigenvalue analysis of $[L][M]$ shows that there are no anomalies in the system. The

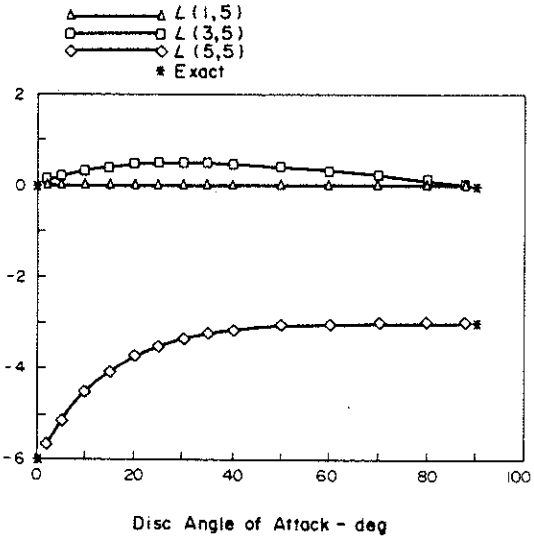

Fig. 10. Fifth column of L-matrix (C_{M2}).

Table 4. Analytic forms of L-matrix and M-matrix

$$[L] = \frac{1}{v}\begin{bmatrix} \frac{1}{2} & 0 & \frac{15\pi}{64}\sqrt{\frac{1-\sin\alpha}{1+\sin\alpha}} \\ 0 & \frac{-4}{1+\sin\alpha} & 0 \\ \frac{15\pi}{64}\sqrt{\frac{1-\sin\alpha}{1+\sin\alpha}} & 0 & \frac{-4\sin\alpha}{1+\sin\alpha} \end{bmatrix}$$

$$[M] = \begin{bmatrix} \frac{128}{75\pi} & 0 & 0 \\ 0 & \frac{-16}{45\pi} & 0 \\ 0 & 0 & \frac{-16}{45\pi} \end{bmatrix}$$

induced flow has three real, stable roots for all values of α between 0° and 90°; and L is always invertible.

6. EXTENSIONS AND FUTURE WORK

There are three major areas in which the preceding results need to be verified or extended. First, the corrected and uncorrected 3×3 and 5×5 models need to be compared in terms of their effect in a coupled, rotor/body dynamic analysis in order to verify the adequacy of the model in Table 4. Second, the results here need to be extended to include the effects of wake contraction and finite number of blades in order to see if these significantly affect the dynamic-inflow model. Third, the complete effect of reduced frequency needs to be investigated with respect to the differences between the assumptions of in-phase velocities and in-phase pressures.

Concerning the effect of wake contraction, there already exists a result from momentum theory that may allow the present results to be directly extended to the lifting case [6]. In particular, it is suggested that the present value of v,

$$v = \sqrt{\mu^2 + \bar{\lambda}^2} \quad \text{(no lift)} \tag{23a}$$

be replaced by a more general mass-flow parameter

$$v = \frac{\mu^2 + (\bar{\lambda} + \bar{v})(\bar{\lambda} + 2v)}{\sqrt{\mu^2 + (\bar{\lambda} + \bar{v})^2}} \quad \text{(steady lift)} \tag{23b}$$

where μ is the inplane component of the aircraft velocity (advance ratio), $\bar{\lambda}$ is the normal component of aircraft velocity (inflow ratio), and $\bar{v}$ is the steady induced flow due to rotor thrust. Similarly, the angle α could be defined as the wake skew angle at the rotor.

$$\alpha = \tan^{-1}\frac{\bar{\lambda} + \bar{v}}{\mu} \tag{23c}$$

In order to verify the usefulness of equations (23b) and (23c), as well as the effect of number of blades, we intend to use an existing, prescribed-wake analysis to calculate the steady L-matrix for various contraction ratios and for rotors with a finite number of blades.

Concerning the effect of reduced frequency, we are currently computing the integrals in equation (19) at various values of k. We already know that, for the second and third rows of L, $dL/dk = \infty$ at $k = 0$. This is analogous to the fixed-wing, Theodorsen theory which also has an infinite derivative at $k = 0$.

$$F = 1 - \frac{k\pi}{2}, \quad G = k\log\frac{k}{2} \tag{24}$$

This implies that no truly first-order model exists for small k. However, it is also known from Ref. [6] that the unsteady terms in dynamic inflow do not become crucial until $k \geq 5$. This is a large reduced frequency but is realistic even for low-frequency motions ($\omega = 0.5$) because v is typically of the order 0.1 ($\omega/v = 5$). Therefore, at these larger values of k, a first-order model may be adequate. As a further verification of the unsteady results, it would be interesting to exercise a transient wake analysis for the response of induced flow to a step input in blade pitch.

7. SUMMARY

An actuator-disc theory has been used to obtain gains and time constants (i.e. the L and M matrices) for both 3-degree-of-freedom and 5-degree-of-freedom dynamic-inflow models. The following conclusions can be made:

(1) In axial flow (e.g. hover), the gains are identical to those obtained from simple momentum theory, and they are independent of the radial lift distribution.

(2) The apparent mass terms (the M matrix) for the simplest pressure distributions are identical to the apparent mass terms of an impermeable disc, but these values vary significantly with lift distribution.

(3) Closed-form results are obtained for all elements of L at $\alpha = 90°$ (axial flow), for all elements of L at $\alpha = 0°$ (edgewise flow), and for the first column of L at all angles of incidence, α.

(4) Numerical results for the elements of L at angles of incidence from 0° to 90° show that they are not strongly dependent upon lift distribution for $10° < \alpha < 90°$, although significant dependence does occur for $\alpha < 10°$.

(5) A 3-degree-of-freedom dynamic-inflow model is probably adequate for rotary-wing dynamics, and this model is expressed in analytic form in Table 4.

(6) More work is required to substantiate the present dynamic-inflow model and to ensure that wake contraction, finite number of blades and reduced-frequency effects will not substantially alter the dynamic–inflow characteristics.

REFERENCES

1. K. B. Amer, Theory of Helicopter Damping in Pitch or Roll and a Comparison with Flight Measurements, NACA TN-2136, October (1948).
2. G. J. Sissingh, The Effect of Induced Velocity Variation on Helicopter Rotor Damping in Pitch or Roll, Aeronautical Research Council Paper No. 101, Technical Note No. Aero. 2132, November (1952).
3. P. J. Carpenter and B. Fridovitch, Effect of Rapid Blade Pitch Increase on the Thrust and Induced Velocity Response of a Full Scale Helicopter Rotor, NACA TN-3044, November (1953).
4. N. K. Shupe, A Study of the Dynamic Motions of Hingeless Rotored Helicopters, Ph.D. Thesis, Princeton University, (1970).
5. R. A. Ormiston and D. A. Peters, Hingeless Helicopter Rotor Response with Nonuniform Inflow and Elastic Blade Bending, *J. Aircraft* **9**, 730–736 (1972).
6. D. A. Peters, Hingeless Rotor Frequency Response with Unsteady Inflow, *Rotorcraft Dynamics* pp. 1–12. NASA SP-352, (1974).
7. S. T. Crews, K. H. Hohenemser and R. A. Ormiston, An Unsteady Wake Model for a Hingeless Rotor, *J. Aircraft*, 11, (1974).
8. R. A. Ormiston, An Actuator Disc Theory for Rotor Wake Induced Velocities, *AGARD Specialists' Meeting on the Aerodynamics of Rotary Wings*, Marseilles, France, (1972).
9. M. Joglekar and R. Loewy, An Actuator-Disc Analysis of Helicopter Wake Geometry and the Corresponding Blade Response, USAAVLABS Technical Report 69-66, (1970).
10. J. P. Jones, An Actuator Disc Theory for the Shed Wake at Low Tip Speed Ratios, MIT Aeroelastic and Structures Laboratory, Technical Report 133-1, (1965).
11. R. G. Loewy, A Two-Dimensional Approximation to the Unsteady Aerodynamics of Rotary Wings, *J. Aeronautical Sci.* **24**, (1957).
12. K. W. Mangler, Fourier Coefficients for Downwash of a Helicopter Rotor, Royal Aircraft Establishment Report No. Aero. 1958 (1948).
13. R. P. Coleman, A. M. Feingold and C. W. Stempin, Evaluation of the Induced-Velocity Field of an Idealized Helicopter Rotor, NACA WR L-126, (1945).

Correlation of Measured Induced Velocities with a Finite-State Wake Model

David A. Peters
Professor

Cheng Jian He
Post-Doctoral Fellow

School of Aerospace Engineering
Georgia Institute of Technology
Atlanta, Ga.

A new rotor induced-flow model is applied to the correlation of a recent set of LDV inflow measurements made by the Army Labs at NASA Langley. This new inflow model is based on an acceleration potential with a skewed cylindrical wake. While this particular flow description is not new, the novel aspect of the present work is that the model is not discretized. Instead, the flow field and the rotor lift are expanded in terms of appropriate inflow modes. The result is a set of closed-form, first-order, ordinary differential equations in time that defines a finite number of modal inflow states, with blade lift as the forcing function. Although the model is intended primarily as a representation of unsteady aerodynamics for aeroelasticity applications, the results here show that it is also effective as a means of finding the inflow distribution in forward flight.

Notation

a = slope of lift coefficient curve, 1/rad
$\bar{c}$ = nondimensional blade chord
$\overline{C}_T$ = steady value of thrust coefficient
C_n^m, D_n^m = arbitrary pressure coefficients
$E[\ ]$ = dynamic inflow acceleration operator
G_n^m = diagnonal mass matrix
H_n^m = factorial ratios, Eq. (26)
i = imaginary number, $i = \sqrt{-1}$
j = polynomial number
$L[\ ]$ = quasi-steady inflow operator
$[\bar{L}_{jn}^{rm}]^c$ = cosine influence coefficients
$[\bar{L}_{jn}^{rm}]^s$ = sine influence coefficients
L_q = blade sectional lift of q^{th} blade, N/m
m = harmonic number
M = total number of harmonics
n = polynomial number
P = pressure across disk divided by $\rho\Omega^2R^2$
$\overline{P}_n^m$ = normalized Legendre function of first kind
P_n^m, Q_n^m = associated Legendre function of first and second kinds
Q = number of blades
q = blade index
q_i = i-th component of perturbation velocity, dimensionless on ΩR
R = rotor radius, m
r = harmonic number
$\bar{r}$ = nondimensional blade radial coordinate
S = total inflow states
t = time, sec
$\bar{t}$ = nondimensional time, $\bar{t} = \Omega t$
V = flow parameter, dimensionless on ΩR
V_T = total flow at rotor plane divided by ΩR
V_∞ = nondimensional freestream speed
w = nondimensional normal component of induced velocity, positive downward
X = function of wake skew angle, $X = \tan|\chi/2|$
α = angle between freestream and rotor disk, positive nose down
α_j^r, β_j^r = induced inflow expansion coefficients
$\overline{\alpha}_1^0$ = steady value of α_1^0
χ = wake skew angle, $\pi/2 - \tan^{-1}|\lambda/\mu|$
θ_q = pitch angle of q^{th} blade, rad
θ_0 = blade collective pitch at blade root, rad
θ_t = blade linear twist, rad
θ_{1c} = blade lateral cyclic pitch, rad
θ_{1s} = blade longitudinal cyclic pitch, rad
λ = total mass-flow inflow, $\lambda = \lambda_f + \lambda_m$

Presented at the 45th Annual National Forum of the American Helicopter Society, Boston, Mass., May 1989

λ_f = inflow due to freestream, $V_\infty \sin(\alpha)$
λ_m = momentum theory inflow, Eq. (35)
μ = advance ratio, $V_\infty \cos(\alpha)$
$\nu, \eta, \bar{\psi}$ = ellipsoidal coordinates, dimensionless
ξ = nondimensional coordinate along freestream line, positive upstream
ρ = air density, kg/m^3
$(\rho_n^m)^2$ = integral (0 to 1) of $(P_n^m(\nu))^2$
σ = rotor solidity
τ_n^{mc} = cosine pressure coefficient
τ_n^{ms} = sine pressure coefficient
$\bar{\tau}_1^{0c}$ = steady part of τ_1^{0c}
$\phi_n^m(\bar{r})$ = inflow expansion functions, $\bar{P}_n^m(\nu)/\nu$
Φ = nondimensional pressure
ψ = spacial position at rotor disk
ψ_q = azimuth of q^{th} blade
Ω = rotor rotational speed, rad/sec
$(\,)^*$ = derivative with respect to nondimensional time, $(\,)^* = \partial/\partial\bar{t}$
$(n)!!$ = double factorial of n,
= $(n)\,(n-2)\,(n-4)\cdots(2)$, for n even;
= $(n)\,(n-2)\,(n-4)\cdots(1)$, for n odd

Introduction

Background

The task of aeroelastic analysis of a rotorcraft involves several key elements. First, appropriate models must be obtained for the various components of the problem. These include a lift model (quasi-steady, dynamic stall, panel code, etc.), an induced-flow model (momentum-theory, Glauert, Drees, prescribed wake, free wake, etc.), a blade model (rigid-blade, linear beam, Hodges-Dowell, etc.), a fuselage model (rigid-body, NASTRAN, etc.), and possibly a feedback control model (stabilizer bar, SCAS, higher-harmonic control, etc.). Second, these models must be coupled together and solved simultaneously to find a trimmed, periodic equilibrium condition. This second task is not at all trivial and is often compounded by the fact that the aerodynamic, structural, and control-system models are often mutually incompatible both in terms of connecting variables and in terms of available solution strategies.

Finally, the trimmed periodic solution to this coupled system must be perturbed (analytically or numerically) in order to obtain a set of linearized, periodic-coefficient equations that can be analyzed for Floquet stability, for frequency and damping, and for the design of active control systems. This third (and crucial) step is often hindered due to the fact that lift or inflow models do not have finite number of state variables that can be identified and perturbed. Instead, these models often contain hidden states (or sometimes an infinite number of states), which precludes efficient aeroelastic analysis and iterative design. What we need are lift and inflow models that are accurate and that are expressive in terms of a reasonable number of state variables. This paper develops a theory and presents applications of such a finite-state inflow model.

Previous Work

At this point, it is instructive to review the various unsteady inflow models that are available to aeroelasticians in the rotary-wing field. One of the best-known models is Loewy theory, Ref. 1. It provides induced velocity in axial flight due to shed vorticity including the returning wake. It is written as a two-dimensional lift-deficiency function that explicitly includes the Theodorsen function. Thus, it is in the frequency domain and has an infinite number of states. Friedmann and Venkatesan, Ref. 2, offer a methodology whereby Loewy theory can be approximated by a finite number of states in the time domain. Still, however, the number of states is large (17 variables at each radial lift element on each blade). Furthermore, the Loewy methodology does not treat induced flow due to trailing vorticity and is not applicable in forward flight. Thus, the finite-state approximation is also limited to hover or climb without trailing vorticity.

Other pertinent methods include actuator-disk theories that assume a skewed cylindrical wake in forward flight, Refs. 3–5. These include both acceleration-potential and vortex-cylinder methods. They are related to our present method, but they are inadequate in that they are steady-state models that must assume an infinite number of blades in order to obtain closed-form performance results. Thus, they are not unsteady, three-dimensional wake models. One alternative model that captures both the unsteady and the three-dimensional aspects of rotor induced flow is that of Miller, Ref. 6. Although the model has some very useful applications (as well as interesting special cases), its solution is in the frequency domain and requires integrals over the wake that can become involved. It also has an infinite number of states and cannot be applied in the aeroelasticity context described in this paper.

Another important class of models is in the set of vortex-filament models, which have dominated performance calculations over the past 20 years (*e.g.*, Refs. 7–9). Some of these have only trailing vorticity (with the shed wake accounted for by Loewy or Theodorsen functions), but others have both shed and trailing filaments. When the wake is prescribed, influence coefficients can be calculated between the strength of vortex filaments and the induced flow at the rotor. The result is a fairly efficient induced flow methodology that is both unsteady and three-dimensional. While these methods are very powerful tools for rotor performance, they still do not meet the needs for aeroelasticity analysis. First, the discretization process, which is adequate for loads, often falls short for unsteady perturbations. There are four major discretizations involved. The first is the spanwise discretization of vortex filaments, the second is the piece-wise discretization of bound vortices, the third is the accompanying discretization of shed filaments (often every 15° of rotor azimuth), and the fourth is the truncation of the wake after a few turns. These discretizations are generally much less accurate for aeroelasticity than they are for performance.

An even more serious problem, however, is that a discretized wake does not have well-defined states and is not easily perturbed. Thus, with conventional dynamic perturbations, one either must freeze the wake (in which case unsteady aerodynamics is lost) or else allow the wake to be implicitly perturbed along with structural states (which contaminates the perturbation dynamics with the dynamics of hidden inflow states). Therefore, vortex filament methods do not satisfy our requirements; and there is a need for a different kind of three-dimensional, unsteady wake model.

Present Approach

The inflow description of this paper is a three-dimensional, unsteady induced-flow model with a finite number of states in the time domain. The basis of the model is an acceleration potential with a skewed cylindrical wake. Thus, its roots are in Refs. 3–5. However, unlike those methods, this model is both unsteady and is applicable to a finite number of blades. Models with a similar basis have been used in rotary-wing work. Ref. 10; but the unique aspect here is the solution methodology. Rather than discretize the wake and couple it to a given blade model, we expand the induced inflow at the disk in terms of modal functions. The blade lift is also expressed as an expression on the disk and is left general. The result is a set of ordinary differential equations (in closed form) that

relate the expansion coefficients of inflow to the expansion coefficients of arbitrary lift. The inflow expansion coefficients thus become states of the model, and the forcing terms can be derived based on any lifting theory (linear or nonlinear).

The theory of dynamic inflow, Ref. 11, can be thought of as a special case of this theory but with only 3 inflow expansion terms (uniform, side-to-side gradient, and fore-to-aft gradient). Furthermore, Ref. 12 (in which the foundations of this new theory are set forth) shows that the new model implicitly includes Theodorsen and Loewy effects (from the shed wake) as well as Prandtl-Goldstein tip losses (due to the trailing wake). Thus, the method is truly an unsteady, three-dimensional wake model with a finite number of states. The method is not expected to replace vortex-filament theories for performance work due to the lack of wake distortion or wake roll-up in the model. Still, the present method should be capable of predicting reasonable unsteady induced-flow distributions in forward flight in order to provide a valid trim state about which to perturb. Therefore, in this paper, we concentrate on correlations of the theory with induced-flow measurements in forward flight.

Formulation of Theory

Fluid Mechanics

For an incompressible potential flow with small perturbations, the continuity and momentum equations can be written in index notation as

$$q_{i,i} = 0 \tag{1}$$

$$\overset{*}{q}_i - V_\infty q_{i,\xi} = -\Phi_{,i} \tag{2}$$

where q_i are the velocity components, Φ is the pressure, $(\ )^*$ is a nondimensional time derivative, and $(\ )_{,\xi}$ is the derivative along the freestream line.

From Eq. (2), it can be seen that spatial gradient of the pressure is a superposition of contributions from both the unsteady rate of change in velocity and the gradient of velocity along the freestream direction. This suggest a division of the pressure into two parts (*i.e.*, the part due to momentum flux, denoted as Φ^V, and the part due to acceleration, noted as Φ^A). Then the pressure can be expressed as

$$\Phi = \Phi^V + \Phi^A \tag{3}$$

$$\Phi_{,i} = \Phi^V_{,i} + \Phi^A_{,i} \tag{4}$$

$$\Phi^V_{,i} = V_\infty q_{i,\xi} \tag{5}$$

$$\Phi^A_{,i} = -\overset{*}{q}_i \tag{6}$$

If we differentiate Eqs. (5) and (6) with respect to the index i and use the continuity equation, Eq. (1), a Laplace's equation can be obtained for each pressure function as follows,

$$\Phi^V_{,ii} = 0; \qquad \Phi^A_{,ii} = 0 \tag{7}$$

Equation (7) indicates that each part of the total pressure satisfies Laplace's equation. Thus, Φ can be represented as an acceleration potential.

When Laplace's equation is written in ellipsoidal coordinates, it can be solved analytically by the method of separation of variables. The potential functions thus obtained can be combined to given an arbitrary pressure discontinuity across a circular disk, Ref. 3. When the condition of a bounded solution is invoked, the general form of the acceleration potential becomes

$$\Phi = \sum_m^\infty \sum_{n=m+1,m+3,\ldots}^\infty P_n^m(\nu) Q_n^m(i\eta)[C_n^m(\bar{t})\cos(m\bar{\psi}) + D_n^m(\bar{t})\sin(m\bar{\psi})] \tag{8}$$

where $P_n^m(\nu)$ and $Q_n^m(i\eta)$ are associated Legendre functions of the first and second kind, respectively; C_n^m and D_n^m are arbitrary, time-dependent coefficients; and ν, η, and $\bar{\psi}$ are ellipsoidal coordinates as described in Ref. 11.

It is important to note that, since ν is positive above the disk and negative below the disk, the functions $P_n^m(\nu)$ with $n + m$ odd yield a discontinuity in pressure across the disc at which $\eta = 0$, $\nu = \sqrt{1 - \bar{r}^2}$, and $\bar{\psi} = \psi$. Therefore, rotor lift can be obtained from the pressure difference between the upper and lower surfaces of the disk,

$$P = \sum_{m,n}^\infty \bar{P}_n^m(\nu)[\tau_n^{mc}(\bar{t})\cos(m\psi) + \tau_n^{ms}(\bar{t})\sin(m\psi)] \tag{9}$$

where

$$\bar{P}_n^m(\nu) = (-1)^m \frac{P_n^m(\nu)}{\rho_n^m} \tag{10}$$

$$(\rho_n^m)^2 = \frac{1}{(2n+1)} \frac{(n+m)!}{(n-m)!} \tag{11}$$

$$\tau_n^{mc} = (-1)^{m+1} 2 Q_n^m(i0) \rho_n^m C_n^m \tag{12}$$

$$\tau_n^{ms} = (-1)^{m+1} 2 Q_n^m(i0) \rho_n^m D_n^m \tag{13}$$

Operator Notation

To establish a relation between the induced flow of a lifting rotor and the blade loads, let us start with Eqs. (5) and (6). Integration of Eq. (5) along the freestream direction results in

$$q_i = -\frac{1}{V_\infty} \int_\xi^\infty \Phi^V_{,i}\, d\xi \tag{14}$$

Then, from Eq. (6), we have

$$\overset{*}{q}_i = -\Phi^A_{,i} \tag{15}$$

Now, if we are only interested in the normal component of induced inflow at the rotor disk, Eqs. (14) and (15) can be placed in the following forms.

$$w = -\frac{1}{V_\infty} \int_0^\infty \frac{\partial \Phi^V}{\partial z}\, d\xi \tag{16}$$

$$\frac{dw}{d\bar{t}} = -\frac{\partial \Phi^A}{\partial z}\Big|_{\eta=0} \tag{17}$$

Equations (16) and (17) can be thought of as linear operators,

$$w = L[\Phi^V] \tag{18}$$

$$\overset{*}{w} = \frac{dw}{d\bar{t}} = E[\Phi^A] \tag{19}$$

At this stage, we assume that the operators L and E are invertable, and then we obtain an equation for inflow in the following form

$$E^{-1}[w]^* + L^{-1}[w] = \Phi^A + \Phi^V = \Phi \tag{20}$$

If we choose a proper series expansion for induced flow, each of the operators L and E can be expressed in a matrix form, which allows a matrix inversion.

Analogous to the expansion of pressure, the induced flow can be represented in terms of azimuthal harmonics and radial distribution functions. The best choice for the radial expansion has been found to be

$$w(\bar{r}, \psi, \bar{t}) = \sum_{r,j}^{\infty} \phi_j^r(\bar{r})[\alpha_j^r(\bar{t})\cos(r\psi) + \beta_j^r(\bar{t})\sin(r\psi)] \quad (21)$$

where $\phi_n^m(\bar{r}) = \bar{P}_n^m(\nu)/\nu$ and $\nu = \sqrt{1 - \bar{r}^2}$. Interestingly, the $\phi_n^m(\bar{r})$ are simple polynomials in the radial position, $\bar{r}$, and have only even (or odd) powers of $\bar{r}$ ranging from m to $n - 1$.

$$\phi_n^m(\bar{r}) = \sqrt{(2n+1)H_n^m} \sum_{q=m,m+2,\cdots}^{n-1} \bar{r}^q(-1)^{(q-m)/2} \frac{(n+q)!!}{(q-m)!!(q+m)!!(n-q-1)!!} \quad (22)$$

With pressure and velocity each represented by the above expansions, the operators in Eq. (20) can be expressed as square matrices that relate the pressure coefficients (τ_n^{mc}, τ_n^{ms}) to the velocity coefficients (α_j^r, β_j^r) (for details, see Ref. 13). Thus, Eq. (20) takes the form

$$[\nwarrow G_n^m \nearrow]\{\alpha_j^r\}^* + 2V[\tilde{L}^c]^{-1}\{\alpha_j^r\} = \{\tau_n^{mc}\} \quad (23)$$

$$[\nwarrow G_n^m \nearrow]\{\beta_j^r\}^* + 2V[\tilde{L}^s]^{-1}\{\beta_j^r\} = \{\tau_n^{ms}\} \quad (24)$$

where G_n^m results from Eq. (17) and is given by

$$G_n^m = \frac{4}{\pi} H_n^m \quad (25)$$

$$H_n^m \equiv \frac{(n+m-1)!!(n-m-1)!!}{(n+m)!!(n-m)!!} \quad (26)$$

and where $\tilde{L}^c$ and $\tilde{L}^s$ arise from Eq. (16) and depend on the wake skew angle χ ($\chi = 0°$ in axial flow through $\chi = 90°$ in pure-edgewise flow).

$$[\tilde{L}_{jn}^{0m}]^c = (X^m)[\Gamma_{jn}^{0m}] \quad (27)$$

$$[\tilde{L}_{jn}^{rm}]^c = (X^{|m-r|} + (-1)^l X^{|m+r|})[\Gamma_{jn}^{rm}] \quad (28)$$

$$[\tilde{L}_{jn}^{rm}]^s = (X^{|m-r|} - (-1)^l X^{|m+r|})[\Gamma_{jn}^{rm}] \quad (29)$$

where $l = \min(r, m)$, and $X = \tan|\chi/2|$. Note that $0 \le X \le 1$. All sine and cosine elements depend on the same coefficients Γ_{jn}^{rm} that can be found in closed-form as follows.

$$\Gamma_{jn}^{rm} = \frac{(-1)^{(n+j-2r)/2}}{\sqrt{H_n^m H_j^r}} \frac{2\sqrt{(2n+1)(2j+1)}}{(j+n)(j+n+2)[(j-n)^2 - 1]} \quad \text{for } r + m \text{ even} \quad (30)$$

$$\Gamma_{jn}^{rm} = \frac{\pi}{2\sqrt{H_n^m H_j^r}} \frac{\operatorname{sgn}(r-m)}{\sqrt{(2n+1)(2j+1)}} \quad \text{for } r + m \text{ odd}, j = n \pm 1 \quad (31)$$

$$\Gamma_{jn}^{rm} = 0 \quad \text{for } r + m \text{ odd}, j \neq n \pm 1 \quad (32)$$

$\tilde{L}$ is partitioned such that the superscripts are row-column indices of the r, m partition, and the subscripts (j, n) are the row-column indices of the elements within each partition. We must note, however, that these indices do not take the traditional matrix values of 1, 2, 3, $\cdots$. Instead, for the cosine equation, $m = 0, 1, 2, 3, \cdots$; for the sine equation, $m = 1, 2, 3, \cdots$; and for either set, $n = m + 1, m + 3, m + 5, \cdots$ (r and j follow the same convention).

As a further extension of the theory, we have replaced V_∞ with an equivalent V to account for energy added to the flow from the rotor

$$V = \frac{\mu^2 + (\lambda + \lambda_m)\lambda}{\sqrt{\mu^2 + \lambda^2}} \quad (33)$$

$$\lambda = \lambda_m + \lambda_f \quad (34)$$

where V comes from momentum considerations, Ref. 11; μ and λ_f are the inplane and normal components of V_∞; and λ_m is the momentum-theory value of steady induced flow for a trimmed rotor,

$$\lambda_m = \frac{1}{2}\frac{\bar{C}_T}{V_T} \cong \sqrt{3}\bar{\alpha}_1^0 \quad (35)$$

In Eq. (35), $\bar{C}_T$ is steady thrust, $\bar{\alpha}_1^0$ is the steady uniform induced flow, and $V_T = \sqrt{\mu^2 + \lambda^2}$. The wake model can then be considered as a model for perturbation pressure and velocity about this steady, uniform pressure

$$\bar{\tau}_1^{0c} = \frac{\sqrt{3}}{2}\bar{C}_T \quad (36)$$

Following Ref. 14, a completely nonlinear version of Eqs. (23) and (24) can also be obtained if we

1) take V as V_T in the first column ($r = 0$) of $[\tilde{L}^c]^{-1}$, but as V for $r \neq 0$.
2) treat all quantities as total rather than perturbation.
3) replace the static λ_m, Eq. (35), by the unsteady value, $\sqrt{3}\alpha_1^0$.

This makes the theory nonlinear, in that V and V_T will depend upon the states, α_n^m. The nonlinear version is used in the correlations in this paper.

Generalized Forces

In order for the model to be coupled with blade lift theory, the τ_n^{mc} and τ_n^{ms} need to be appropriately related to the blade lift. If we treat the pressure across the disk as a lifting line for each blade, rotating with angular velocity Ω, then the azimuth of the q^{th} lifting line (i.e., blade) is $\psi_q = \Omega t + (q-1)2\pi/Q$. These rotating pressure spikes can then be expanded as in Eq. (9) to obtain the pressure harmonics, Ref. 12.

$$\tau_n^{0c} = \frac{1}{2\pi}\sum_{q=1}^{Q}\left[\int_0^1 \frac{L_q}{\rho\Omega^2 R^3}\phi_n^m(\bar{r})d\bar{r}\right] \quad (37)$$

$$\tau_n^{mc} = \frac{1}{\pi}\sum_{q=1}^{Q}\left[\int_0^1 \frac{L_q}{\rho\Omega^2R^3}\,\phi_n^m(\bar{r})d\bar{r}\right]\cos(m\psi_q) \quad (38)$$

$$\tau_n^{ms} = \frac{1}{\pi}\sum_{q=1}^{Q}\left[\int_0^1 \frac{L_q}{\rho\Omega^2R^3}\,\phi_n^m(\bar{r})d\bar{r}\right]\sin(m\psi_q) \quad (39)$$

where L_q is blade sectional circulatory lift that can be evaluated from a lift theory. Since the wake and lift are now treated separately, the lift theory need not be linear. It can include dynamic stall or other nonlinear effects. Although the above integrals assume that the lift is concentrated along a lifting line at ψ_q, Ref. 12 shows that the integrals are easily modified to include lift distributed over a chordwise surface. Note also that the τ_n^m take on the character of generalized forces. Thus, we have a complete, three-dimensional unsteady wake model written in terms of a finite number of states α_j^r and β_j^r.

Computation of Induced Flow

The generalized dynamic wake equations have been applied to the prediction of dynamic response of the flow field associated with an isolated rotor in forward flight. The computation of induced inflow at the rotor disk consists of solving the system of Eqs. (23) and (24), simultaneously. In order to do this, the forcing functions on the right-hand side of the equations (*i.e.*, τ_n^{mc}, and τ_n^{ms}) need to be evaluated from Eqs. (37)–(39). Therefore, in addition to the basic dynamic wake equations, we will proceed to establish the expressions for lift.

Blade Lift Model

For this induced inflow computation, we have made the following main assumptions: 1) reversed flow neglected, 2) blade angle of attack is assumed small, 3) there is no blade dynamics, 4) there is no interaction between fuselage and rotor aerodynamics, and 5) the reduced frequency is small enough that $\dot{\theta}$ and $\ddot{\theta}$ terms can be neglected.

Based on these assumptions, the blade sectional lift can be written as

$$\frac{L_q(\bar{r},\psi_q,\bar{t})}{\rho\Omega^2R^3} = \frac{1}{2}a\bar{c}(\bar{r}+\mu\sin\psi_q)^2\left\{\theta_q - \frac{[w(\bar{r},\psi_q,\bar{t})+\lambda_f]}{(\bar{r}+\mu\sin\psi_q)}\right\} \quad (40)$$

where θ_q, the q^{th} blade pitch angle, is

$$\theta_q = \theta_0 - \theta_t\bar{r} + \theta_{1c}\cos\psi_q + \theta_{1s}\sin\psi_q \quad (41)$$

and w is the induced inflow as given in Eq. (21). It is noted that the induced inflow, w, enters the blade lift expression and couples the sine and cosine parts of the dynamic wake equations. Substitution of the blade lift, Eq. (40), into Eqs. (37)–(39) yields generalized-force integrals, (τ_n^{0c}, τ_n^{mc}, and τ_n^{ms}). Although Eq. (40) appears to be a two-dimensional quasi-steady model, the inflow feedback through w implies that both the unsteady effects (e.g., Theodorsen and Loewy) and tip relief effects (*e.g.*, Prandtl and Goldstein tip-loss) are included implicitly.

Solution Method

The resultant set of coupled inflow and lift equations is a system of ordinary differential equations with periodic coefficients. These can be solved by a variety of methods including harmonic balance or direct time-marching. In either event, one must also find the trim settings to give a desired thrust coefficient and desired roll and pitch moments. In our model, $\bar{C}_T = (2/\sqrt{3})\bar{\tau}_1^{0c}$; and roll and pitch moments are proportional to τ_2^{1c} and τ_2^{1s}. This makes trimming a straightforward process. In the work here, we use time-marching with the auto-pilot system described in Ref. 15. For a typical problem with 33 flow states, the method requires 2 minutes CPU on a CDC 855. About half of this is to find trim. This CPU time is much faster than either free-wake programs or prescribed-wake codes.

The choice of inflow states is based on the relationships in Table 1. The table shows the number of radial shape functions for each harmonic (m) in order to have radial terms up to a given power of $\bar{r}$. For example, for terms up to $\bar{r}^4$, the m = 0 harmonic would have three radial terms; the m = 1 and m = 2 sine and cosine harmonics would have 2 terms each; and the m = 3 and m = 4 sine and cosine harmonics would have one term each. Thus, a total of 15 terms (or state variables) would be used. If we desire more polynomials without increasing the total number of harmonics, we choose a row corresponding to a larger power of $\bar{r}$. For example, for m = 4 and $\bar{r}^8$, this would be 5 + 2 (4 + 4 + 3 + 3) = 33 total states, S.

Experimental Data

All of the experimental data used in this paper are from the LDV measurements made by the Army Labs at NASA Langley, Ref. 16. There are two different blade planforms for which data are available. One set of blades has 13° of linear twist, a uniform chord over the inner 75 percent radius, and a 3-to-1 blade taper over the outer 25 percent. The other blades have 8° of linear twist and are constant-chord. Each set has a 25 percent root cutout, a solidity of 0.0977, and was tested as a 4-bladed configuration at $\bar{C}_T$ = .0064. Results for the tapered blades are available at μ = .15 and μ = .23. Results for the rectangular blades are available at these two advance ratios and at μ = 0.3. Data at the lower advance ratios are for 3° nose down shaft angle, and data at μ = 0.3 are for 4° nose down shaft angle. The measurements are taken one chord above the tip-path plane in contrast to our calculations, which are at the rotor plane. All results have cyclic flapping trimmed to zero.

The experimental data also include values of the trimmed pitch settings for each data condition. We have compared these with the trimmed pitch settings from our auto-pilot. The average difference in settings for the tapered blades is 0.5°, and the average difference for rectangular blades is 1.1°. From our model, the 3/4 radius trim settings are nearly identical for the two sets of blades.

Contour Plots for Tapered Blades

Figure 1a gives computed induced flow contours with four harmonics and with 15 state-variables at μ = 0.15. Figure 1b gives the measured values at the same condition. One can see that the computation with 15 state variables gives a good representation of all flow characteristics including: 1) The existence of upwash at the front of the disk, 2) the "double-S" shape of the w = .02, .03, and .04 contours around the w =

Table 1 Number of Shape Functions per Harmonic

Highest Power of $\bar{r}$	Harmonic Number, m 0	1	2	3	4	5	6	7	8	Total Inflow States
0	1									1
1	1	1								3
2	2	1	1							6
3	2	2	1	1						10
4	3	2	2	1	1					15
5	3	3	2	2	1	1				21
6	4	3	3	2	2	1	1			28
7	4	4	3	3	2	2	1	1		36
8	5	4	4	3	3	2	2	1	1	45

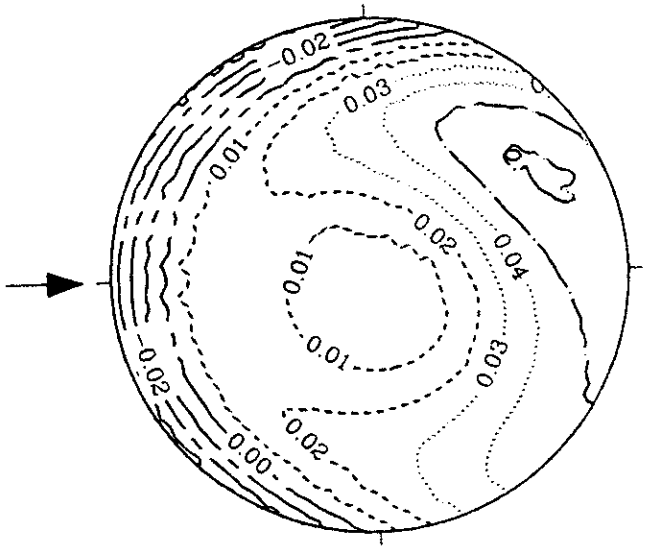

Figure 1a Theoretical induced flow distribution, tapered blades, μ = 0.15, M = 4, S = 15.

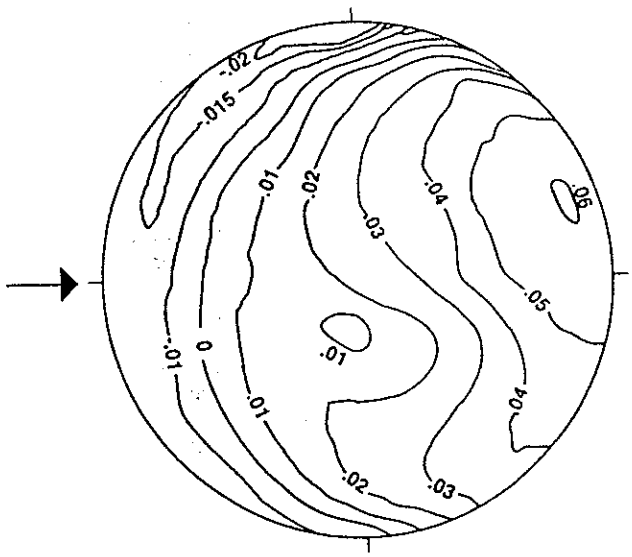

Figure 1b Experimental induced flow distribution, tapered blades, μ = 0.15.

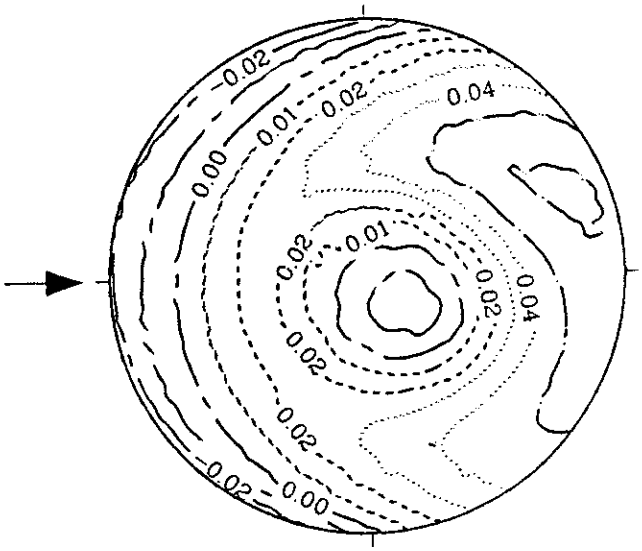

Figure 1c Theoretical induced flow distribution, tapered blades, μ = 0.15, M = 4, S = 33.

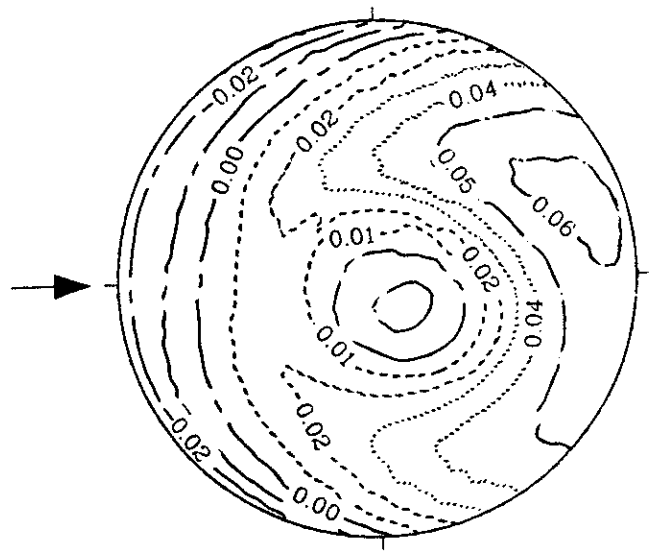

Figure 1d Theoretical induced flow distribution, tapered blades with fuselage, μ = 0.15, M = 4, S = 33.

.01 contour on the retreating side, and 3) the skewing of induced flow toward the advancing side with a maximum of w = 0.06 at ψ = 30°, $\bar{r}$ = 0.85. One discrepancy, however, is the overly large gradient in computed induced flow at ψ = 180°. This discrepancy is alleviated, however, when (with M = 4) we increase to 33 state variables, Fig. 1c. The correlation becomes better yet when we add the flow over the fuselage from Ref. 17, Fig. 1d. A similarly good correlation is seen for μ = 0.23 when we include 33 states and fuselage flow, Figs. 2a–2b.

We have seen in Fig. 1 that the flow over the fuselage gives a marked improvement in data correlation. Figures 3 and 4 show the effect of fuselage flow in more detail. In these figures, we plot induced flow with and without fuselage flow both on the longitudinal centerline (ψ = 0°, 180°) and on the lateral center line (ψ = 90°, 270°) at μ = 0.15 and 0.23. Results show no effect of the fuselage on the flow at the lateral centerline, but they show a noticeable improvement in correlation on the longitudinal centerline. This improvement is more significant at μ = 0.23 due to the larger relative freestream. Therefore, flow over the fuselage is included in all results to follow.

Convergence of Method

We have seen in Figs. 1a–1c that the correlation at μ = 0.15 improves at the leading edge of the disk if more inflow states are added. To study this effect further, we now investigate in detail the influence of the number of states on the convergence and correlation. Figure 5 shows the identical centerline results as in Fig. 4 (μ = 0.23 with flow over the fuselage), but the number of states is increased from 15 ($\bar{r}^4$ terms) to 33 ($\bar{r}^8$ terms). Convergence to the measured values at the leading edge is clearly seen from comparison of Figs. 4 and 5. Figure 6 details this convergence for μ = 0.15. Figure 6a gives results at ψ = 180°, the leading edge, where we saw the greatest effect in Fig. 1. The three results are for 15, 33, and 51 state variables, respectively. It is clear from the curves that the

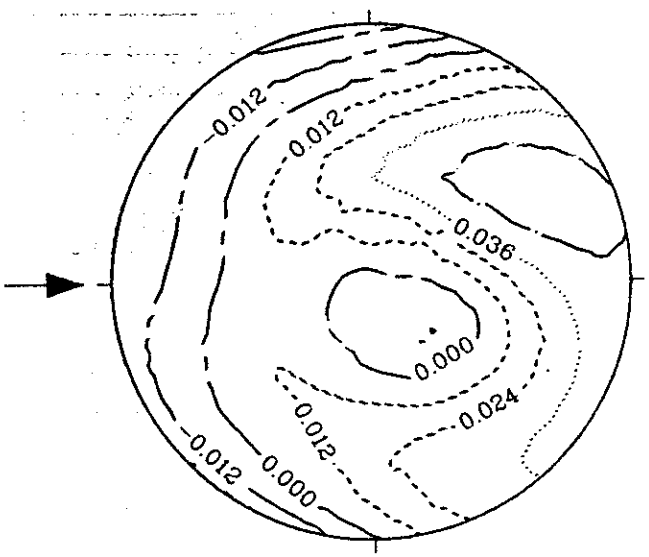

Figure 2a Theoretical induced flow distribution, tapered blades with fuselage, $\mu = 0.23$, $M = 4$, $S = 33$.

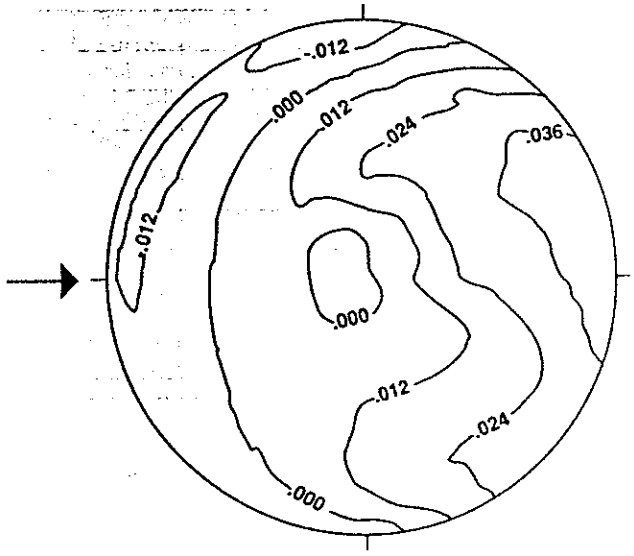

Figure 2b Experimental induced flow distribution, tapered blades, $\mu = 0.23$.

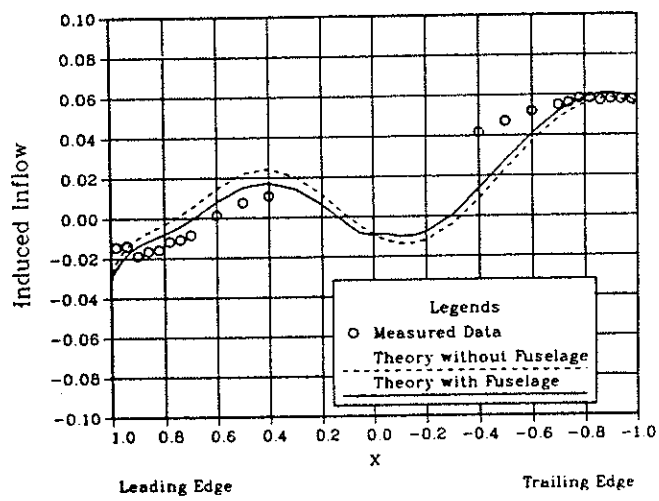

Figure 3a Longitudinal variation of induced flow, tapered blades, $\mu = 0.15$, $M = 4$, $S = 33$.

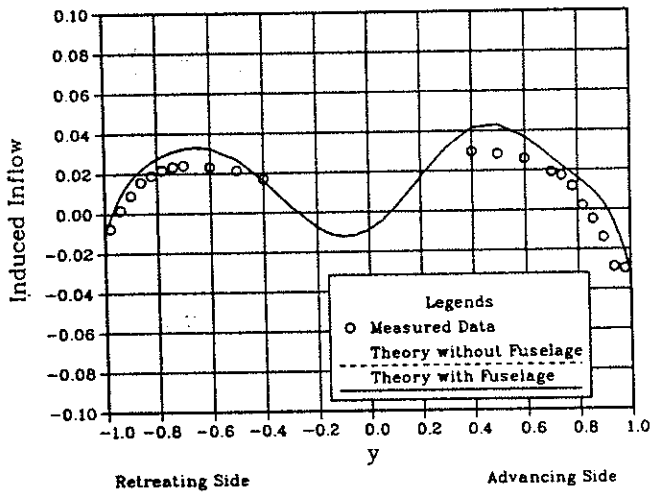

Figure 3b Lateral variation of induced flow, tapered blades, $\mu = 0.15$, $M = 4$, $S = 33$.

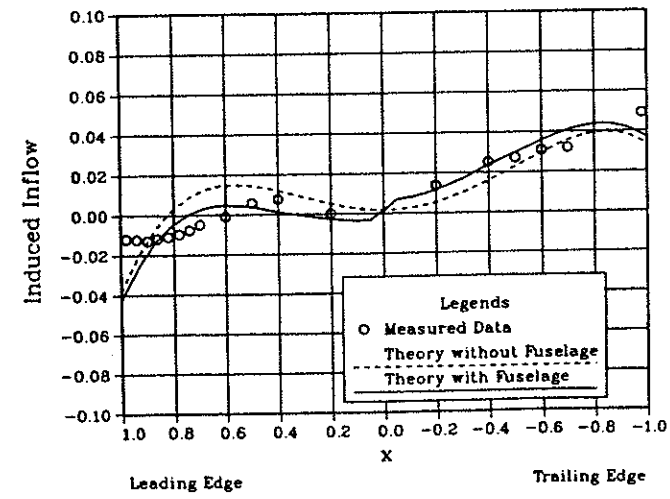

Figure 4a Longitudinal variation of induced flow, tapered blades, $\mu = 0.23$, $M = 4$, $S = 15$.

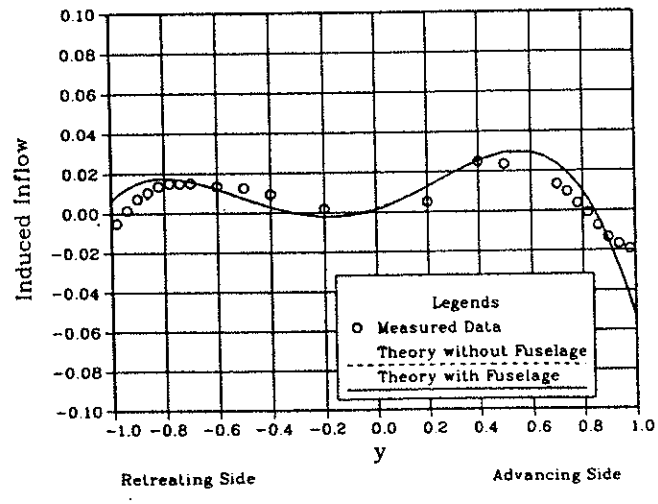

Figure 4b Lateral variation of induced flow, tapered blades, $\mu = 0.23$, $M = 4$, $S = 15$.

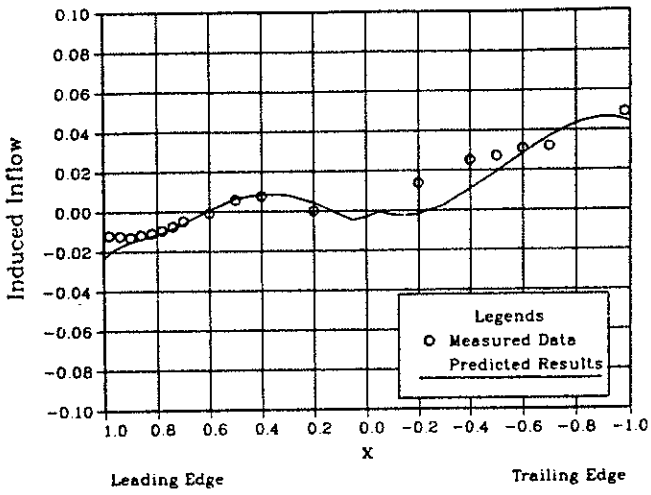

Figure 5a Longitudinal variation of induced flow, tapered blades with fuselage, $\mu = 0.23$, $M = 4$, $S = 33$.

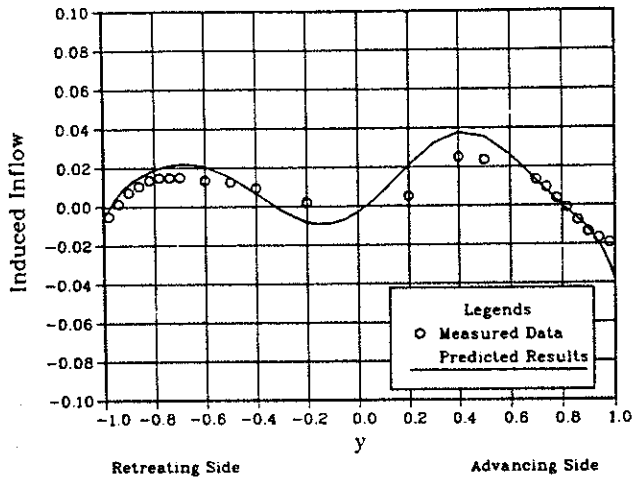

Figure 5b Lateral variation of induced flow, tapered blades with fuselage, $\mu = 0.23$, $M = 4$, $S = 33$.

computed flow at the rotor edge is converging to an answer very close to the measured flow. The results with $S = 15$ show an excessive inflow gradient near $\bar{r} = 1$, whereas results for $S = 33$ and $S = 51$ are moving toward the data and have a "flat" distribution for $0.8 < \bar{r} < 1.0$. Figures 6b and 6c show the same comparison for $\psi = 0°$ and $\psi = 30°$ (the latter being the azimuth of maximum induced flow). In these cases, the flow at the trailing edge has already converged; but the flow in the center of the disk is changing with S, due to convergence on the effect of the root vortex. Interestingly, the data at $\psi = 0°$ do not seem to agree with the calculations at $\bar{r} < 0.4$, while those at $\psi = 30°$ do. We believe that the hub and fuselage-wake interaction may account for the discrepancy at $\psi = 0°$, $\bar{r} < 0.4$.

In general, 15 state variables capture the major flow effects, but 33 states capture more detail at the rotor edge. We have also computed inflow with 8 and 12 harmonics, respectively. There is no appreciable change in time-averaged inflow. Therefore, $M = 4$ is sufficient for the tapered blades.

Comparison with other Methods

Although our model is not designed as a detailed performance model, it is interesting to compare it with other, more performance-oriented models. Figure 7 shows contour plots for the tapered blade at $\mu = 0.15$ from free-wake and prescribed-

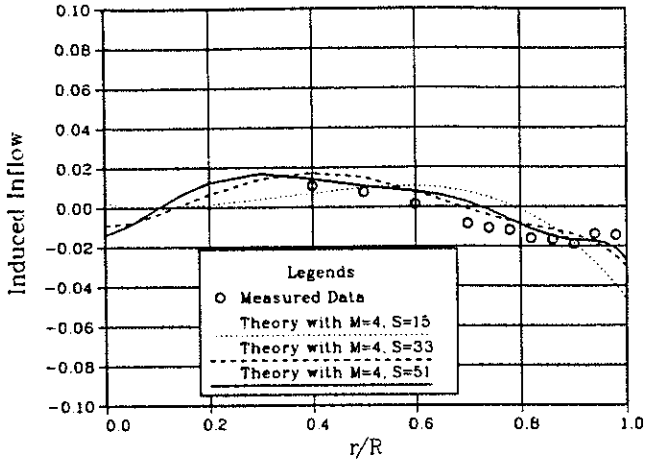

Figure 6a Effect of number of shape functions on time-averaged induced flow modeling, tapered blades with fuselage, $\mu = 0.15$, $\psi = 180°$.

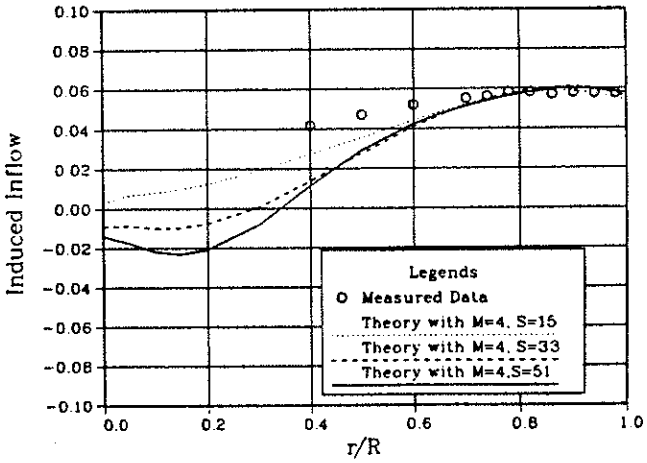

Figure 6b Effect of number of shape functions on time-averaged induced flow modeling, tapered blades with fuselage, $\mu = 0.15$, $\psi = 0.0°$.

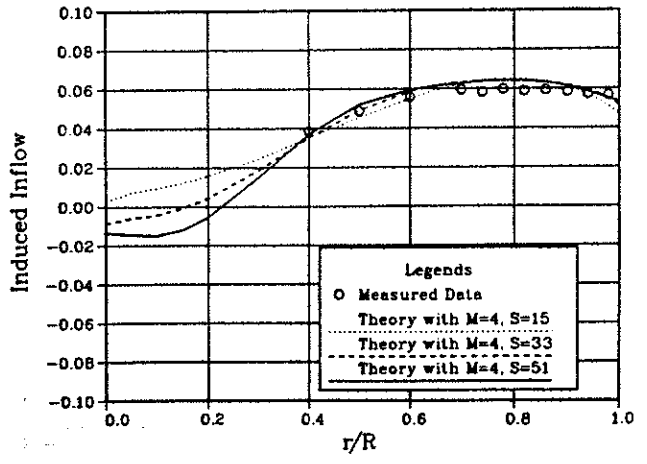

Figure 6c Effect of number of shape functions on time-averaged induced flow modeling, tapered blades with fuselage, $\mu = 0.15$, $\psi = 30.0°$.

wake models, Ref. 18 (neither of these results includes flow over the fuselage). These can be compared with the data and with our computations in Fig. 1. We see that the present model is as good or better than these other methodologies, despite its simpler assumptions. For example, the current model predicts

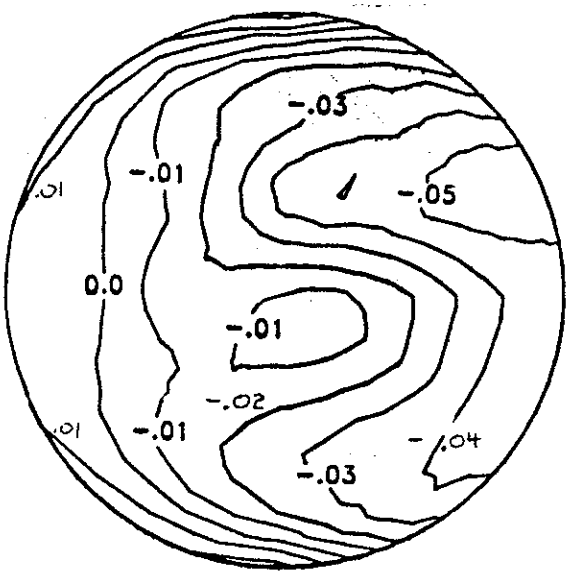

Figure 7a Computed induced flow distribution, prescribed wake, tapered blades, $\mu = 0.15$.

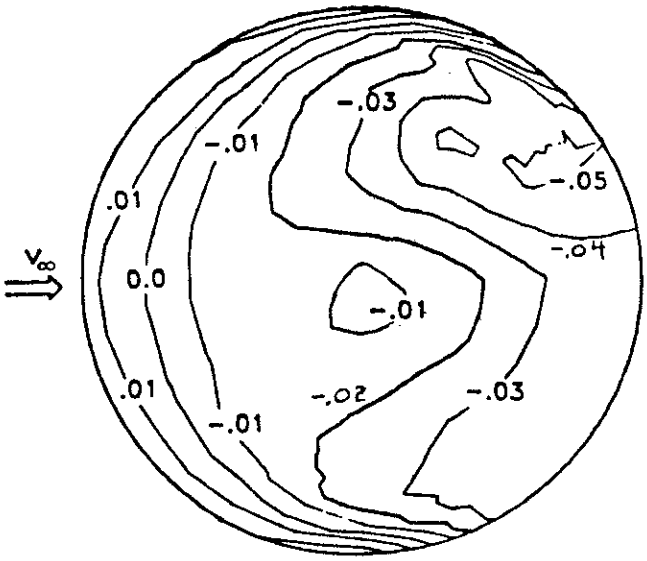

Figure 7b Computed induced flow distribution, free wake, tapered blades, $\mu = 0.15$.

the maximum measured contour of 0.06, whereas the methodologies in Fig. 7 do not. A possible explanation for this better correlation is that, although our model lacks wake distortion and wake roll-up, it has no discretization errors. In other words, the wake is continuous along the blade span and is shed continuously behind the blade rather than being modeled by a few vortex panels. Thus, for some problems (especially nearly flat wakes as we have for this data set), our model may sometimes out-perform other wake models due to reduced computational approximations.

Rectangular Blades

We now turn to correlation with the data for rectangular blades. Figures 8a–f compare theoretical and experimental contour plots at $\mu = 0.15$, 0.23, and 0.30. The theoretical results are for $S = 33$ and include flow over the fuselage. In general, the theory shows good agreement with the major flow features, but the correlations are not as good as for the tapered blades.

This discrepancy at the tip can be seen more clearly in results along the lateral and longitudinal axes, Figs. 9a–f. Figures 9a–b show small errors in the tip regions near $\bar{r} = 1$, similar to the unconverged results in Fig. 4. However, the correlation at the center is better than in Fig. 4. The overall correlation deteriorates at $\mu = 0.23$, Figs. 9c–d, and at $\mu = 0.30$, Figs. 9e–f. We have also done this computation with up to 51 states. Correlation improves at the tips, but is still not completely accurate.

The difference in convergence between rectangular blades and tapered blades is due to the fact that rectangular blades with 8° of twist have less lift inboard and more lift outboard than do the tapered blades with 13° twist. Thus, the tapered blades have a stronger root vortex (slowing convergence in the center), while the rectangular blades have a stronger tip vortex (slowing convergence at the blade tips).

Although the above correlation is not as good as it was for the tapered blades, the accuracy must be placed in perspective. Reference 19 provides a comparison of these data with five other wake models. A comparison of our results with those in

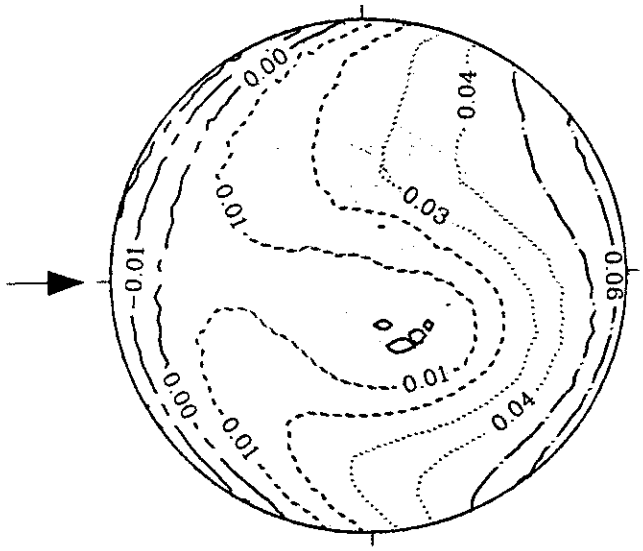

Figure 8a Theoretical induced flow distribution, rectangular blades with fuselage, $\mu = 0.15$, $M = 4$, $S = 33$.

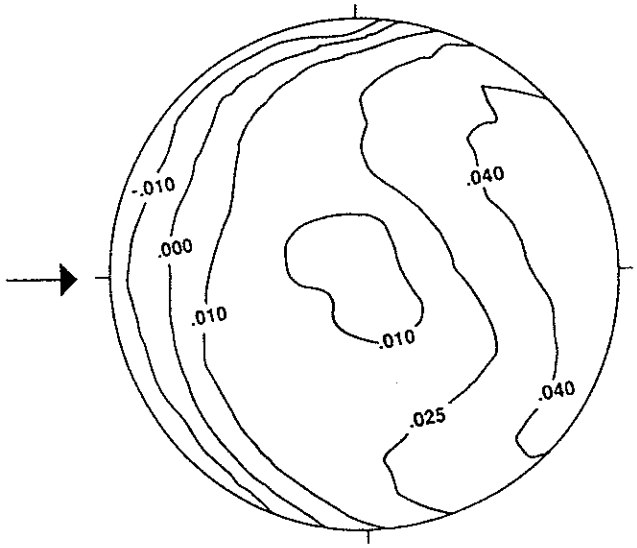

Figure 8b Experimental induced flow distribution, rectangular blades, $\mu = 0.15$.

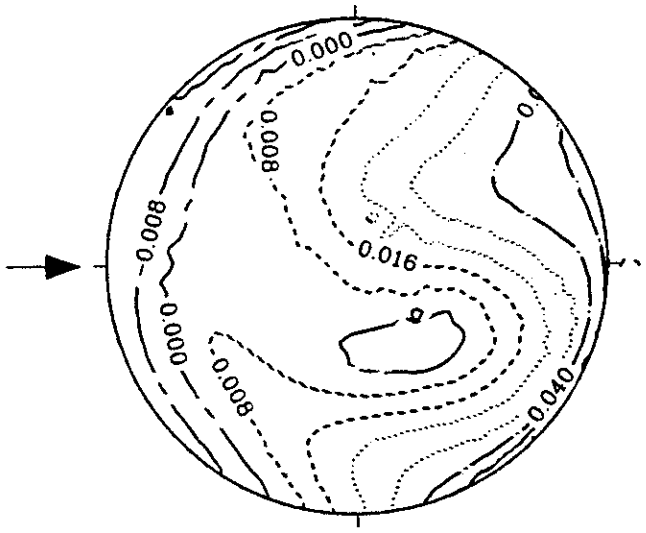

Figure 8c Theoretical induced flow distribution, rectangular blades with fuselage, $\mu = 0.23$, $M = 4$, $S = 33$.

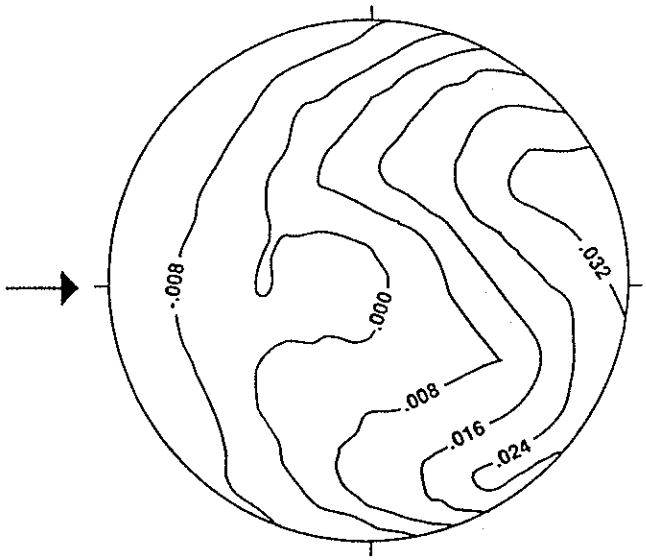

Figure 8d Experimental induced flow distribution, rectangular blades, $\mu = 0.23$.

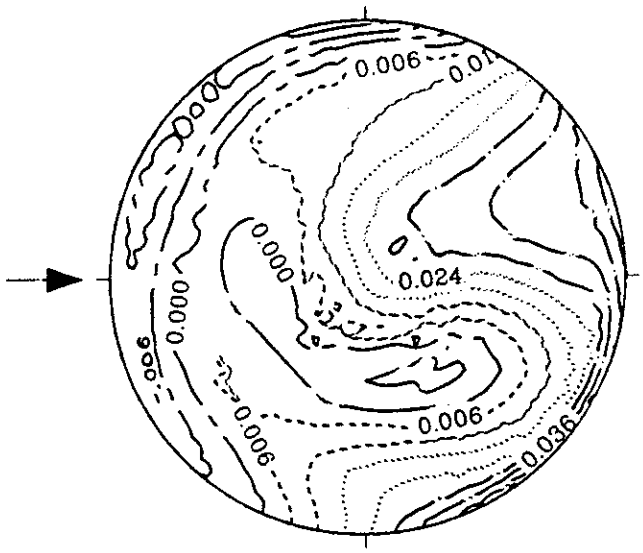

Figure 8e Theoretical induced flow distribution, rectangular blades with fuselage, $\mu = 0.30$, $M = 4$, $S = 33$.

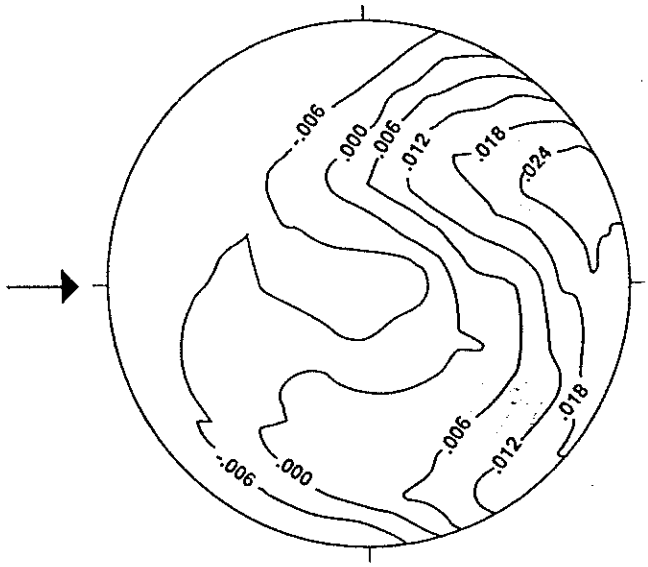

Figure 8f Experimental induced flow distribution, rectangular blades, $\mu = 0.30$.

Ref. 19 shows that, despite the slow convergence, the present model with $S = 33$ does as well or better than the other models tested.

An important point is that, despite the fact that our model does well for tapered blades (and fairly well for rectangular blades), a detailed induced flow computation is not the end product of this theory. The utility of our model comes from the need to perturb the wake about this steady-state solution. It is these aeroelastic perturbation equations that are best formulated with our finite-state model. Thus, we do not need to be completely accurate on induced flow or even on lift. We do need to be accurate on the generalized lifting forces associated with wake perturbation. Thus, modeling of flow details is much less important for aeroelasticity than it is for performance.

Summary and Conclusions

An unsteady, three-dimensional induced-flow model has been successfully applied to the computation of the induced-flow distribution of a rotor in forward flight, and numerical results have been compared against LDV measurements for induced flow at the disk. The major conclusions of this comparison are given below. However, these must be tempered by the facts that the comparisons are only for two particular blade planforms at three advance ratios, and that results are obtained only for two shaft angles, one value of $\bar{C}_T$, and one solidity.

1. The time-averaged induced flow from this method gives good correlation with measured data with the exception of just behind the pylon at the lowest advance ratio, and near the blade tips for rectangular blades at high advance ratios.
2. The method performs as well as or better than other codes that have been applied to this data; but the new method takes less computing time, and it is better suited for aeroelastic analysis.
3. Results with only 4 harmonics and 15 state variables converge to all fundamental characteristics of the time-averaged flow. However, for accurate flow near blade tips (especially at $\psi = 180°$), we require 33 state variables for tapered blades and more than 51 states for the rectangular blades.

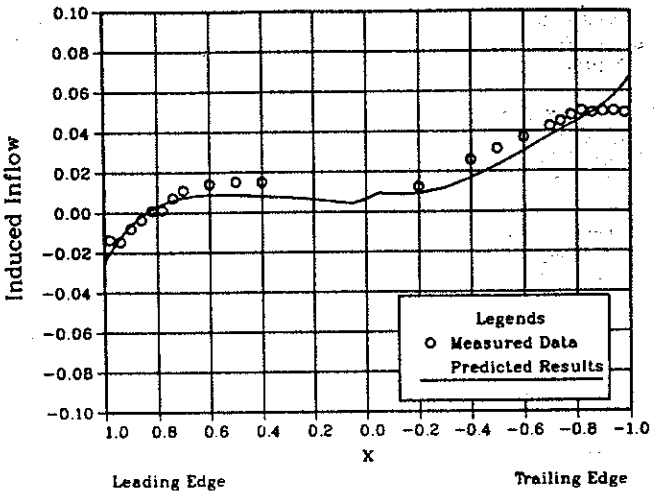

Figure 9a Longitudinal variation of induced flow, rectangular blades with fuselage, $\mu = 0.15$, $M = 4$, $S = 33$.

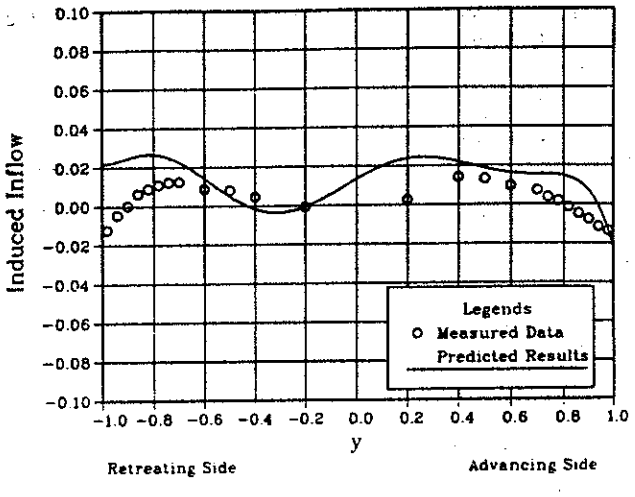

Figure 9d Lateral variation of induced flow, rectangular blades with fuselage, $\mu = 0.23$, $M = 4$, $S = 33$.

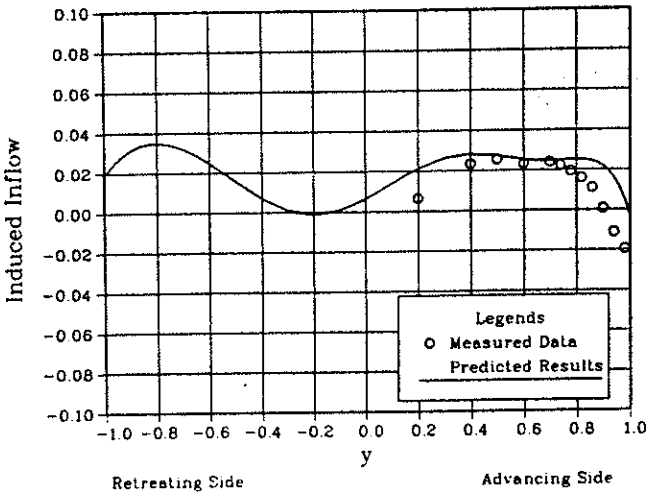

Figure 9b Lateral variation of induced flow, rectangular blades with fuselage, $\mu = 0.15$, $M = 4$, $S = 33$.

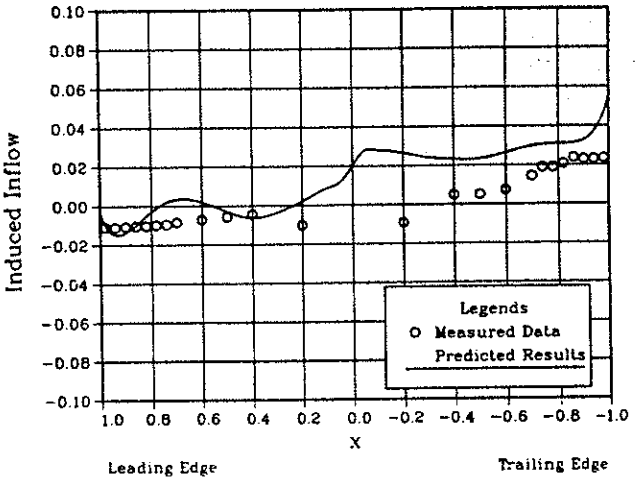

Figure 9e Longitudinal variation of induced flow, rectangular blades with fuselage, $\mu = 0.30$, $M = 4$, $S = 33$.

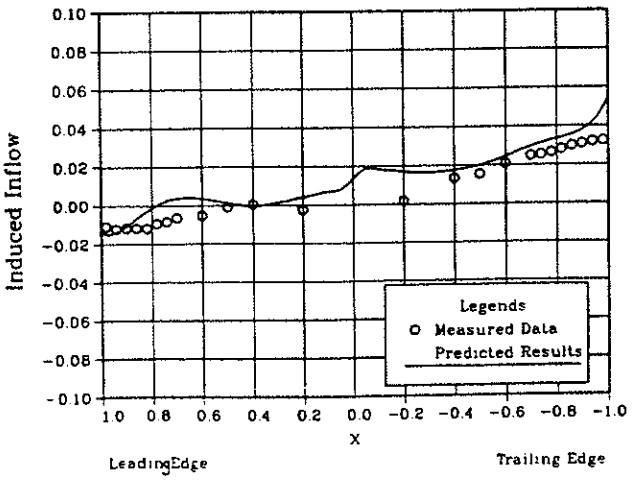

Figure 9c Longitudinal variation of induced flow, rectangular blades with fuselage, $\mu = 0.23$, $M = 4$, $S = 33$.

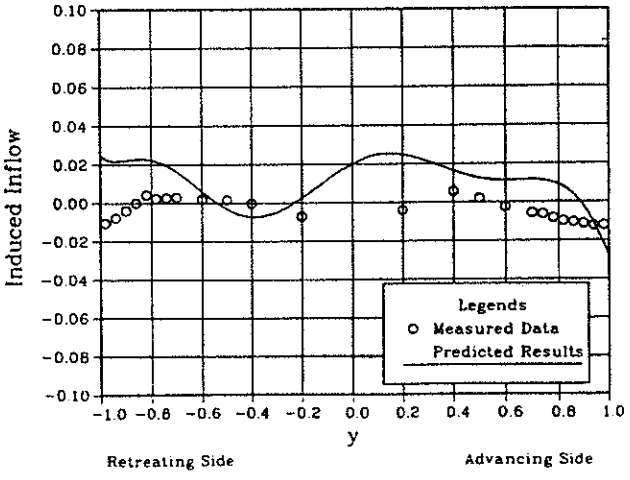

Figure 9f Lateral variation of induced flow, rectangular blades with fuselage, $\mu = 0.30$, $M = 4$, $S = 33$.

4. For accurate correlation, one needs the flow over the fuselage to be included in the analysis.

Acknowledgment

This work was sponsored by a joint NASA-Army grant, NAG-2-462, Bob Ormiston, Bill Warmbrodt, and Benton Lau technical monitors. Additional funding was provided by the Georgia Tech Center of Excellence for Rotary Wing Aircraft Technology, sponsored by the Army Research Office.

References

[1]Loewy, R. G., "A Two Dimensional Approach to the Unsteady Aerodynamics of Rotary Wings," *Journal of the Aeronautical Sciences*, Vol. 24, (2), Feb 1957.

[2]Friedmann, P. P., and Venkatesan, C., "Finite State Modeling of Unsteady Aerodynamics and Its Application to a Rotor Dynamic Problem," 11th European Rotorcraft Forum, London, Sep 1985.

[3]Mangler, K. W., "Calculation of the Induced Velocity Field of a Rotor," Royal Aircraft Establishment, Report No. Aero 2247, Sep 1948.

[4]Heyson, H. H., and Kotzoff, S., "Induced Velocities Near a Lifting Rotor with Nonuniform Disk Loading," NASA TR 1319, 1957.

[5]Wang, Shi-Cun, "Generalized Rotor Vortex Theory, Problems of Helicopter Rotor Aerodynamics," U.S.S.R., 1961 (see also, Mil, M. J., *Helicopters, Calculation and Design*, NASA TT F-494, Sep 1967).

[6]Miller, R. H., "Rotor Blade Harmonic Air Loading," *AIAA Journal*, Vol. 2, (7), Jul 1964.

[7]Scully, M. P., "A Method of Computing Helicopter Vortex Wake Distortion," MIT, ASRL TR138-1, Jun 1967.

[8]Landgrebe, A. J., "An Analytical Method for Predicting Rotor Wake Geometry," *Journal of the American Helicopter Society*, Vol. 14, (4), Oct 1969.

[9]Sadler, S. G., "Development and Application of a Method for Predicting Rotor Free Wake Positions and Resulting Blade Airloads," NASA CR-1911 Vol. I: Model and Results, NASA CR-1912 Program Listing, 1971.

[10]Runyan, Harry L., and Tai, Hsiang, "Application of a Lifting Surface Theory for a Helicopter in Forward Flight," 11th European Rotorcraft Forum, London, Sep 1985.

[11]Pitt, D. M., and Peters, D. A., "Theoretical Prediction of Dynamic Inflow Derivatives," *Vertica*, Vol. 5, (1), Mar 1981.

[12]Peters, D. A., Boyd, D. D., and He, Chengjian, "Finite-State Induced-Flow Model for Rotors in Hover and Forward Flight," *Journal of the American Helicopter Society*, Vol. 34, (4), Oct 1989.

[13]He, Chengjian, *Development and Application of a Generalized Dynamic Wake Theory for Lifting Rotors*, Ph.D. Thesis, School of Aerospace Engineering, Georgia Institute of Technology, Jul 1989.

[14]Peters, D. A., and Ninh HaQuang, "Dynamic Inflow for Practical Application," *Journal of the American Helicopter Society*, Vol. 33, (4), Oct 1988.

[15]Peters, D. A., Kim, B. S., and Chen, H. S., "Calculation of Trim Settings for a Helicopter Rotor by an Optimized Controller," *Journal of Guidance, Control and Dynamics*, Vol. 7, (1), Jan–Feb 1984.

[16]Elliott, J. W., and Althoff, S. L., "Inflow Measurement Made with a Laser Velocimeter on a Helicopter Model in Forward Flight," Vols. I–V, NASA TM's 100541-100545, Apr 1988.

[17]Berry, John D., and Althoff, Susan L., "Computing Induced Velocity Perturbations due to a Helicopter Fuselage in a Freestream," NASA TM 4113, Jun 1989.

[18]Berry, J. D., Hoad, D. R., Elliott, J. W., and Althoff, S. L., "Helicopter Rotor Induced Velocities-Theory and Experiment," AHS National Specialists' Meeting on Aerodynamics, and Aeroacoustics, Arlington, Tex., Feb 1987.

[19]Hoad, Danny R., Althoff, Susan, L., and Elliott, J. W., "Rotor Inflow Variability with Advance Ratio," American Helicopter Society 44th Annual Forum, Washington, D.C., Jun 1988.

FINITE-STATE AIRLOADS FOR DEFORMABLE AIRFOILS ON FIXED AND ROTATING WINGS

David A. Peters, Director
Center for Computational Mechanics
Mark J. Johnson, Graduate Student
Department of Mechanical Engineering

Washington University
Campus Box 1129
St. Louis, Missouri 63130

INDIVIDUAL BLADE CONTROL

- Servo-Flaps
- Dynamic Camber
- Smart Structures

MODELING NEEDS

- Lift and Drag
- All Generalized Forces
- Large Frame Motions
- State-Space Representation

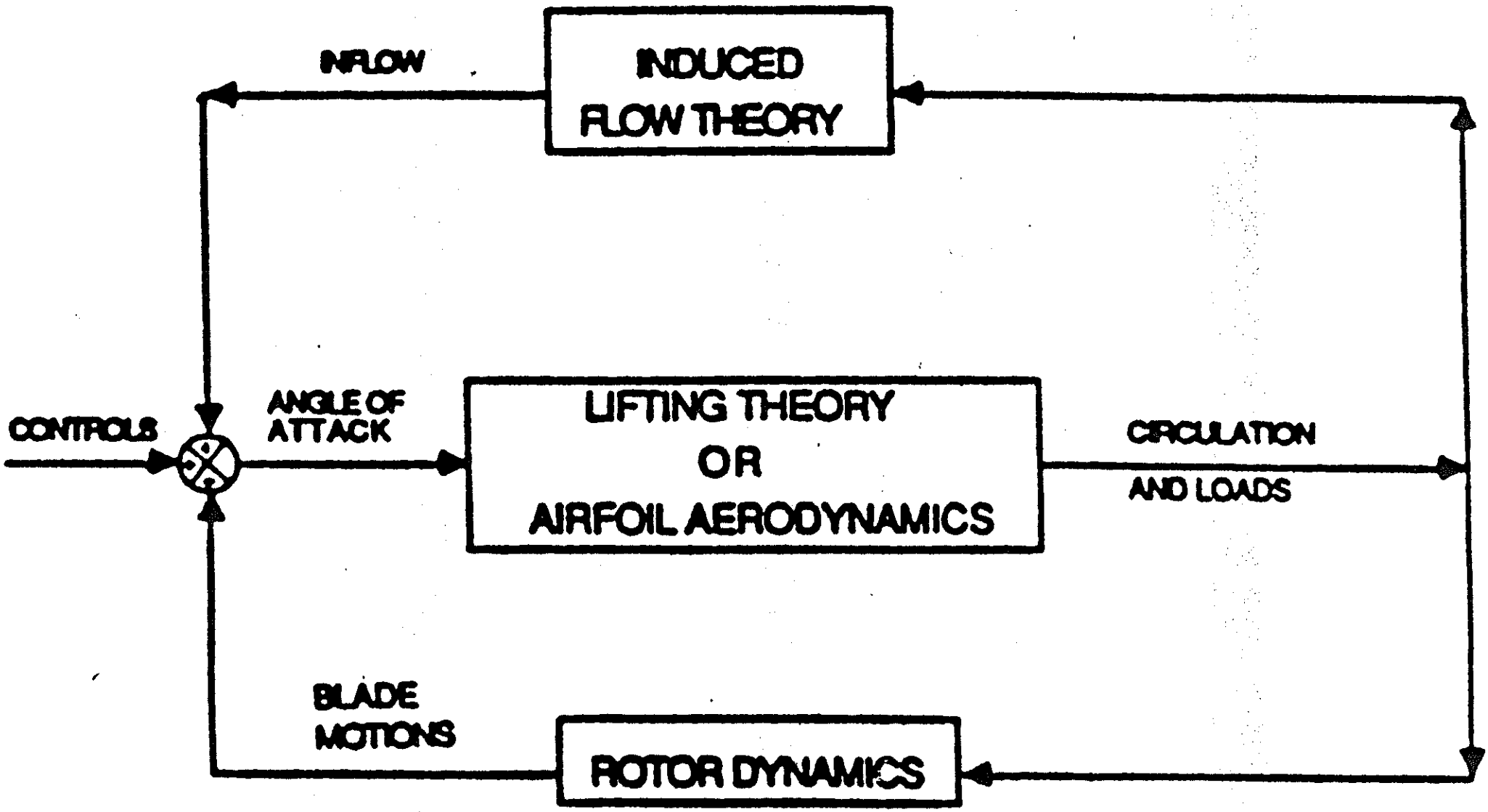
INFLOW
INDUCED
FLOW THEORY
CONTROLS
ANGLE OF
ATTACK
LIFTING THEORY
OR
AIRFOIL AERODYNAMICS
CIRCULATION
AND LOADS
BLADE
MOTIONS
ROTOR DYNAMICS

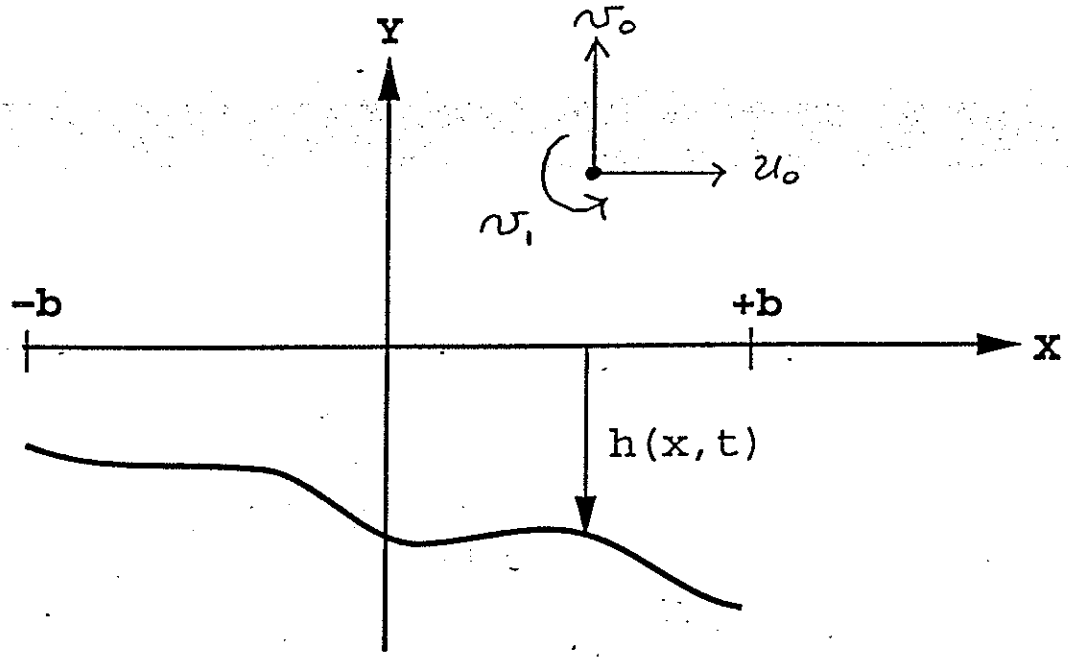

Figure 1. General Airfoil Coordinate System.

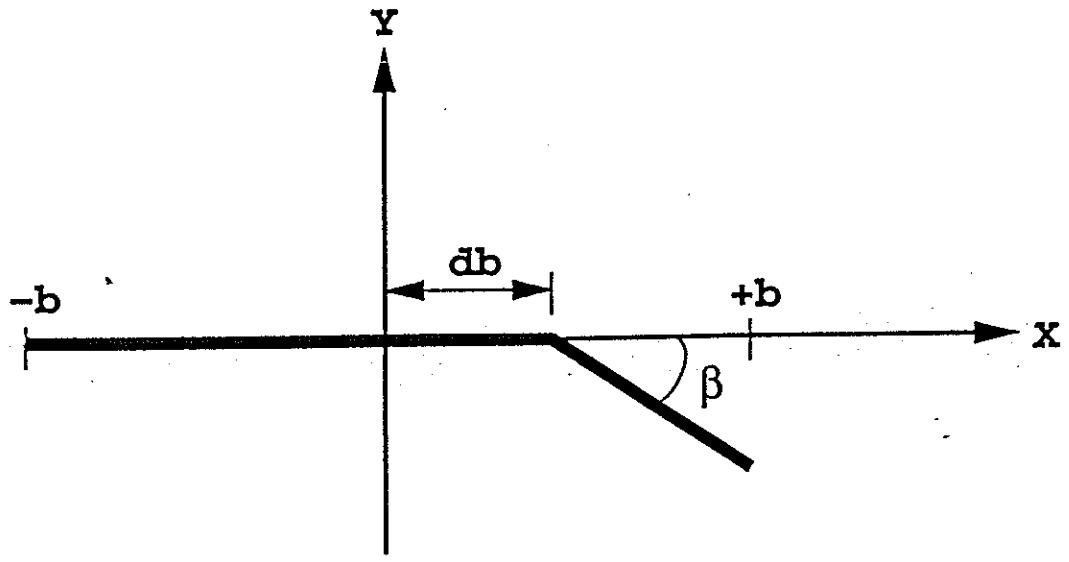

Figure 2. Geometry of Trailing-Edge Flap.

FLUID DYNAMICS

$$\bar{v} = \overbrace{u_0 \partial h/\partial x + \partial h/\partial t + v_0 + v_1 x/b}^{\omega} - \lambda$$

$$\bar{v} = \frac{-1}{2\pi} \int_{-b}^{+b} \frac{\gamma_b(\xi, t)}{x - \xi} d\xi$$

$$\Delta P = \rho u_0 \gamma_b + \rho \int_{-b}^{x} \partial \gamma_b / \partial t \; d\xi$$

$$\partial \lambda/\partial t + u_0 \partial \lambda/\partial x = \frac{1}{2\pi} \frac{d\Gamma/dt}{b - x}$$

EXPANSIONS

$$x = b \cos\phi$$

$$\gamma_b = 2 \left[\frac{+\gamma_s}{\sin\phi} - \frac{\gamma_0 \cos\phi}{\sin\phi} + \sum_{n=1}^{\infty} \gamma_n \sin(n\phi) \right]$$

$$\Delta P = 2\rho \left[\frac{+\tau_s}{\sin\phi} - \frac{\tau_0 \cos\phi}{\sin\phi} + \sum_{n=1}^{\infty} \tau_n \sin(n\phi) \right]$$

$$\bar{v} = \sum_{n=0}^{\infty} \gamma_n \cos(n\phi)$$

$$h = \sum h_n \cos(n\phi)$$

VELOCITY DUE TO BOUND VORTICITY

$$u_0\gamma_s = \tau_s, \quad u_0\gamma_0 = \tau_0$$

$$b(\dot{\gamma}_0 - \frac{1}{2}\dot{\gamma}_2) + u_0\gamma_1 = \tau_1 - \dot{\Gamma}/\pi$$

$$\frac{b}{2n}(\dot{\gamma}_{n-1} - \dot{\gamma}_{n+1}) + u_0\gamma_n = \tau_n - \dot{\Gamma}/(n\pi) \quad n \geq 2$$

VELOCITY DUE TO SHED VORTICITY

$$b(\dot{\lambda}_0 - \frac{1}{2}\dot{\lambda}_2) + u_0\lambda_1 = \dot{\Gamma}/\pi$$

$$\frac{b}{2n}(\dot{\lambda}_{n-1} - \dot{\lambda}_{n+1}) + u_0\lambda_n = \dot{\Gamma}/(n\pi) \quad n \geq 2$$

$$\lambda_0 = \frac{1}{2}\sum_{n=0}^{\infty} b_n\lambda_n$$

PRESSURE-VELOCITY RELATIONSHIP

$$w_n = \gamma_n + \lambda_n$$

$$u_0(w_0 - \lambda_0) = \tau_0$$

$$b(\dot{w}_0 - \frac{1}{2}\dot{w}_2) + u_0 w_1 = \tau_1$$

$$\frac{b}{2n}(\dot{w}_{n-1} - \dot{w}_{n+1}) + u_0 w_n = \tau_n \quad n > 2$$

REVERSED FLOW AND KUTTA CONDITION

$$\tau_s = f\tau_0$$

$$f = 1 \text{ (reversed flow neglected)}$$

$$f = u_0/|u_0| = sgn(u_0) \text{ (full reversed flow)}$$

$$f = u_0/\sqrt{u_0^2 + (v_0 + \dot{h}_0 - \lambda_0)^2} = \cos\alpha \text{ (weak reversed flow)}$$

GENERALIZED LOADS

$$L_n = -\int_{-b}^{+b} \Delta P \cos(n\phi) dx = -\int_0^{\pi} b\Delta P \cos(n\phi)\sin\phi d\phi$$

$$D = \int_{-b}^{+b} (\Delta P)(\partial h/\partial x) dx \; - 2\pi\rho b f (w_0 - \lambda_0)^2$$

$$= \int_0^{\pi} b(\Delta P)(\partial h/\partial x)\sin\phi d\phi - 2\pi\rho b f (w_0 - \lambda_0)^2$$

BOUNDARY CONDITIONS

$$h = \sum_{n=0}^{\infty} h_n \cos(n\phi)$$

$$w_0 = v_0 + \dot{h}_0 + u_0 \sum_{n=1,3,5}^{\infty} n h_n / b$$

$$w_1 = v_1 + \dot{h}_1 + 2u_0 \sum_{n=2,4,6}^{\infty} n h_n / b$$

$$w_m = \dot{h}_m + 2u_0 \sum_{n=m+1,m+3,}^{\infty} n h_n / b \quad m \geq 2$$

$$w_0 + \frac{1}{2} w_1 = v_0 + \frac{1}{2} v_1 + \dot{h}_0 + \frac{1}{2} \dot{h}_1 + u_0 \sum_{n=1,2,3}^{\infty} n h_n / b$$

$$w_0 - \frac{1}{2} w_2 = v_0 + \dot{h}_0 - \frac{1}{2} \dot{h}_2 + u_0 h_1 / b$$

$$w_{n-1} - w_{n+1} = \dot{h}_{n-1} - \dot{h}_{n+1} + 2n u_0 h_n / b \quad n \geq 2$$

Matrix Form of Theory

$$\{L_n\} = -2\pi\rho b u_0[c]\begin{Bmatrix} v_0 - \lambda_0 \\ v_1 \end{Bmatrix} - \pi\rho b^2[m]\begin{Bmatrix} \dot{v}_0 \\ \dot{v}_1 \end{Bmatrix}$$

$$-2\pi\rho u_0^2[K]\{h_n\} - 2\pi\rho b u_0[C]\left\{\dot{h}_n\right\}$$

$$-\pi\rho b^2[M]\left\{\ddot{h}_n\right\} - 2\pi\rho b\dot{u}_0[\overline{C}]\{h_n\}$$

STIFFNESS AND DAMPING

$$[K] = \begin{bmatrix} 0 & f & 2 & 3f & 4 & 5f & 6 & \cdots \\ 0 & -1/2 & 0 & 0 & 0 & 0 & 0 & \\ 0 & 0 & -2/2 & & 0 & 0 & 0 & \\ 0 & 0 & 0 & -3/2 & 0 & 0 & 0 & \\ 0 & 0 & 0 & 0 & -4/2 & 0 & 0 & \\ 0 & 0 & 0 & 0 & 0 & -5/2 & 0 & \\ 0 & 0 & 0 & 0 & 0 & 0 & -6/2 & \cdots \end{bmatrix}$$

$$[C] = \begin{bmatrix} f & 1 & 0 & 0 & 0 & \\ -\frac{1}{2} & 0 & \frac{1}{2} & 0 & 0 & \cdots \\ 0 & -\frac{1}{2} & 0 & \frac{1}{2} & 0 & \cdots \\ 0 & 0 & -\frac{1}{2} & 0 & \frac{1}{2} & \cdots \\ 0 & 0 & 0 & -\frac{1}{2} & \ddots & \ddots \\ \vdots & \vdots & \vdots & \ddots & \ddots & \ddots \end{bmatrix}$$

MASS MATRIX

$$M_{00} = 1 \quad M_{11} = 1/8, \quad M_{02} = M_{20} = -1/2$$

$$M_{nn} = \frac{n}{2(n^2-1)} , \quad n \geq 2$$

$$M_{n-1,n+1} = M_{n+1,n-1} = -1/4n , \quad n \geq 2$$

$$[M] = \begin{bmatrix} x & 0 & x & 0 & 0 & 0 \\ 0 & x & 0 & x & 0 & 0 \\ x & 0 & x & 0 & x & 0 \\ 0 & x & 0 & x & 0 & x \\ 0 & 0 & x & 0 & x & 0 \\ 0 & 0 & 0 & x & 0 & x \end{bmatrix}$$

INDUCED DRAG

$$D = -2\pi\rho b(v_0 + \dot{h}_0 - \lambda_0)\left[f(v_0 + \dot{h}_0 - \lambda_0)\right.$$

$$\left. + u_0 \sum_{n=1,3,5}^{\infty} f n h_n/b + u_0 \sum_{n=2,4,6}^{\infty} n h_n/b\right]$$

$$+2\pi\rho \sum_{n=1}^{\infty} h_n \left[\frac{b}{4}(\ddot{h}_{n-1} - \ddot{h}_{n+1}) + n u_0 \dot{h}_n + \frac{1}{2} n \dot{u}_0 h_n\right]$$

$$+2\pi\rho h_1 \left(\frac{b}{2}\dot{v}_0 + \frac{b}{2}\ddot{h}_0\right) + 2\pi\rho h_2 \frac{b}{4}\dot{v}_1 + \pi\rho u_0 v_1 h_1$$

VALIDATION CASES

- Theodorsen (add $\dot{u}_0$ for Greenberg)

$$v_0 = v_1 = \dot{u}_0 = 0\,,\ \ f = 1\,,\ \ h_0 = h - ba\alpha\,,\ \ h_1 = b\alpha\,,\ \ h_n = 0\ n \geq 2$$

$$\lambda_0 = (w_0 + \frac{1}{2}w_1)[1 - C(k)] = [u_0\alpha + \dot{h} + b(\frac{1}{2} - a)\dot{\alpha}][1 - C(k)]$$

- Trailing-Edge Flap

$$h(x) = \begin{cases} 0 & x \leq bd \\ \beta(x - bd) & x > bd \end{cases}$$

- Combined/Garrick

$$\{h_n\} = [T]\begin{Bmatrix} h \\ \alpha \\ \beta \end{Bmatrix}$$

LARGE-ANGLE CORRELATION

Case 1: Conformal Mapping

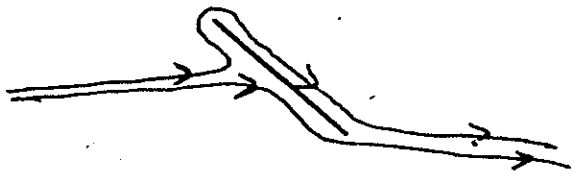

a.) $C_\ell = a \sin \alpha$

b.) lift perpendicular to free stream

Case 2: Large Frame Motions

Still Air

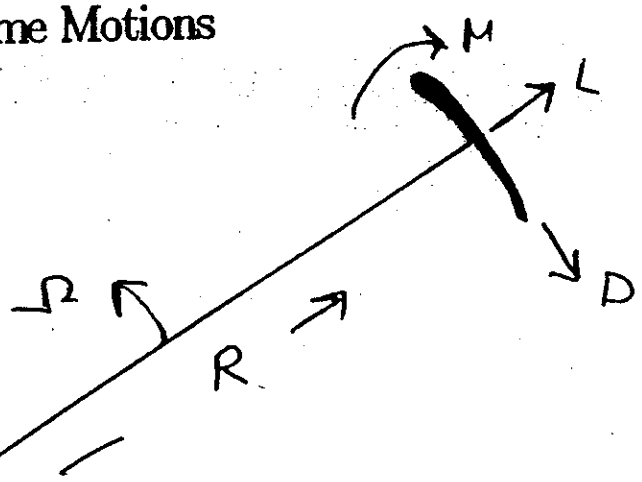

a.) Camber = Curvature $\Rightarrow$ No Loads

b.) Angle of Attack $\Rightarrow$ Conservation of Energy

$$M + DR = 0$$

NACA 4-DIGIT AIRFOILS

$$\bar{m}\bar{p}xy, \quad m = .01\bar{m}, \quad p = .10\bar{p}$$

$$w_0 = 4m(4/\pi - 1)(2p - 1)$$

$$w_1 = 4m\ , \quad w_2 = \frac{32}{3\pi}m(2p - 1)$$

Table 1: NACA Four-Digit Airfoils, Angle of Attack for Zero Lift

Airfoil	$w_0/4m$	$w_1/4m$	Predicted α_0	Measured α_0
0012	0	0	0°	0°
2412	-.056	1.019	-2.1°	-2.0°
4412	-.056	1.019	-4.2°	-4.1°
6412	-.056	1.019	-6.2°	-6.1°
4409	-.056	1.019	-4.1°	-4.0°
4415	-.056	1.019	-4.1°	-4.1°
8318	-.123	1.082	-7.7°	-7.4°

Figure 1 : Airloads from various Theories

$k = 0.2, \mu = 0.8, N = 8$

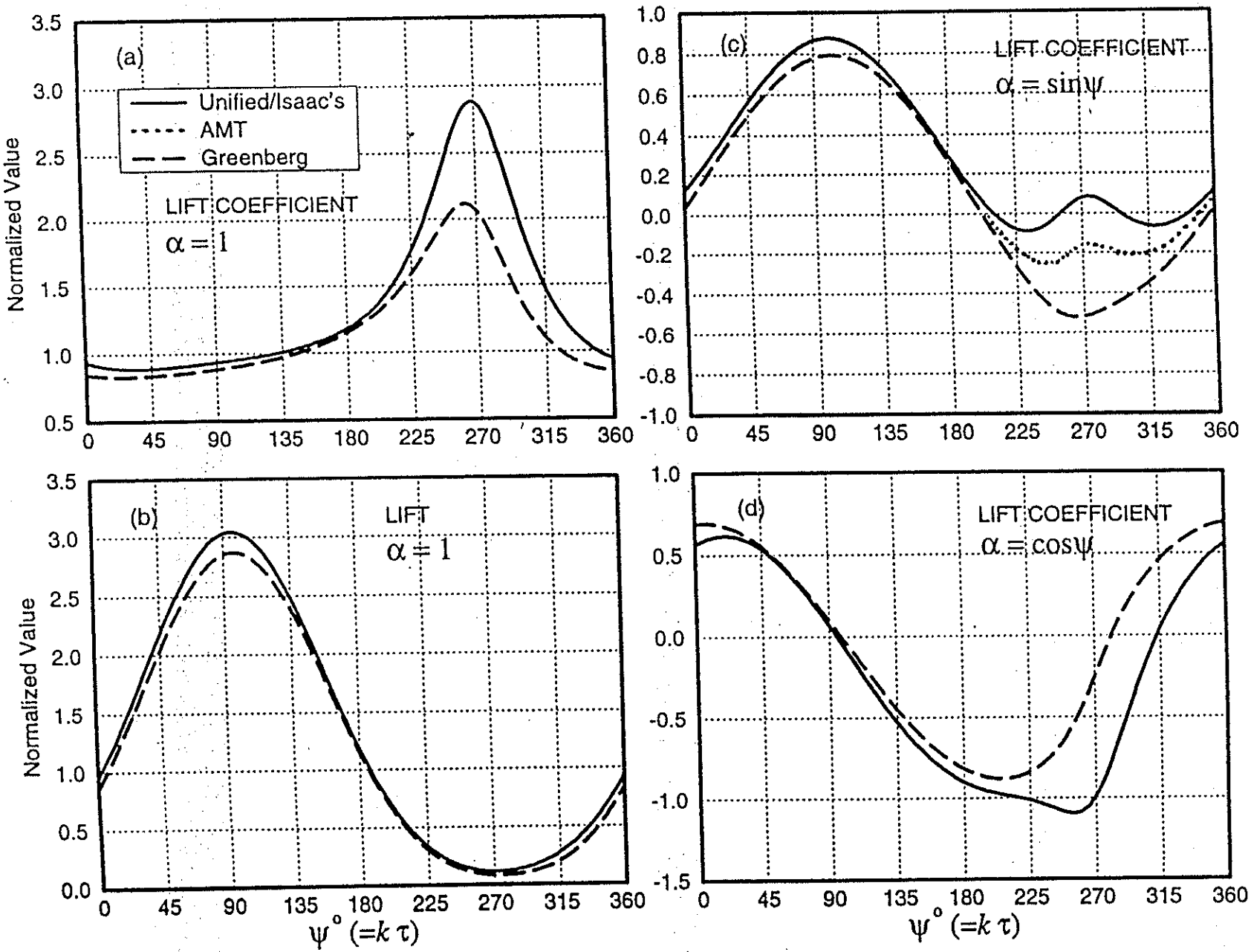

4-29-05

APPLICATION OF FINITE-STATE AIRLOADS

$w_0 = U_T$, $v_0 - \lambda_0 = -U_P$ * , $f = 1$

$v_1 + \dot{h}_1 = \dot{\alpha} b$ $\quad h_1 = b\theta$, $b = c/2$

all other $h_n \equiv 0$, $2\pi = a$

Lift $= -L_0$, Moment $= bL_1$

Lift/unit length =

$$\frac{1}{2}\rho a c \left[U_T^2 \theta - U_P U_T + L_T \frac{c}{4}\dot{\alpha} - \frac{c}{4}\dot{U}_P + \frac{c}{4}\dot{U}_T\theta \right]$$

Moment/unit length (mid-chord) $= \frac{1}{8}\rho a c^2 \left[U_T^2 \theta - U_P U_T - \frac{1}{32}\ddot{\alpha} \right]$

$$\underline{\text{Drag}}_{\text{unit length}} = +\frac{1}{2}\rho a c \left[U_P U_T \theta - U_P^2 + U_T\theta\left(\frac{c}{2}\right)\left(\dot{\theta} + \dot{\alpha}/2\right) + \theta\left(\frac{c}{4}\right)\left(\theta \dot{U}_T - \dot{U}_P\right) \right]$$

* $U_P \equiv -w_0$

STALL

$$\Delta C_n = C_{qn} - C_{sn}$$

C_{qn}: theory; C_{sn}: measured

$$L_n|_{corrected} = L_n|_{theory} - \rho b U_T^2 \Delta C_n$$

$$= L_n + \rho U_T \Gamma_n$$

$$\ddot{\Gamma}_n + (U_T/b)\eta\dot{\Gamma}_n + (U_T/b)^2\omega^2\Gamma_n =$$

$$-\omega^2 U_T^3 \Delta C_n/b - \omega^2 e U_T \frac{d}{dt}(U_T \Delta C_n$$

η, ω^2, e — from dynamic-stall experiments

SUMMARY

- We have developed a finite-state airloads model for deformable airfoils.
- All generalized forces and drag are present.
- The theory is in matrix form in terms of deformation expansions.
- An inflow theory for λ_0 must be used, and such theories already exist.

CONCLUSIONS

- The theory is validated against Theodorsen, Garrick, Greenberg, and Large-Angle Potential Flow.
- The theory is validated against static airfoil data.
- The theory is in a useful form for control analysis.

TRIG IDENTITIES

$$\sin(a+b) = \sin a \cos b + \cos a \sin b$$
$$\sin(a-b) = \sin a \cos b - \cos a \sin b$$
$$\cos(a+b) = \cos a \cos b - \sin a \sin b$$
$$\cos(a-b) = \cos a \cos b + \sin a \sin b$$

$$\cos a \cos b = \tfrac{1}{2}\left[\cos(a-b) + \cos(a+b)\right]$$

$$\sin a \sin b = \tfrac{1}{2}\left[\cos(a-b) - \cos(a+b)\right]$$

$$\sin a \cos b = \tfrac{1}{2}\left[\sin(a-b) + \sin(a+b)\right]$$

$$\cos a \sin b = \tfrac{1}{2}\left[-\sin(a-b) + \sin(a+b)\right]$$

$a = b = \theta$

$$\sin(2\theta) = 2\sin\theta\cos\theta$$
$$\cos(2\theta) = \cos^2\theta - \sin^2\theta$$
$$\cos^2\theta = \tfrac{1}{2}\left[1 + \cos 2\theta\right]$$
$$\sin^2\theta = \tfrac{1}{2}\left[1 - \cos 2\theta\right]$$
$$\sin\theta\cos\theta = \tfrac{1}{2}\sin 2\theta$$

TERMINOLOGY FOR MEMS 5703 (revised)
You should be able to define these, know what they are for, and locate them on a drawing or photograph.

helicopter
auto-gyro
main rotor
rotor blades
swashplate
pitch link
pitch horn
flap hinge
lag hinge
pitch (or feathering) hinge
lag damper
tail rotor
servo-flap
collective stick
collective pitch
cyclic stic
cyclic pitch
rudder pedals
blade root cut-out
tail boom
delta-3 angle
precone angle
fuselage
gyro stabilizer bar

MEMS 5703 GLOSSARY

Roman	definition
a	slope of lift curve
a_n	Fourier cosine terms
A	area of stream tube
A_0	A(0)
$A(t)$	periodic eigenvectors
$A(t_1, t_2)$	multiple time-scale constant
b	number of blades
b_n	Fourier sine terms
B	tip loss factor
$B(t_1, t_2)$	multiple time-scale constant
c	blade chord
c_D, c_d	drag coefficient
c_l	lift coefficient
C_{xxx}	xxxx coefficient
$C(\psi)$	periodic damping
d	vertical distance between vortex sheets
dC	element of centrifugal force
D	blade drag
$[D(t)]$	periodic state matrix
e	hinge offset
EF	wind turbine efficiency
f	Prandtl potential factor
F	induced mass flow
F_β	flap loading
F_ζ	inplane loading
F_1	thrust component of lift
F_2	inplane component of lift
FM	figure of merit
g	acceleration of gravity
h	height above ground/R
h	height above CG
I_y, I_β	flapping inertia of blade
i	sqrt(−1)
$[I]$	identity matrix
k	Prandtl tip loss function
k_G	ground effect factor
K_I	apparent inertia of air
K_m	apparent mass of air
K_β	root spring
K_{ij}	elements of flap-lag stiffness matrix
$K(\psi)$	periodic stiffness

L	roll moment, advancing side down
$\mathcal{L}$	blade lift
m	mass per unit length
m-dot	total mass flow
M	pitch moment, nose up
M	Mach number
M_β	flap moment
M_ζ	inplane moment
n	Lowis constant $\gamma/8$
p	flapping frequency
P	power into rotor
P_I	ideal power
q	roll rate
Q	power out of rotor
$\bar{Q}$	Ground resonance inertia ratio
Q_T	power in wind
[Q]	Floquet Transition matrix at end of period
r	nondimensional radial coordinate, x/R
R	blade radius
R_e	elastic coupling parameter
S	Laplace transform
s	wake spacing
t	time
T	thrust
T	period of coefficients
T( )	kinetic energy
U_P	flow perpendicular to blade
U_T	flow tangential to blade
v	induced flow
V	climb rate
V( )	potential energy
V	mass flow parameter
$\mathcal{V}$	total flow at blade
W	wind speed
x	radial coordinate
x, y	change of variable flapping coordinates
z	percent of wind stopped

Greek

α	angle of attack
α	angle of shift of disk plane re
β	blade flapping angle
β_0	steady coning angle
β_{pc}	pre-cone angle
γ	blade Lock number
γ_t	tip loss Lock number
γ^*	equivalent Lock number
δW	virtual work
δ_3	delta-3 for pitch-flap coupling
Δ	elastic coupling
Δ_n	parameter for region boundary
$\Delta( )$	perturbation of ( )
ε	nondimensional offset, e/R
ε	perturbation quantity in multiple time scales
ζ	blade inplane angle
η	nondimensional climb rate
η_j	characteristic exponents
θ	pitch angle
θ_β	pitch-flap coupling
$\theta\gamma$	pitch-lag coupling
λ	total inflow, $\eta + \nu$
Λ_j	eigenvalues of Floquet Transition Matrix
μ	advance ratio
ν	induced flow ratio, $v/(\Omega R)$
ξ	dummy integration variable
ρ	density of air
σ	rotor solidity, $bc/(\pi R)$
$\bar{\sigma}$	ground resonance blade ratio
τ	reduced time
ϕ	inflow angle
ϕ_A	inflow angle with no tip loss at blade tip
$[\Phi(t)]$	Floquet Transition Matrix
χ	wake skew angle
ψ	rotor azimuth angle
ψ	nondimensional time, Ωt
$[\Psi]$	decoupled transition matrix
ω	excitation frequency
ω	natural frequency in flapping change of variable
ω_β	nonrotating flap frequency
ω_ζ	nonrotating lag frequency
Ω	rotor speed, rad/sec

Symbols

$(\,-\,)^*$	$d(-)/d\psi$
$(-)_0$	constant component
$(-)_s$, $(-)_c$	sine and cosine components
$(\,\bar{}\,)$	normalized quantity or average, static value
Σ	summation
$(-)_{eq}$	equivalent average value
$(\,)_n$	n-th term in perturbation expansion
tr( )	trace of ( )